University of Zurich[UZH]

Land surface dynamics of the Canadian Arctic Archipelago and adjacent Greenland observed using optical and SAR time series

GEO 511 Master's Thesis

Author
Marius Vögtli
13-720-016

Supervised by
Dr. David Small
Dr. Rogier De Jong

Faculty representative
Prof. Dr. Michael Schaepman

27.09.2018
Department of Geography, University of Zurich

University of Zurich[UZH]

Department of Geography

Land surface dynamics of the Canadian Arctic Archipelago and adjacent Greenland observed using optical and SAR time series

GEO 511 Master's Thesis

Author:
Marius Vögtli
13-720-016
marius.voegtli@geo.uzh.ch

Supervised by:
Dr. David Small
david.small@geo.uzh.ch
&
Dr. Rogier de Jong
rogier.dejong@geo.uzh.ch

Faculty representative:
Prof. Dr. Michael Schaepman

27th September 2018
Department of Geography, University of Zurich

Abstract

In recent years, the Arctic cryosphere has faced numerous changes, including a continuing shrinkage of glaciers and ice caps and a decreasing snow cover extent. These changes have strong implications on Earth's climate and water cycle, calling for accurate and timely knowledge about the state of the cryosphere. Satellite remote sensing has proven to be a valuable tool for monitoring the cryosphere with good temporal and spatial resolutions.

In this Master's thesis, the potential of satellite remote sensing for cryosphere applications is assessed using an 18 years long time series of optical data from Moderate Resolution Imaging Spectro-Radiometer (MODIS) and four years of Synthetic Aperture Radar (SAR) data from RADARSAT-2 and Sentinel-1 covering the north-eastern most part of Canada and adjacent Greenland. On the one hand, the changes that occurred to the Canadian Arctic Archipelago and surrounding Greenland are analysed. On the other hand, the capabilities and the complementarity of optical data and SAR data is evaluated.

Different optical methods, such as the Normalised Difference Snow Index (NDSI) and the Normalised Difference Vegetation Index (NDVI), and SAR methods, such as a widely-used snow wetness algorithm, were applied to receive various land cover metrics (snow/ice-covered days (SCD), minimum snow/ice-covered area (MSCA), melting days (MD), average melting intensity (AMI) and vegetation days (VD)). Using these metrics, a characterisation of the changes in land cover during the 18 years of observations could be obtained and the complementarity of optical and SAR data could be analysed.

A significant decrease in SCD of -2.0 days per decade and in MSCA of $-1.5\,\%$ could be observed. The largest changes occurred in the north-western part of the Canadian Arctic Archipelago, while Greenland generally showed smaller changes. The melting activity revealed by the SAR data correlated clearly with meteorological variables and well-described events could be observed in the data. The ice cover of Lake Hazen, the largest High Arctic lake, showed a clear decrease. In contrast, an increase in vegetation activity could be observed throughout the study area with a clear correlation to areas of retreating cryosphere.

Optical data and SAR data have proven to be valuable for cryosphere research. Both provide parameters that allow analyses of the changes the cryosphere faces with climate change. Although at current times optical data provide a broader variety of metrics, SAR data are of special value in areas with frequent cloud cover and with a lack of daylight in winter. Moreover, they can detect melting processes without a visible loss of snow or ice.

Zusammenfassung

In den letzten Jahren hat sich die arktische Kryosphäre mit zahlreichen Veränderungen konfrontiert gesehen, darunter einem anhaltenden Rückgang der Gletscher und Eiskappen und einer abnehmenden Schneedecke. Diese Veränderungen haben starke Auswirkungen auf das Klima und den Wasserkreislauf der Erde und erfordern genaue und zeitnahe Kenntnisse über den Zustand der Kryosphäre. Die Satellitenfernerkundung hat sich als wertvolles Werkzeug zur Überwachung der Kryosphäre mit guten zeitlichen und räumlichen Auflösungen erwiesen.
In dieser Masterarbeit wird das Potenzial der Satellitenfernerkundung für Kryosphärenanwendungen anhand einer 18 Jahre langen Zeitreihe von optischen Daten von *Moderate Resolution Imaging Spectro-Radiometer (MODIS)* und vier Jahren *Synthetic Aperture Radar (SAR)*-Daten von RADARSAT-2 und Sentinel-1 bewertet, die den nordöstlichsten Teil Kanadas und das angrenzende Grönland abdecken. Auf der einen Seite werden die Veränderungen analysiert, die sich auf den kanadischen arktischen Archipel und das umliegende Grönland auswirkten. Auf der anderen Seite werden die Fähigkeiten und die Komplementarität von optischen Daten und SAR-Daten bewertet. Verschiedene optische Methoden, wie z.B. *Normalised Difference Snow Index (NDSI)* und *Normalised Difference Vegetation Index (NDVI)*, und SAR-Methoden, wie z.B. ein weit verbreiteter Schneefeuchtigkeitsalgorithmus, wurden angewendet, um verschiedene Bodenbedeckungskennwerte zu erhalten (schnee-/eisbedeckte Tage, minimale schnee-/eisbedeckte Fläche, Schmelztage, durchschnittliche Schmelzintensität und Vegetationstage). Mit Hilfe dieser Kennwerte konnte eine Charakterisierung der Veränderungen der Bodenbedeckung in den 18 Jahren der Beobachtungen gewonnen und die Komplementarität von optischen und SAR-Daten analysiert werden.
Ein signifikanter Rückgang der schnee-/eisbedeckten Tage von -2.0 Tagen pro Jahrzehnt und der minimalen schnee-/eisbedeckten Fläche von $-1.5\,\%$ konnte beobachtet werden. Die grössten Veränderungen gab es im nordwestlichen Teil des kanadischen arktischen Archipels, während Grönland im Allgemeinen kleinere Veränderungen zeigte. Die Schmelzaktivität, die durch die SAR-Daten detektiert wurde, korrelierte eindeutig mit meteorologischen Variablen und gut beschriebene Ereignisse konnten in den Daten beobachtet werden. Die Eisbedeckung von Lake Hazen, des grössten hocharktischen Sees, zeigte einen deutlichen Rückgang. Im Gegensatz dazu konnte im gesamten Untersuchungsgebiet eine Zunahme der Vegetationsaktivität beobachtet werden, mit einer klaren Korrelation zu den Bereichen der zurückweichenden Kryosphäre.
Optische Daten und SAR-Daten haben sich für die Kryosphärenforschung als wertvoll erwiesen. Beide liefern Parameter, die eine Analyse der Veränderungen der Kryosphäre durch den Klimawandel ermöglichen. Obwohl optische Daten zu aktuellen Zeiten eine grössere Vielfalt an Metriken bieten, sind SAR-Daten in Gebieten mit häufiger Bewölkung und wenig Tageslicht im Winter von besonderem Wert. Darüber hinaus können sie Schmelzvorgänge ohne sichtbaren Verlust von Schnee oder Eis erkennen.

Contents

List of Figures

Page

List of Tables

Page

List of Abbreviations

AMI	Average Melting Intensity
AMSR-E	Advanced Microwave Scanning Radiometer for the Earth Observing System
AVHRR	Advanced Very High Resolution Radiometer
CCRS	Canadian Centre for Remote Sensing
CDED	Canadian Digital Elevation Data
CDEM	Canadian Digital Elevation Model
CoReH2O	Cold Regions Hydrology High-Resolution Observatory
CSA	Canadian Space Agency
DJF	December, January, February
DEM	Digital Elevation Model
ESA	European Space Agency
GIMP	Greenland Ice Mapping Project
HH	Horizontally polarised sent, Horizontally polarised received
HV	Horizontally polarised sent, Vertically polarised received
ICESat-2	Ice, Cloud and land Elevation Satellite-2
IPCC	Intergovernmental Panel on Climate Change
JJA	June, July, August
LRW	Local Resolution Weighting
MAM	March, April, May
MD	Melting Days
MODIS	Moderate Resolution Imaging Spectro-Radiometer
MSCA	Minimum Snow/Ice-covered Area
NDSI	Normalised Difference Snow Index
NDVI	Normalised Difference Vegetation Index
NIR	Near Infrared
PDD	Positive Degree Days
QuikSCAT	Quick Scatterometer
RCM	RADARSAT Constellation Mission
RTC	Radiometrically Terrain Corrected
RSL	Remote Sensing Laboratories
SAR	Synthetic Aperture Radar
SCD	Snow/Ice-covered Days
Suomi NPP	Suomi National Polar-orbiting Partnership
SWIR	Short-wave Infrared
UTM	Universal Transverse Mercator
VD	Vegetation Days
VH	Vertically polarised sent, Horizontally polarised received
VIIRS	Visible Infrared Imager Radiometer Suite
VIS	Visible
VV	Vertically polarised sent, Vertically polarised received

1 Introduction

1.1 Motivation

The cryosphere is one of the key components of Earth's climate. Not only does it play a crucial part in Earth's water cycle, but also in Earth's climate system. In recent years, the cold regions have faced numerous changes. In the 5th assessment report of the Intergovernmental Panel on Climate Change (IPCC) Vaughan et al. (2013) note that:

- most of Earth's glaciers have continued to shrink
- most of the ice loss of glaciers was concentrated to Alaska, the Canadian Arctic, Greenland, the Southern Andes and the Asian Mountains
- the snow cover extent, especially in spring, has decreased throughout the Northern Hemisphere

Satellite remote sensing has proven to be a valuable tool for monitoring the state of the cryosphere. This thesis gives, using remotely sensed data, insights into the changes the cryosphere in the Canadian Arctic and adjacent Greenland has faced during the last 18 years.

1.2 The Arctic Cryosphere

Compared to other regions of the Earth, the Arctic faces a warming rate twice as high as the global average (Trishchenko and Wang, 2018). As one of many consequences, the melt of glaciers and ice caps in the Canadian Arctic contributed to 25 % of the global sea level rise (Gregory et al., 2013). In their research, Fisher et al. (2012) found that the ice caps in the Canadian Arctic have shown the highest melt rates in the last four millennia, which led to a glacier (and ice cap) surface loss. As an explanation for the increased melt they found a strong correlation to the number of positive degree days.

Owing to their large albedo, snow and ice have a cooling effect on the climate. The snow cover duration is, however, projected to decrease by 10 % to 20 % (Callaghan et al., 2011). Trishchenko and Wang (2018) analysed the changes in minimum snow/ice extent of the Canadian Arctic landmass between 2000 and 2016 using optical satellite imagery. They found the smallest minimum snow/ice extent in 2012 with an area of $1.53 \times 10^5\,\mathrm{km}^2$ and the largest extent in 2013 with an area of $2.09\,\mathrm{km}^2$, see figure 1.1 on the following page. The average minimum snow/ice extent over the 17 years period was $1.7 \times 10^5\,\mathrm{km}^2$.

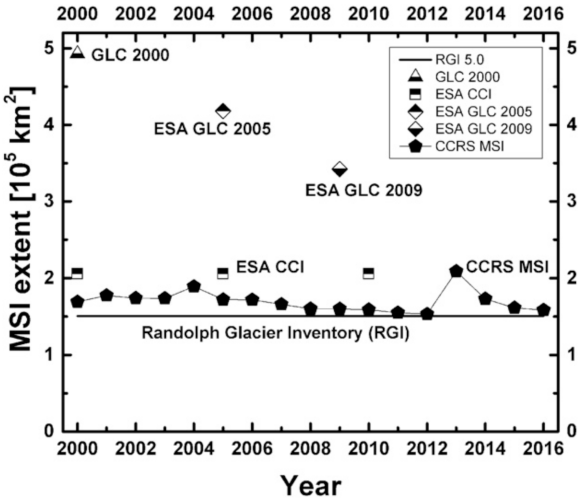

Figure 1.1: Time series of the minimum sea/ice extent between 2000 and 2016, based on the calculations using CCRS MODIS imagery. Image from Trishchenko and Wang (2018).

The authors concluded from the 17 years of observations that there was an inter-annual variability in minimum snow/ice extent, mostly concentrated to the low-altitude regions, whereas the areas above 1400 m elevation remained almost 100 % glaciated. The authors did not draw any conclusions about trends in minimum snow/ice extent. AMAP (2017) note, however, that the snow cover in the Arctic has declined by 2 to 4 days per decade in recent years and that the duration of the snow cover might decrease by 10 % to 20 % compared to current levels by 2050.

The impacts of a warming climate do, however, not only appear on global or regional, but also on local scales. In a recent study, another group of researchers, Lehnherr et al. (2018), analysed Lake Hazen on Ellesmere Island, the world's largest High Arctic lake. The hypothesis of the thesis was that Lake Hazen, owing to its large size, would be relatively resilient to the impacts of a warming climate. They found, however, a distinctly increased mass loss from glaciers in the watershed of Lake Hazen due to increased summer air temperatures, which led to a cascade of effects on the lake and its surroundings. A ten times higher inflow of glacial melt waters with associated sediments, organic carbon and contaminants was observed. Furthermore, the residence time of the lake water shrank by 70% and the lake was projected to be summer ice-free in the near future. These factors caused distinct changes in the ecology of the lake area, such as an algal bloom and damages to the Arctic Char population.

1.3 Satellite Remote Sensing

The large impacts of a warming climate, described in the previous chapter, call for accurate and timely knowledge about the state of the cryosphere. Satellite remote sensing first emerged in the middle of the 20$^{\text{th}}$ century and has ever since been used for monitoring the cryosphere. On the one hand, the vast archive of satellite imagery can be used for the analysis of processes on Earth over a long period in time, making assumptions about the development of these processes possible. On the

other hand, the near real-time sensing capabilities of recent optical and SAR sensors offer great opportunities for observing Earth's surface with a good temporal and spatial resolution at reasonable costs.

Various algorithms using different acquisition technologies have been used in recent years and have delivered promising results. Dietz et al. (2012) give a comprehensive overview of the available methods for monitoring snow and ice. They mention MODIS-based methods as the gold standard in the reflective part of the spectrum and rate SAR methods and the integration of both approaches as promising new directions.

Due to their different acquisition technologies, optical and SAR sensors observe different processes on Earth. In this Master's thesis, time series acquired by both types of sensor will be used to (a) assess their complementarity or differences and to (b) characterise the changes the Canadian Arctic and adjacent Greenland have faced during the last 18 years. The anticipated outcome is a deeper insight into the behaviour of the land cover in the Canadian Arctic and surroundings as well as its change in time. Furthermore, conclusions about the potential of combining optical and SAR data for such analyses might be drawn.

1.4 Research Questions

The aims of this thesis follow multiple directions. On the one hand, questions about the characterisation of the land surface and its changes over a longer period provide an environmental and climatological dimension. On the other hand, an analysis of the complementarity of different satellite remote sensing products provide a more methodological dimension. The key questions that will be answered are:

- Which aspects of snow dynamics can be derived from SAR data, from optical data, and from both?
- Using these, what changes in land and snow/ice cover can be observed between 2000 and 2017?
- (How) can the observed changes in land and snow/ice cover be explained?

1.5 Outline

The first two sections of the thesis cover a description of the study site and the available data — from satellite data to auxiliary data. Then, the different methods applied to the optical and SAR data are introduced, followed by the presentation of the results. Finally, the results are discussed in a broader context and conclusions are drawn.

2 Study Site

The following chapter introduces the study site of this Master's thesis; the north-eastern most part of Canada as well as adjacent Greenland. Furthermore, considerations about the suitability of the study site are presented.

2.1 The Canadian Arctic Archipelago

The Canadian Arctic Archipelago consists of 94 islands with a size of more than 130 km^2 and 36'469 smaller islands, adding up to a total area of 1.4×10^6 km^2 (Adams and Dunbar, 2016).

Figure 2.1: Major islands of the Canadian Arctic Archipelago. Image from Adams and Dunbar (2016).

The largest islands of the archipelago are Baffin Island (507 451 km^2), Victoria, Island (217 291 km^2), Ellesmere Island (196 236 km^2), Banks Island (70 028 km^2), Devon Island (55 247 km^2), Axel Heiberg Island (43 178 km^2), Melville Island (42 149 km^2) and Prince of Wales Island (3339 km^2) (Marsh, 2018a).

The climate of the archipelago is described as truly polar with annual mean temperatures as low as -20 °C on the northern islands and -6 °C further south. With 100 mm to 400 mm, yearly precipitation rates are small, which makes parts of the archipelago a polar desert.

The largest part of the Canadian Arctic Archipelago and the study site is covered by Ellesmere Island. With a size of 196 236 km^2, Ellesmere Island is the third largest island in Canada and the tenth largest island in the world (Marsh, 2018b). The highest point on Ellesmere Island is Barbeau Peak with an elevation of 2616 m (The Editors of Encyclopaedia Britannica, 2017). The geography of the island is dominated by fjords, ice shelves, ice caps and Nunataks (exposed rocks or mountain peaks within a glacier or an ice cap). Lake Hazen, the largest polar lake, is located in the north-eastern part of Ellesmere Island. The island is only sparsely vegetated, but has some

populations of muskoxen, caribous, numerous bird species and other land mammals (Marsh, 2018b). There are a couple of inhabited places on Ellesmere Island. Grise Fiord (or *Aujuittuq*, an important Inuit community) and Eureka and Alert (two weather stations) are the most important ones (The Editors of Encyclopaedia Britannica, 2017).

For more details on the geography of the Canadian Arctic Archipelago and Ellesmere Island, see Adams and Dunbar (2016) and Marsh (2018a).

2.2 Lake Hazen

Lake Hazen is the largest High Arctic lake, situated in the north-eastern part of Ellesmere Island, at an altitude of 159 m above sea level. In their extensive bathymetric measurements of the lake, Köck et al. (2012) obtained an area of approximately 540 km^2, a volume of 5.14×10^{10} km^3 and a maximum depth of 267 m. Their bathymetric map of the lake can be seen in figure 2.2. Several glacial inflows provide water input into the lake, while Ruggles River is the only outflow. The lake was described as a polar oasis by Köck et al. (2012) and Surdu et al. (2016), i.e. a thermal oasis with summer temperatures as high as 20 °C within a polar desert. Surdu et al. (2016) explain the warmer temperatures by the Grand Land Mountains in the north and a plateau in the south of the lake, that give shelter from cold air from the Arctic Ocean.

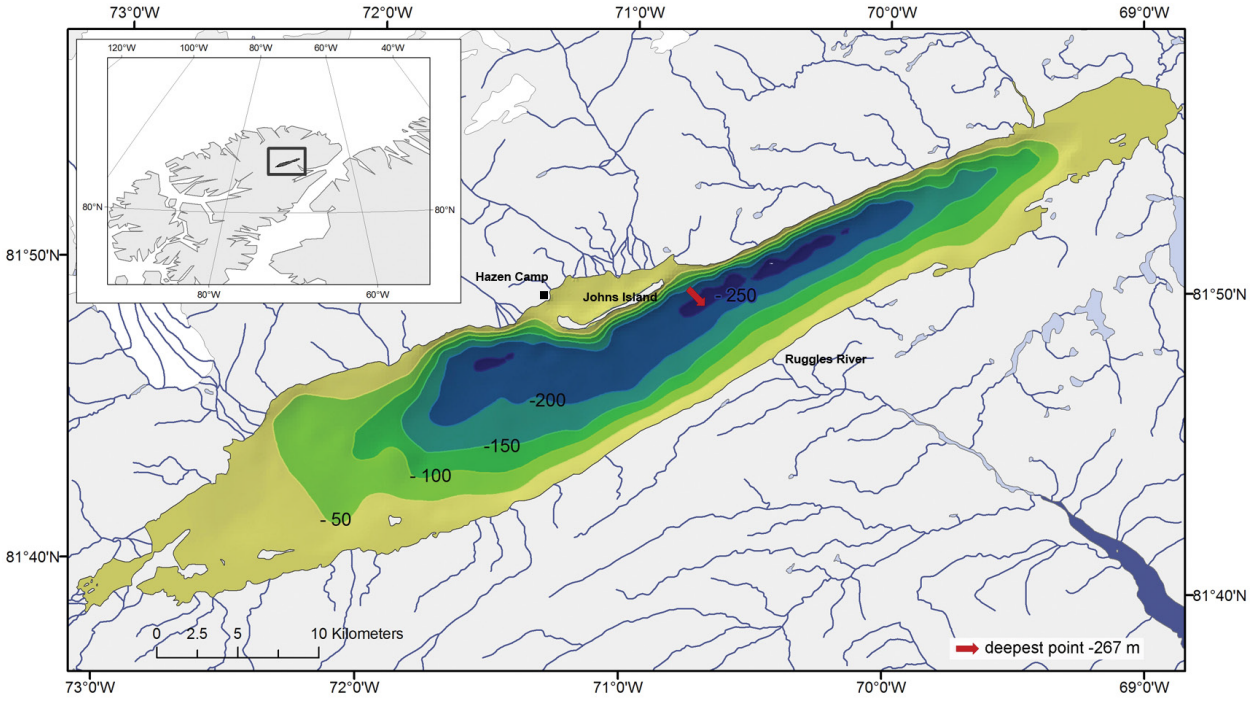

Figure 2.2: Bathymetry of Lake Hazen. Image from Köck et al. (2012).

2.3 Suitability of the Study Site

The satellite imagery available for the thesis covers Ellesmere Island, the surrounding Canadian Arctic Archipelago as well as the westernmost part of Greenland. This provides an interesting study

site. Ellesmere Island, taking up large parts of the study site, has a north-south extent of roughly 800 km allowing the analysis of different phenomena on different latitudes. Furthermore, there is an elevation difference of roughly 2600 m between the highest point (Barbeau Peak) and the sea level, enabling elevation-dependent analyses. And due to the surrounding Canadian Arctic Archipelago and Greenland, comparisons between these different areas are possible.

2.4 Subsets

During the research, the data and phenomena were analysed in three different subsets: the whole area (WA) of the available imagery, the Canadian Arctic Archipelago (CA), and adjacent Greenland (GL). Table 2.1 below and figure 2.3 on the next page give an overview of the subset regions.

Table 2.1: Overview of the three different subset regions.

Region	Abbr.	Area	Rel.
Whole Area	WA	442 156 km^2	100 %
Canadian Arctic Archipelago	CA	282 881 km^2	64 %
Greenland	GL	159 275 km^2	36 %

Additionally, five different elevation bands (E05 to E25) were used for the analysis. Table 2.2 below provides an overview. Since the elevation bands are rather chaotic when displayed graphically, no image was produced. Figure 3.5 on page 14, showing the DEMs can, however, give an idea of the elevation distribution.

Table 2.2: Overview of the five different elevation bands.

Elevation Band	Abbr.	Area	Rel.
0 - 499m	E05	189 096 km^2	43 %
500 - 999m	E10	119 609 km^2	27 %
1000 - 1499m	E15	83 444 km^2	19 %
1500 - 1999m	E20	46 263 km^2	10 %
2000 - 2533m	E25	2262 km^2	1 %

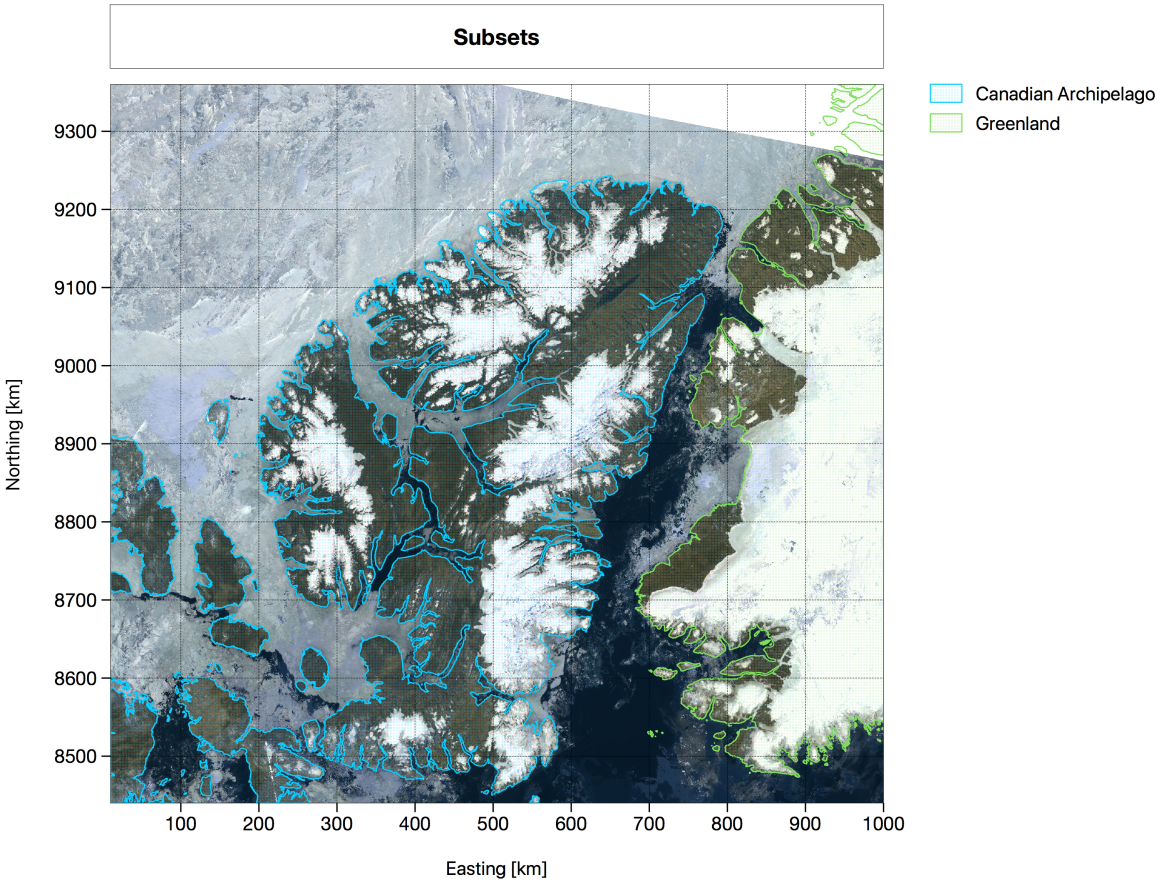

Figure 2.3: The Canadian Arctic Archipelago (CA) and Greenland (GL) as two subsets, which together make the whole area (WA). Background: MODIS 10d composite RGB image, 21 July - 31 July 2017.

3 Data

This chapter provides a description of the data used for the research. First, the optical and the Synthetic Aperture Radar (SAR) satellite data are described, followed by a description of different auxiliary data, such as digital elevation models and weather data.

3.1 Optical Imagery

The optical data used in the thesis were acquired by the Moderate Resolution Imaging Spectro-Radiometer (MODIS) sensor.

3.1.1 MODIS

The MODIS sensor takes measurements onboard the Aqua and Terra satellites. Terra was launched in 1999, Aqua followed in 2002. Both satellites have a sun-synchronous orbit at an altitude of 705 km. The swath has a size of 2330 km cross-track and 10 km along-track. The revisit time is one to two days. This allows a new complete image of the Earth roughly every two days. MODIS has 36 bands (0.4 µm to 14.4 µm) with spatial resolutions of 250 m to 1000 m. The first MODIS images were acquired in March 2000 and data are available until today.

For more information on MODIS, see for example Salomonson et al. (1989).

3.1.2 CCRS MODIS Data

The Level 3 MODIS data used in the thesis were processed by the Canadian Centre for Remote Sensing (CCRS), see Trishchenko (2017). Data are available for the years 2000 - 2017. Three original Level 1B products were used for the generation of the final product:

- MOD02QKM: Level 1B 250 m swath data, 5-min granules
- MOD02HKM: Level 1B 500 m swath data, 5-min granules
- MOD03-Level 1 Geolocation information: 1 km swath data, 5-min granules

The data were composited in 10-day intervals, making for 36 10-day Canada-wide, clear-sky, cloud-free and shadow-free images. Table 3.1 below shows the available bands in the visible (VIS), near infrared (NIR) and short-wave infrared (SWIR) portion of the electromagnetic spectrum.

Table 3.1: MODIS bands available in the CCRS product (Trishchenko, 2017).

Band	Spatial resolution	Bandwith	Band name
1	250 m	0.620 - 0.670 µm	VIS (Red)
2	250 m	0.841 - 0.876 µm	NIR
3	500 m	0.459 - 0.479 µm	VIS (Blue)
4	500 m	0.545 - 0.565 µm	VIS (Green)
5	500 m	1.230 - 1.250 µm	NIR
6	500 m	1.628 - 1.652 µm	SWIR
7	500 m	2.105 - 2.155 µm	SWIR

In order to make the data comparable to the SAR data (see following chapter), the Universal Transverse Mercator (UTM) projection 17N (EPSG code: 26917) at a spatial resolution of 400 m was used. Figure 3.1 below provides an example.

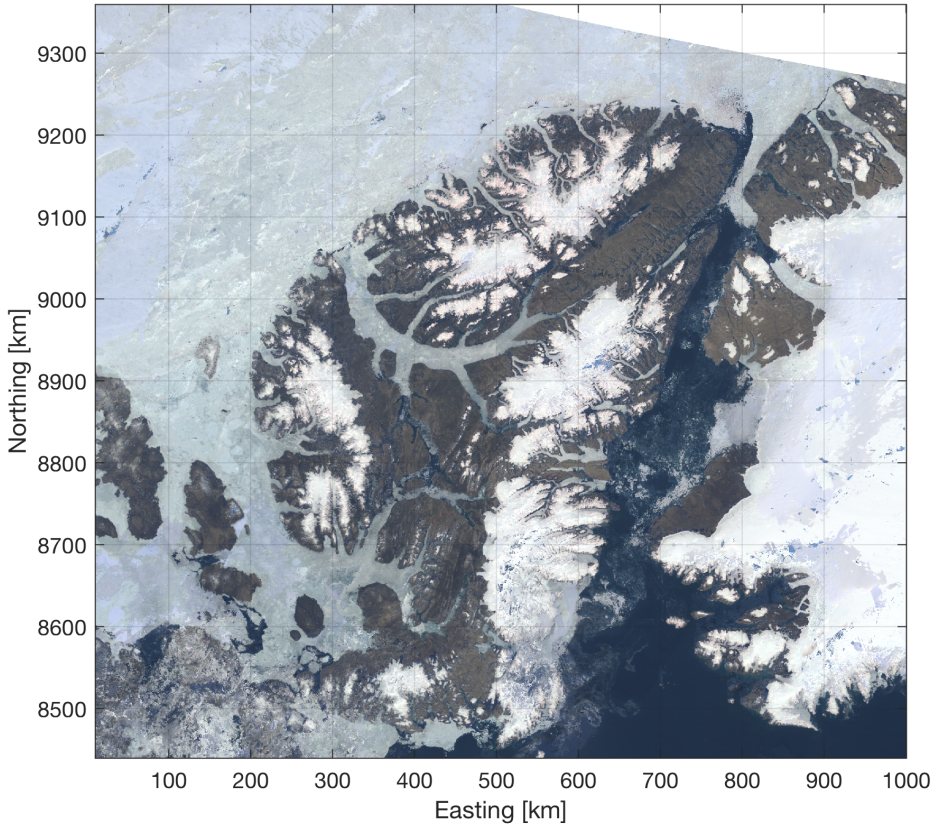

Figure 3.1: An example Moderate Resolution Imaging Spectro-Radiometer (MODIS) RGB image based on a 10-day composite between 21 July and 31 July 2017.

3.2 SAR Imagery

The Synthetic Aperture Radar (SAR) data used in the thesis originated from two different platforms: Sentinel-1A/B and RADARSAT-2.

3.2.1 Sentinel-1A/B

Sentinel-1A and Sentinel-1B are a pair of polar orbiting SAR satellites. Sentinel-1A was launched in 2014 and Sentinel-1B in 2015. They have a sun-synchronous orbit at an altitude of 693 km. The sensor onboard the two satellites is a C-band SAR with a centre frequency of 5.405 GHz, offering acquisitions in VV, VH, HH and HV polarisations. The Sentinel-1 satellites have four different acquisition modes with spatial resolutions between 5 m and 40 m and swaths between 80 km and 400 km.

For more information on Sentinel-1A/B, see for instance European Space Agency (2012) or Torres et al. (2017).

3.2.2 RADARSAT-2

RADARSAT-2 is a polar-orbiting SAR satellite launched in 2007. It has a sun-synchronous orbit at an altitude of 798 km. The sensor onboard RADARSAT-2 is a C-band SAR with a centre frequency of 5.405 GHz, offering acquisitions in HH, HV, VV and VH polarisations. Many different acquisition modes, depending on the polarisation, are available, with swath widths between 18 km and 530 km, and spatial resolutions between 1 m and 100 m.

For more information on RADARSAT-2, see for example Livingstone et al. (2005).

3.2.3 Local Resolution Weighting

All SAR images were processed at the Remote Sensing Laboratories (RSL) of the University of Zurich to so-called local resolution weighting (LRW) images. The LRW method uses multiple radiometrically terrain corrected (RTC) backscatter images (see Small (2011)) in combination with their co-registered local illuminated areas to generate composite SAR imagery (Small, 2012). By weighing each contributing image by the local resolution, a higher level SAR product with a better local resolution and a smaller amount of looks can be obtained. Figure 3.2 below provides an example.

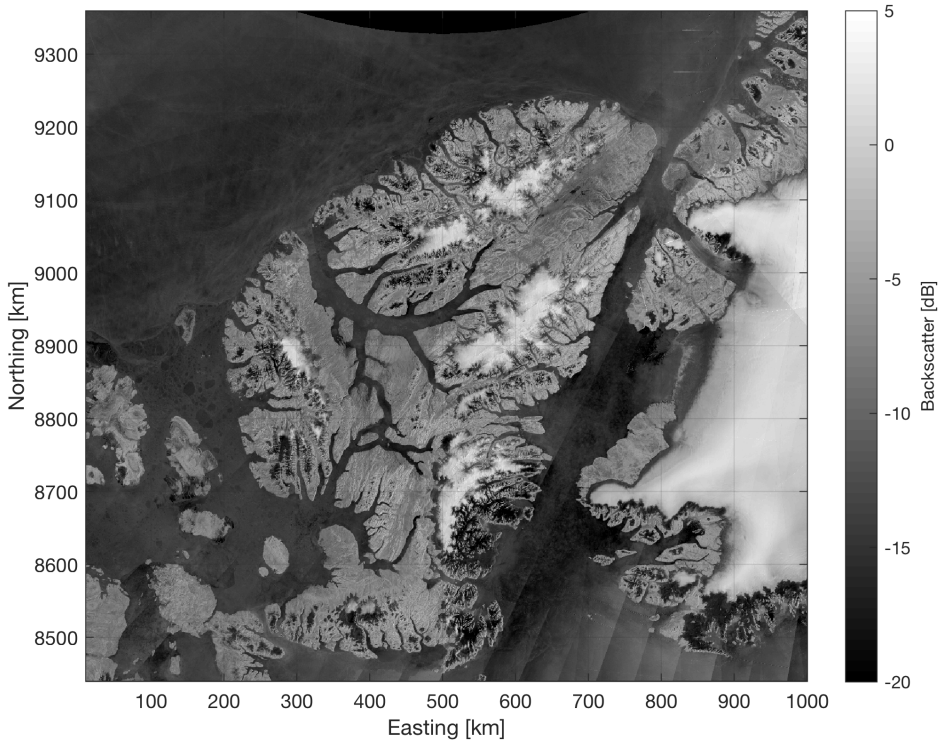

Figure 3.2: An example Sentinel-1 LRW image (HH) based on a 10-day composite between 21 July and 31 July 2017.

3.2.4 Compositing Intervals and Data Quality

The SAR data were available in different compositing intervals. Table 3.2 below gives an overview of the available data and compositing intervals.

Example composites are as follows:

- 1d composites: `20170301000000_20170301235959`, then `20170302000000_20170302235959`
- 2d composites: `20170301000000_20170302235959`, then `20170302000000_20170303235959`
- 10d composites: `20170301000000_20170310235959`, then `20170311000000_20170320235959`

For the 1d and 10d composites there was no overlap between consecutive composites; 1d composites covered exactly 24h and 10d composites cover 240h. The 2d composites, however, had an overlap of 24 hours. Each day was covered by two consecutive 48h composites — once as the first half of the composite, once as the second half of the composite.

Table 3.2: Overview of the available SAR data.

Year	Interval	Satellite(s)	Images	Date Coverage
2010	10d	RADARSAT-2	15	04/01-08/21
2015	10d	Sentinel-1	36	01/01-12/31
2016	10d	Sentinel-1	36	01/01-12/31
2017	10d	Sentinel-1	36	01/01-12/31
2017	2d	Sentinel-1	365	01/01-12/31
2017	1d	RADARSAT-2 & Sentinel-1	184	03/01-08/31

Due to the nature of composites, not every pixel of the study area was mapped on every image. The pixel coverage in table 3.3 below gives information about on how many of the images per year the area is represented. Figure 3.3a to 3.3d on the following page provide an overview of the spatial distribution of the coverage of the 10d composites, and figure 3.3e and 3.3f of the 2d and 1d composites.

Table 3.3: SAR data quality (pixel coverage) for the three subsets. WA = whole area, CA = Canadian Arctic Archipelago, GL = Greenland.

Year	Interval	WA	CA	GL
2010	10d	93.4%	99.9%	79.7%
2015	10d	91.0%	89.0%	99.1%
2016	10d	99.0%	98.8%	100.0%
2017	10d	99.9%	100.0%	99.9%
2017	2d	97.8%	97.7%	98.8%
2017	1d	93.5%	95.0%	91.8%

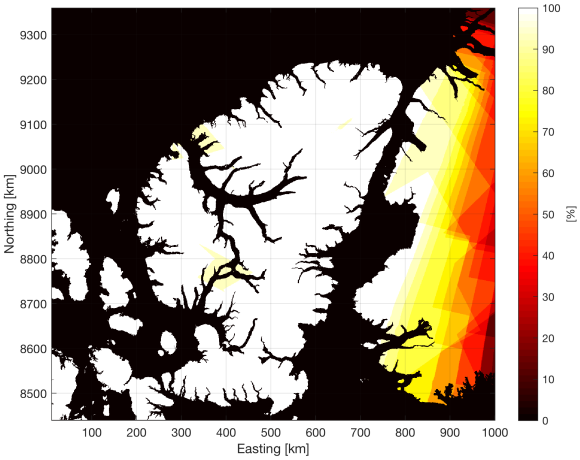

(a) 2010: 10d

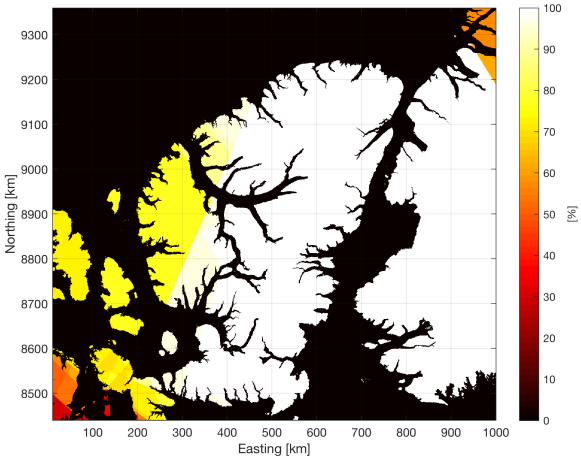

(b) 2015: 10d

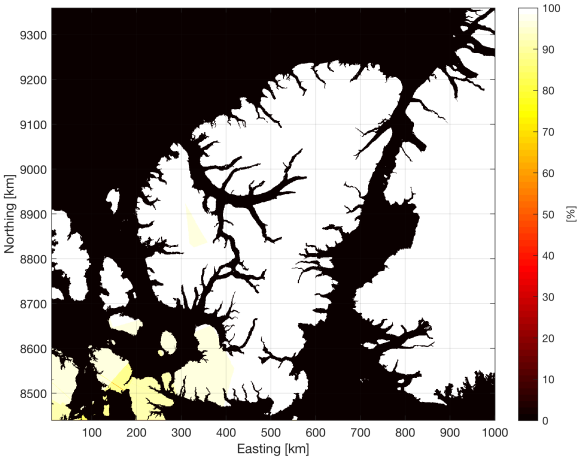

(c) 2016: 10d

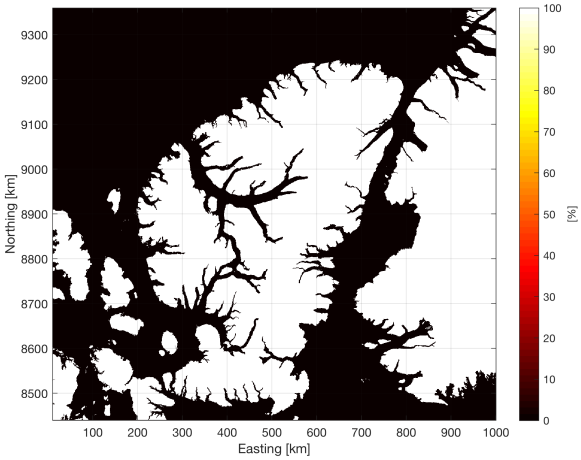

(d) 2017: 10d

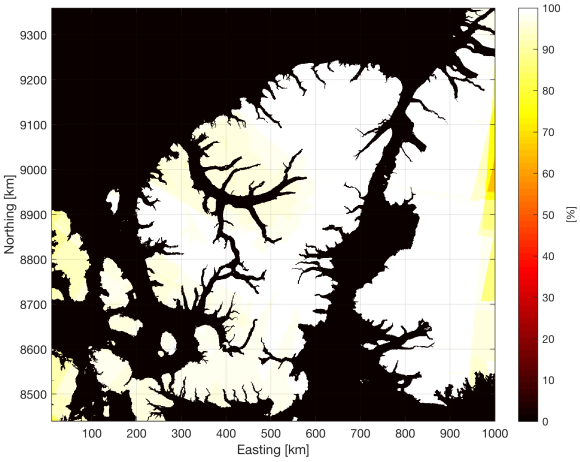

(e) 2017: 2d

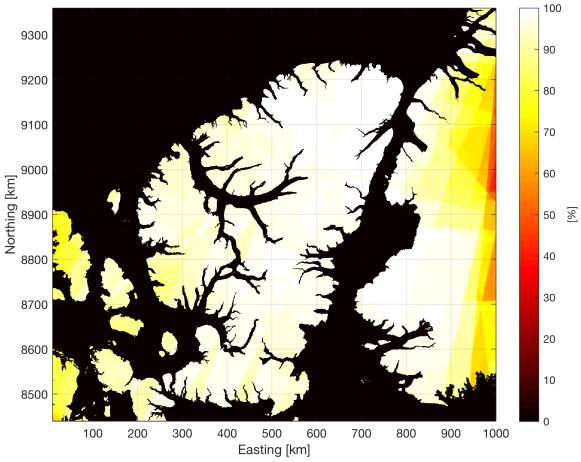

(f) 2017: 1d

Figure 3.3: Coverage of the 1d/2d/10d SAR composites.

Furthermore, it was decided to work with HH polarised data only, and to omit the HV polarised data for two reasons:

- The HV data had a lower coverage than the HH data. Figure 3.4 below provides an example.
- Thermal noise had an impact on the data quality of Sentinel-1, especially in the cross polarised channel (thus the HV channel), see e.g. Park et al. (2018).

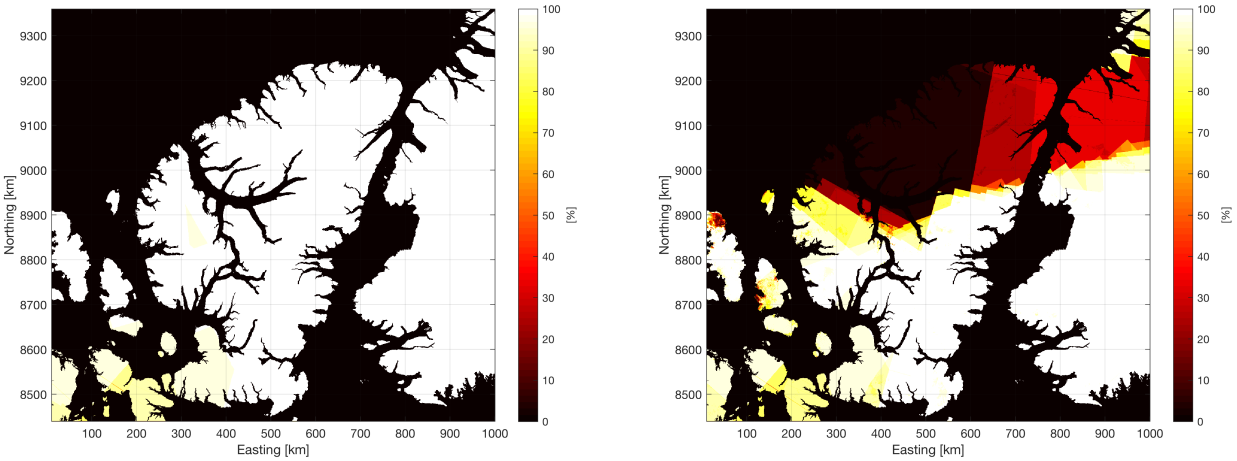

(a) HH **(b)** HV

Figure 3.4: Comparison of the coverage of the 10d Sentinel-1 composites in 2016, HH vs. HV.

3.3 Auxiliary Data

In addition to the satellite imagery, different auxiliary data were available for the thesis, such as Digital Elevation Models (DEMs) and weather data from different stations.

3.3.1 Digital Elevation Models (DEMs)

Since the area of interest of this thesis is partly in Canada and partly in Greenland, two different DEMs were necessary (see figure 3.5 on the following page).

For the Canadian part of the scene, the Canadian Digital Elevation Model (CDEM) was used. The origin of the CDEM are the Canadian Digital Elevation Data (CDED) (Natural Resources Canada, 2016). The elevation data were available at different spatial resolutions. A 90 m spatial resolution was used for the thesis. The CDEM data were, however, re-sampled to a resolution of 400 m to fit the satellite data.

For the Greenland part of the scene, the Greenland Ice Mapping Project (GIMP) DEM was used. The GIMP DEM is based on an existing low-resolution DEM of Greenland, enhanced by the integration of high-quality topography data from photogrammetry (Howat et al., 2014). The 90 m

spatial resolution version of the GIMP DEM was used for the thesis. Similar to the CDEM, the GIMP DEM was re-sampled to a spatial resolution of 400 m to fit the satellite data.

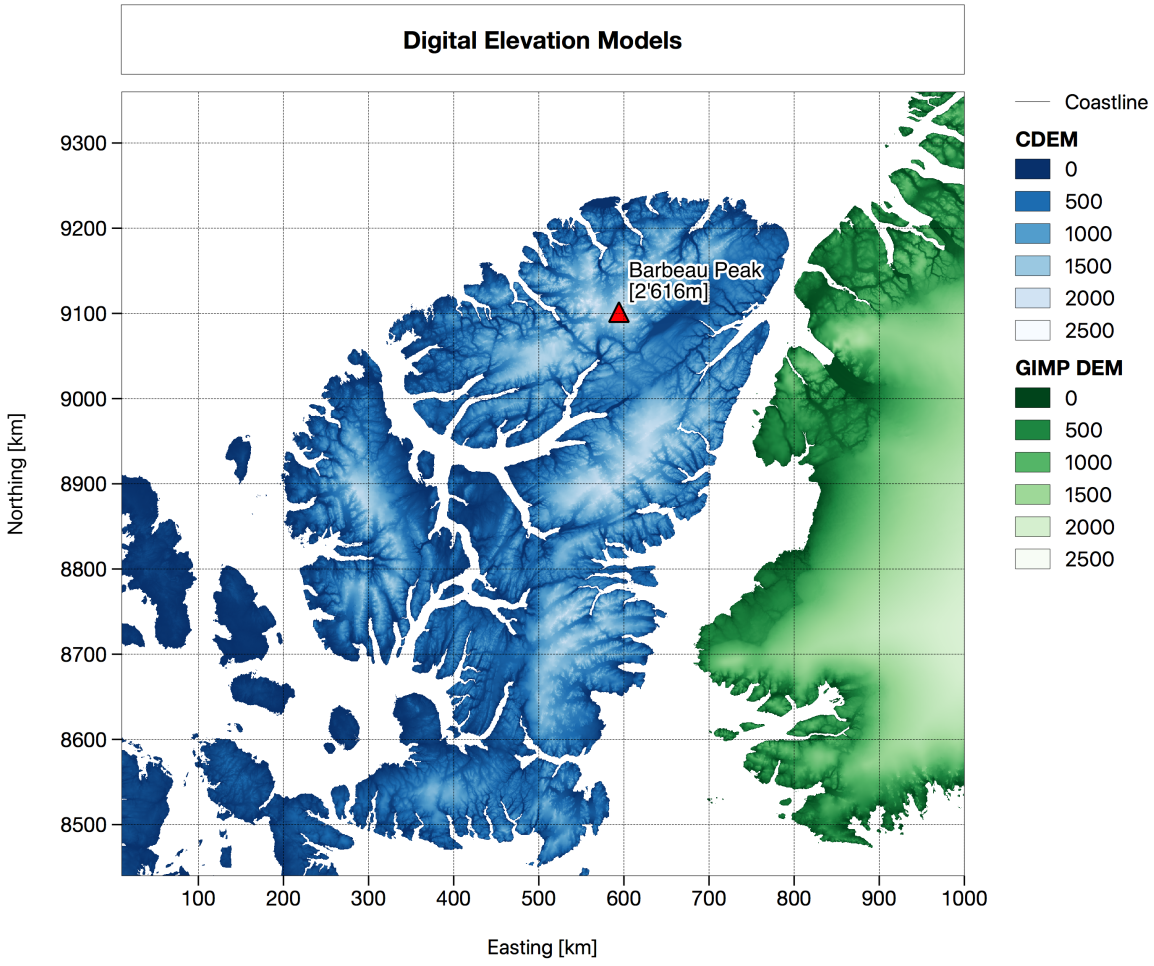

Figure 3.5: The two different Digital Elevation Models (DEMs) and Barbeau Peak on Ellesmere Island, the highest point in the Canadian Arctic Archipelago.

3.3.2 Weather Data

The weather data of five weather station were available (see figure 3.6 on the next page). Four were run by Environment Canada's Meteorological Service: Alert, Eureka, Grise Fiord and Svartevaeg. Milne Ice Shelf weather station was run by the University of Ottawa. All stations provided hourly measurements, while the stations run by Environment Canada also provided daily measurements. Table 3.4 on the following page gives an overview of the main characteristics of the weather stations, based on Environment and Climate Change Canada (2018b) and University of Ottawa (2018). The data of Milne Ice Shelf could unfortunately not be used for the research, since the data access service was not available between the first and last few weeks of the thesis.

Table 3.4: Weather stations in the Canadian Arctic Archipelago. Measurement Abbreviations: Max = Maximum Temperature, Min = Minimum Temperature, Mean = Mean Temperature, HDD = Heating Degree Days, CDD = Cooling Degree Days, TR = Total Rain, TS = Total Snow, TP = Total Precipitation, S = Snow on ground, DG = Gust Direction, SG = Gust Speed, T@1m = Temperature at 1m, T@2m = Temperature at 2m, P = Pressure, RH = Relative Humidity, SR = Solar Radiation, WS = Wind Speed, WD = Wind Direction. ** Elevation of Milne Ice Shelf Weather Station estimated from DEM.

	Lat/Lon	**Elevation**	**Measurements**	Years
Alert	82.5/-62.3	65.4 m	Daily: Max, Min, Mean, HDD, CDD, TR, TS, TP, S, DG, SG	1950 -
Eureka	79.98/-85.93	10 m	Daily: Max, Min, Mean, HDD, CDD, TR, TS, TP, S, DG, SG	1947 -
Grise Fiord	76.42/-82.9	35.1 m	Daily: Max, Min, Mean, HDD, CDD, TR, TS, TP, S, DG, SG	1984 -
Milne Ice Shelf	82.42/-81.34	769 m**	Hourly: T@1m, T@2m, P, RH, SR, S, WS, SG, WD	2008 -
Svartevaeg	81.17/-91.82	72 m	Daily: Max, Min, Mean, HDD, CDD, TR, TS, TP, S, DG, SG	2012 -

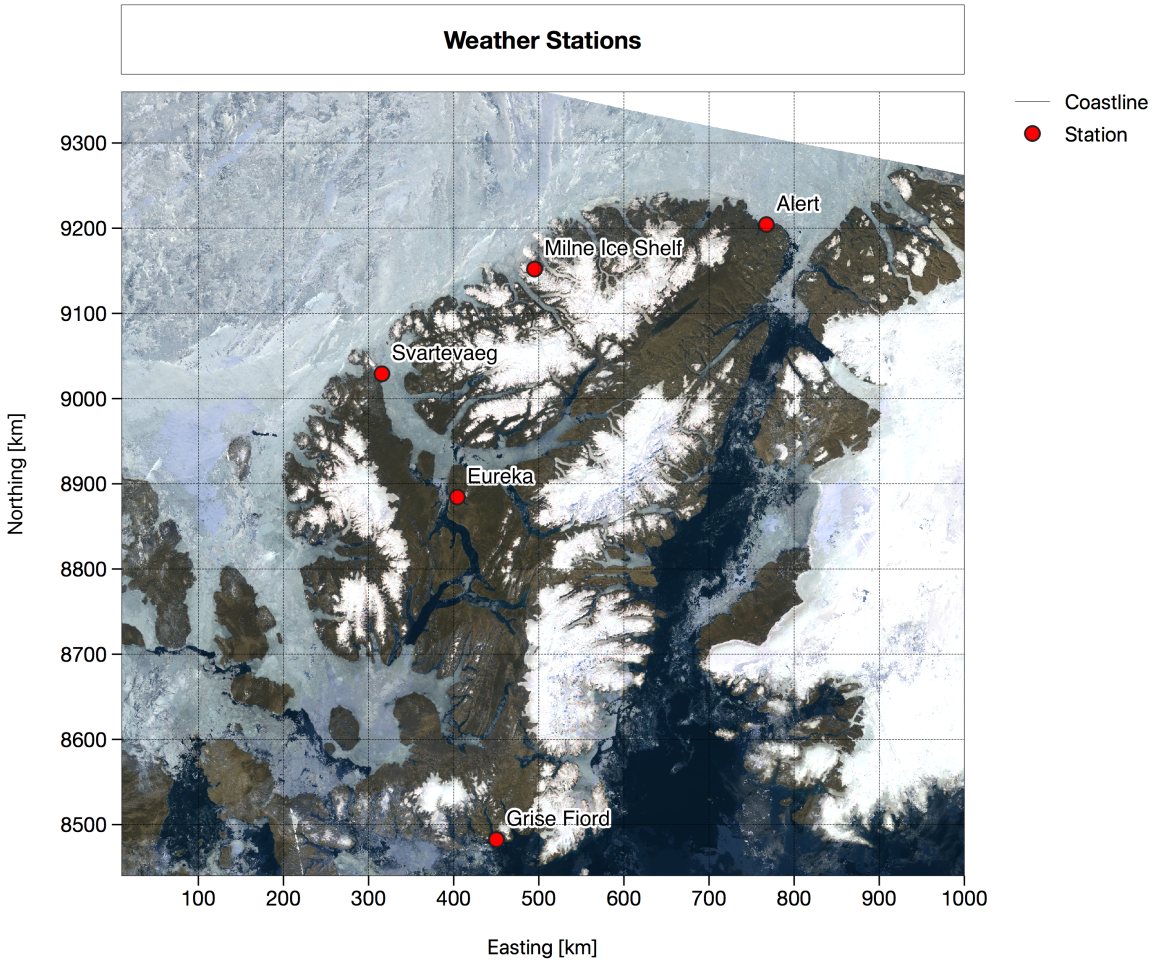

Figure 3.6: The five weather stations in the Canadian Arctic Archipelago. Background: MODIS 10d composite RGB image, 21 July - 31 July 2017.

4 Methods

The following chapter covers the methods applied during research. First, algorithms for the detection of snow/ice using optical data are introduced, followed by some examples of their application. Then, the SAR-based snow wetness detection algorithms are introduced, also followed by some examples of their application.

4.1 Snow/Ice Cover Mapping

4.1.1 Optical Properties of Snow/Ice

Due to its high albedo, snow reflects a major part of the incoming radiation in the visible wavelengths. Factors that have an impact on the amount of reflection are for example the snow impurity, the grain size or the age of the snow (Dietz et al., 2012). In longer wavelengths, however, the reflectance of snow decreases distinctly. In the NIR region, for instance, the values are close to zero, as can be seen in figure 4.1 on the next page. Snow can easily be discriminated from all land classes but not from clouds. Since the reflective behaviour of snow and clouds is quite similar in the shorter wavelengths (i.e. visible) region, it is the longer wavelengths that allow a discrimination between snow and clouds.

4.1.2 Algorithms

The Normalised Difference Snow Index (NDSI), introduced by Crane and Anderson (1984) and first applied for global snow-monitoring by Hall et al. (1995), is a normalised-difference index which makes use of the normalised difference of the reflectance in the green (R_G) and the SWIR (R_{SWIR}) portion of the electromagnetic spectrum (Hall et al., 1995):

$$\mathrm{NDSI} = \frac{R_G - R_{SWIR}}{R_G + R_{SWIR}} \tag{1}$$

Since snow has a large reflectance in the VIS and a large absorption in the SWIR and NIR portion of the electromagnetic spectrum, and clouds have a lower absorption in these portions, combining them in the NDSI allows for a good separation between snow and clouds (Hall and Riggs, 2011). This behaviour can be observed in figure 4.1 on the following page from Dietz et al. (2012), especially after 1.4 µm, where snow absorbs most of the radiative energy, while clouds still show some reflectance.

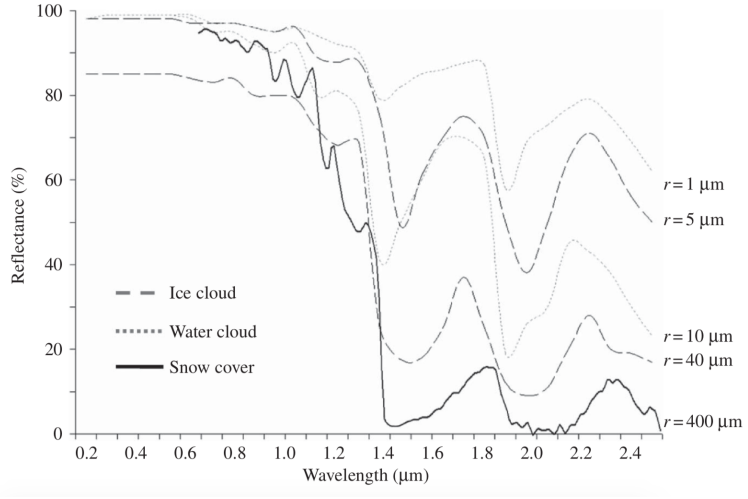

Figure 4.1: The reflectance of snow and different clouds. Figure from Dietz et al. (2012)

When the NDSI was originally applied by Hall et al. (1995), they observed that NDSI values of 0.4 or more imply the presence of snow cover. In their later work two further criteria in addition to a NDSI value of ≥ 0.4 were introduced:

- Hall et al. (1998) found that water pixels also show NDSI values ≥ 0.4. They thus added a new criterion that the reflectance in the NIR portion of the electromagnetic spectrum ($\approx 0.8\,\mu m$) must be higher than 11 % with an NDSI value ≥ 0.4 to mark a snow pixel.
- Hall et al. (2002) added another criterion: if the reflectance in the green portion of the electromagnetic spectrum ($\approx 0.55\,\mu m$) is $< 10\,\%$ the pixel should not be classified as snow, even if the other two criteria are met.

4.1.3 Application in the Literature

Besides methods to map fractional snow cover or snow water equivalent, Dietz et al. (2012) mention the NDSI as one of the most widely used algorithms to map snow cover extent. They conclude that "(...) the MODIS snow-cover product processed by the Snowmap algorithm should be preferred amongst the datasets generated from the reflective part of the spectrum." (Dietz et al., 2012, p. 4125), since it has been proven to be accurate in many studies and for many regions.

4.2 Application of the NDSI

The NDSI calculations in this work were performed using the CCRS MODIS data. The NDSI equation (equation 1 on the previous page) was adapted using MODIS band 4 (B4, 0.545 - 0.565 μm) and band 6 (B6, 1.628 - 1.652 μm):

$$\mathrm{NDSI} = \frac{\mathrm{B4} - \mathrm{B6}}{\mathrm{B4} + \mathrm{B6}} \tag{2}$$

For the two further criteria, MODIS band 4 (B4, 0.545 - 0.565 μm) and band 2 (B2, 0.841 - 0.876 μm) were used.

Using the NDSI calculations, a couple of secondary products were generated. They are described in the following sub-chapters.

4.2.1 Snow/Ice-Covered Days

For every year, the number of MODIS images with full illumination of the study site were selected (20 images per year, from 11 March until 21 September, 2300 px × 2475 px). Then for every image NDSI calculations were performed according to equation 2 on the preceding page. All pixels with values > 0.4 were classified as snow/ice, while all other pixels were classified as no-snow/ice. This resulted in 20 binary images, which were then stacked into a cube with dimensions 2300 px × 2475 px × 20 (x × y × z). In a next step, all NDSI values of a pixel (x/y) in dimension z were extracted. This resulted in a vector of length 20, which looked for example as follows:

Vector	1	1	1	0	1	1	0	0	0	0	0	0	0	0	0	0	1	1	1	1
Image No.	1	2	3	4	5	6	7	8	9	10	11	12	13	14	15	16	17	18	19	20

As a first means of analysis, a straight-forward approach of counting the number of snow/ice-covered images (NDSI = 1) was applied:

Vector	**1**	**1**	**1**	0	**1**	**1**	0	0	0	0	0	0	0	0	0	0	**1**	**1**	**1**	**1**
Image No.	1	2	3	4	5	6	7	8	9	10	11	12	13	14	15	16	17	18	19	20

For the example pixel this results in 9 snow/ice-free images. Given the fact, that the images are 10-day composites, this can roughly be converted to 90 snow/ice-covered days (SCD). Since the cut-off images (due to no available light) are between January and March and between September and December, it can be assumed that the images are snow-covered, too. So another 160 days (16 images) can be added to the results, which finally results in an amount of 250 SCD.

4.2.2 Minimum Snow/Ice-Covered Area

The minimum snow/ice-covered area (MSCA) is a widely used measure to track changes in snow cover over a certain period in time. It consists of the areas of permanent snow/ice (e.g. ice caps). The applied approach to calculate this metric was straight-forward:

1. Calculation of the NDSI for every 10d composite (see chapter 4.2.1), resulting in 20 binary images per year.
2. Determination of the lowest snow/ice cover out of these 20 images, i.e. image with the lowest number of pixels with snow/ice.
3. Conversion of pixels into area.
4. Normalisation to the land area, resulting in relative snow/ice-covered area.

4.2.3 Snow/Ice-free Season

Using the same NDSI cube and the pixel-based NDSI vectors as mentioned in chapter 4.2.1, a slightly more computationally intensive approach was developed. The length of the snow-free or ice-free season was defined as the pixel-based difference between the first and the last occurrence of

no-snow/no-ice. To determine the start and the end, certain patterns in the vector were looked for. The start of the snow/ice-free season was defined as the first occurrence of two images without snow/ice after one image with snow/ice, i.e. the pattern [1 0 0] and the end of the snow/ice-free season as the first occurrence of two images with snow after one image without snow/ice, i.e. the pattern [0 1 1].

Vector	1	1	1	0	1	**1**	**0**	**0**	0	0	0	0	0	0	0	**0**	**1**	**1**	1	1
Image No.	1	2	3	4	5	6	**7**	8	9	10	11	12	13	14	15	**16**	17	18	19	20

In the above example, this results in image 7 as the start and in image 16 as the end of the snow/ice-free season. Including these two images, this gives a length of the snow/ice-free season of 10 images. Here again, due to the 10-day composite characteristics of the images, a rough conversion to days can be made, resulting in a snow/ice-free season of 100 days.

4.2.4 Change Analysis

Since 18 years of MODIS data were available (2000-2017), the snow/ice-covered days (SCD) were further used for change analysis (mainly due to their lower computational complexity). The number of snow/ice-covered images of an exemplary pixel over a period of 18 years looked as follows in raw data or graphically in figure 4.2 on the next page:

Images	15	15	14	16	16	14	12	12	14	13	12	12	13	16	14	1	14	16
Year 20..	00	01	02	03	04	05	06	07	08	09	10	11	12	13	14	15	16	17

Since the data were not normally distributed, non-parametric methods were necessary to analyse changes. One of these methods is Kendall's Tau. Kendall's Tau measures how strong a monotonic relationship between two variables is (Heisel and Hirsch, 2002). The test is applied on the ranks of the data and takes values between -1 and 1, where a positive number means that the ranks of the two variables increase together, whereas a negative number means that while the rank of one variable increases, the rank of the other variable decreases (Crichton, 2001). According to Heisel and Hirsch (2002), Kendall's Tau can be calculated as

$$\tau = \frac{\mathrm{S}}{\mathrm{n} \cdot (\mathrm{n}-1)/2} \tag{3}$$

where the test statistic S = P – M is defined as the difference of the number of concordant pairs M (i.e. the number of times one variable increases while the other variable increases too) and the number of discordant pairs P (i.e. the number of times one variable decreases while the other increases). The calculation of Kendall's Tau for the exemplary pixel results in a value of $\tau = -0.174$.

Kendall's Tau tells whether a positive or negative correlation between two variables exists and how strong the correlation is. If information about the trend is of interest, other methods are required. One method is the ordinary least squares (OLS) method, which fits a linear slope. OLS-based methods are, however, very sensitive to outliers. The Theil-Sen approach, which works by calculating the median of the slopes between each pair of data points, is more resistant to outliers (Ohlson and Kim, 2015). For the exemplary data Sen's slope has a value of -0.0625.

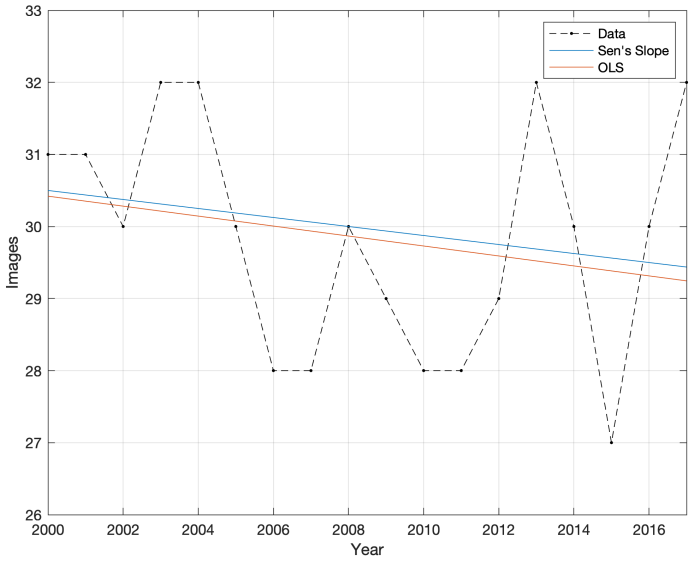

Figure 4.2: Yearly number of snow/ice-covered images with Sen's slope and OLS.

4.3 Wet Snow/Ice Detection

4.3.1 Physical Properties of Snow/Ice

C-band SAR data can only be used for mapping wet snow, because under dry conditions the ground below the snow cover dominates the backscattering signal (Dietz et al., 2012). In the case of dry snow, snow is a mixture of ice crystals and air, while in the case of wet snow, snow is a mixture of ice crystals, air and liquid water (Tiuri et al., 1984). Since the dielectric constants ϵ of liquid water and frozen water are distinctly different ($\epsilon_{\text{air}} = 1$, $\epsilon_{\text{ice}} = 3.15$, $\epsilon_{\text{water}} = 80$), the interactions of microwaves with the respective material are too (Snehmani et al., 2015). The high dielectric constant ϵ of water leads to high dielectric losses of wet snow and thus to a distinctly reduced backscattering coefficient σ_0 of wet snow, compared to dry-snow or snow-free regions (Nagler et al., 2016).

4.3.2 Algorithms

Nagler and Rott (2000) developed an algorithm which makes use of this interaction of the microwaves with the different states of snow. The algorithm is based on the pixel-based ratio (R) of the backscattering coefficient of a dry-snow or no-snow reference image (σ^0_{ref}) and the potential wet snow image to be analysed (σ^0_{ws}).

$$\text{R} = \frac{\sigma^0_{\text{ws}}}{\sigma^0_{\text{ref}}} \tag{4}$$

Applying a threshold to the ratio allows to determine whether a pixel contains wet snow or not. By signature analysis and by analysing the frequency distribution of the ratios, Nagler and Rott (2000) found a threshold (TR) of $-3\,\text{dB}$. If the ratio of a pixel is $<$ TR, the pixel contains wet snow, if

the ratio of a pixel is > TR, the pixel does not contain wet snow. In their later work, Nagler et al. (2016) revised the algorithm and found a threshold of −2 dB to be more appropriate.

4.3.3 Application in the Literature

The algorithm introduced by Nagler and Rott (2000) has been widely analysed, discussed and used in studies, see for example Solberg et al. (2004), Luojus et al. (2006) and Luojus et al. (2009). The approach has proven to be successful in monitoring snow wetness. Different studies have extended the approach, for example by altering the wet snow threshold to fit specific study areas, such as highly forested areas (e.g. Luojus et al. (2009)).

4.4 Application of the Wet Snow/Ice Algorithm

During the work for this thesis, the algorithm of Nagler et al. (2016) was applied to generate maps of the extent of wet snow, as well as to generate different secondary products. The basic procedure was based on equation 4 on the preceding page.

4.4.1 Melting Days

Similar to the NDSI calculations (see chapter 4.2.1 on page 18), the wet snow algorithm was applied image-based pixel-based. For every image, the wet snow calculations were performed according to the approach described in chapter 4.3.2 on the preceding page. All pixels with a threshold < −2 dB were classified as wet snow/ice, all other pixels were classified as no-wet snow/ice. Depending on the number of images available per year, this resulted in a binary data cube of dimensions 2300 px × 2475 px × *nn* (x × y × z) images. Then for every pixel (x/y) a vector in dimension z was extracted. This resulted in a vector of length nn, which could have looked as follows:

Value	0	0	0	0	0	0	0	0	0	0	0	0	0	0	0	0	1	1
Image No.	1	2	3	4	5	6	7	8	9	10	11	12	13	14	15	16	17	18
Value	1	1	1	1	1	1	0	0	0	0	0	0	0	0	0	0	0	0
Image No.	19	20	21	22	23	24	25	26	27	28	29	30	31	32	33	34	35	36

Here, again similar to the NDSI calculations, the first approach was rather straight-forward: counting the number of wet snow/ice pixels (value = 1).

Value	0	0	0	0	0	0	0	0	0	0	0	0	0	0	0	0	**1**	**1**
Image No.	1	2	3	4	5	6	7	8	9	10	11	12	13	14	15	16	17	18
Value	**1**	**1**	**1**	**1**	**1**	**1**	0	0	0	0	0	0	0	0	0	0	0	0
Image No.	19	20	21	22	23	24	25	26	27	28	29	30	31	32	33	34	35	36

In this example, this results in 8 wet snow/ice images. Borne in mind that the images are 10-day composites, this can roughly be approximated to 80 wet snow/ice days.

4.4.2 Average Melting Intensity

Another approach is the calculation of the average melting intensity. In this approach, the raw decibel values of all pixels with wet snow/ice are considered. Since more melting leads to wetter snow and wetter snow leads to lower backscattering coefficients (Nagler and Rott, 2000), an approach considering raw decibel values should give insights into how strong the melting at certain locations was. An example pixel looked like this:

Value	-0.2	-0.3	-0.2	0.0	-0.1	-0.5	0.2	-0.1	-0.2	-0.4	-0.5	-0.4
Image No.	1	2	3	4	5	6	7	8	9	10	11	12
Value	-0.6	-0.6	-0.8	-1.0	-3.4	-5.8	-5.3	-4.1	-3.0	-4.6	-2.4	-2.1
Image No.	13	14	15	16	17	18	19	20	21	22	23	24
Value	-1.4	-1.3	-1.3	-1.3	-1.0	-0.9	-0.8	-0.6	-0.8	-1.0	-0.8	-0.5
Image No.	25	26	27	28	29	30	31	32	33	34	35	36

Then, the average of all values $< -2\,\mathrm{dB}$ (pixels with wet snow/ice) was calculated:

Value	-0.2	-0.3	-0.2	0.0	-0.1	-0.5	0.2	-0.1	-0.2	-0.4	-0.5	-0.4
Image No.	1	2	3	4	5	6	7	8	9	10	11	12
Value	-0.6	-0.6	-0.8	-1.0	**-3.4**	**-5.8**	**-5.3**	**-4.1**	**-3.0**	**-4.6**	**-2.4**	**-2.1**
Image No.	13	14	15	16	17	18	19	20	21	22	23	24
Value	-1.4	-1.3	-1.3	-1.3	-1.0	-0.9	-0.8	-0.6	-0.8	-1.0	-0.8	-0.5
Image No.	25	26	27	28	29	30	31	32	33	34	35	36

$$\frac{-(3.4 + 5.8 + 5.3 + 4.1 + 3.0 + 4.6 + 2.4 + 2.1)\,\mathrm{dB}}{8} = -3.8\,\mathrm{dB}$$

In this example, this results in an average melting intensity of $-3.8\,\mathrm{dB}$.

4.4.3 Radar Composites

The different SAR compositing intervals were described in chapter 3.2.4 on page 11. Each image set had to be treated individually:

- The 1d composites could be processed as they were — they covered exactly 24 hours and thus described the relevant processes of one day.
- The 2d composites, however, had an overlap of 24 hours. To deal with this overlap, only every second 2d composite was used. In this way they described the processes of two days. By a multiplication by factor two, the processes could be broken down into one day.
- The 10d composites covered exactly 240 hours without overlap between consecutive composites. By a multiplication by factor ten, the processes represented one day.

4.5 Vegetation Detection

For the detection of possible vegetation signals, the Normalised Difference Vegetation Index (NDVI) was used. The NDVI is another normalised-difference index (similar to the NDSI) and was first introduced by Rouse et al. (1973). The index makes use of the normalised difference of the reflectance in the NIR (R_{NIR}) and the red (R_R) portion of the electromagnetic spectrum:

$$\mathrm{NDVI} = \frac{R_{NIR} - R_R}{R_{NIR} + R_R} \tag{5}$$

NDVI values range from -1 to 1, while vegetation usually shows values of 0.2 or more (Esau et al., 2016). Every pixel with an NDVI larger than 0.2 was thus defined as vegetation.

The vegetation data were further analysed using the same change analysis technique as for the snow/ice-covered days (SCD), see chapter 4.2.4 on page 19.

5 Results

The first part of the results chapter covers the calculations based on the optical imagery. Insights into the number of snow/ice-covered days (SCD) as well as the minimum snow/ice-covered area (MSCA) through 18 years of observations are presented, followed by an analysis of the changes that occurred. The second part covers reults derived from the SAR data, such as the number of melting days and the average melting intensity, including comparisons between different compositing intervals in 2017. In the third part, NDVI-based results are presented, giving insights into the presence of vegetation as well as its change over time. Then, the relation between optical data-based NDSI measurements and SAR data-based backscatter measurements is explained. Finally, as a topic of special interest, an analysis of the Lake Hazen ice cover during the 18 years of observations is presented.

5.1 Snow and Ice Cover

5.1.1 Snow/Ice-Covered Days

The number of snow/ice-covered days (SCD) was calculated as described in chapter 4.2.1 on page 18 for the subsets described in chapter 2.4 on page 6, based on the 10d MODIS composites. The results can be seen in table 5.1 and figure 5.1 on the next page. The results were masked to the area of non-permanent snow cover within the respective regions.

For the whole area (WA), the average number of SCD ranged from 271 in 2012 to 309 in 2013 (15 days below and 23 days above the average). In the Canadian Arctic Archipelago (CA), 2012 and 2013 were the years with the smallest and largest number of SCD, with 273 days in 2012 (16 days below average) and 313 days in 2013 (24 days above average). And for Greenland (GL), the lowest number of SCD occurred in 2012 with 264 days (16 days below average), while the largest number of snow/ice-covered was measured in 2017 with 300 days (20 days above average).

Hence, in all three regions the year 2012 showed the lowest average number of SCD, while the following year 2013 showed the highest average number, except for Greenland, where the maximum was observed in 2017. Generally, the record high year had a higher deviation from the 18-year average than the record low year.

Table 5.1: Average number of snow/ice-covered days (SCD), based on 10d MODIS NDSI calculations, for different locations. WA = Whole Area, CA = Canadian Arctic Archipelago, GL = Greenland.

	WA	CA	GL
2000	295	298	287
2001	287	290	275
2002	280	282	275
2003	286	292	268
2004	293	296	285
2005	282	283	283
2006	291	292	290
2007	282	282	280
2008	280	284	272
2009	284	285	282
2010	281	283	274
2011	279	280	277
2012	**271**	**273**	**264**
2013	**309**	**313**	296
2014	288	292	277
2015	274	277	266
2016	288	291	280
2017	304	305	**300**
Mean	286	289	280

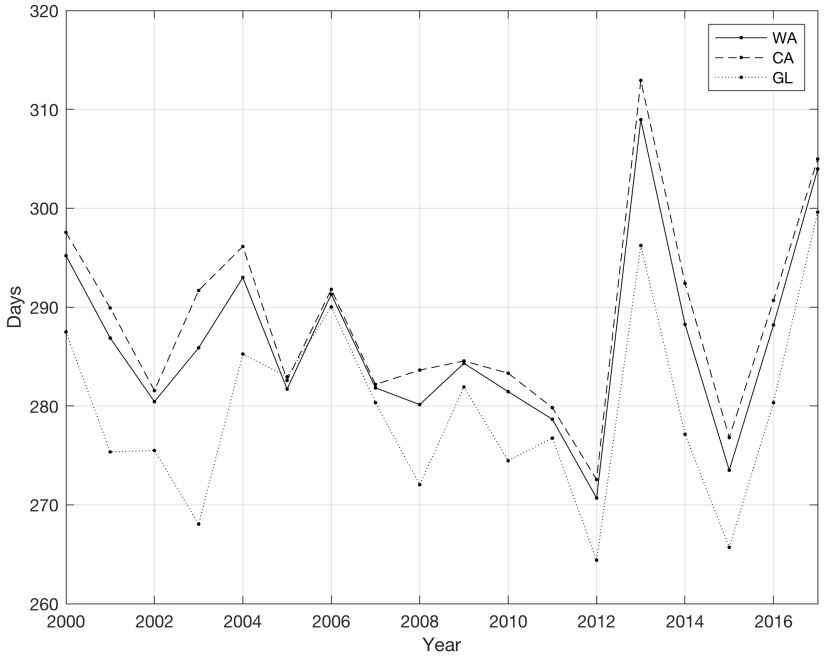

Figure 5.1: Average number of snow/ice-covered days (SCD), based on 10d MODIS NDSI calculations, for different locations. WA = Whole Area, CA = Canadian Arctic Archipelago, GL = Greenland.

In addition to the regional subsets, different elevation bands (described in chapter 2.4 on page 6) were analysed, see table 5.2 on the next page and figure 5.2 on page 27: E05 (0-499m), E10 (500-999m) and E15 (1000-1499m). Two further elevation bands, E20 (1500-1999m) and E25 (2000-2533m) were almost completely covered by permanent snow. Since the data were masked to the area of non-permanent snow cover, they were left out.

In the first and second elevation band (E05 and E10), the smallest average number of SCD was observed in 2012 with a value of 269 and 274 (15 days and 16 days below the 18-year average), while the largest number of days was observed in 2013 (306 and 314 respectively, 22 days and 24 above average). In the highest elevation band (E15), the smallest number of days was observed in 2001 with 297 days (22 days below average) and the largest in 2004 with 344 days (25 days above average).

Hence, E05 and E10 behaved similar to the subset regions, with the record years 2012 and 2013. E15, however, had different record years. Here again, the deviation from the 18-year average was larger for the record high year than the record low year.

Table 5.2: Average number of snow/ice-covered days (SCD), based on 10d MODIS NDSI calculations, for different elevation bands. E05 = 0 - 499m, E10 = 500 - 999m, E15 = 1000 - 1499m.

	E05	E10	E15
2000	293	298	335
2001	285	286	**297**
2002	279	284	340
2003	283	289	338
2004	290	295	**344**
2005	280	287	309
2006	288	302	319
2007	280	287	308
2008	277	285	308
2009	282	288	307
2010	279	288	312
2011	277	283	306
2012	**269**	**274**	302
2013	**306**	**314**	330
2014	286	290	341
2015	272	279	303
2016	285	292	311
2017	301	307	325
Mean	284	290	319

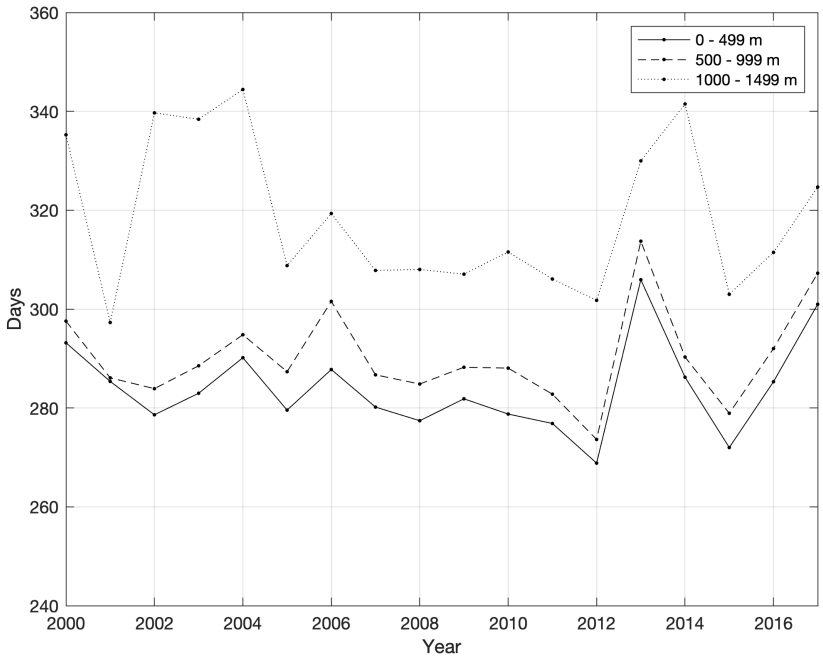

Figure 5.2: Average number of snow/ice-covered days (SCD), based on 10d MODIS NDSI calculations, for different elevation bands. E05 = 0 - 499m, E10 = 500 - 999m, E15 = 1000 - 1499m.

5.1.2 Minimum Snow/Ice-Covered Area

The minimum snow/ice-covered area (MSCA) was calculated as described in chapter 4.2.2 on page 18 for the three regions of interest described in chapter 2.4 on page 6, again using the 10d MODIS composites. Table 5.3 and figure 5.3 on the next page provide insights into the results.

For the whole area, the MSCA varied between 45.4 % in 2011 and 51.1 % in 2013, 2.6 % below and 3.1 % above the average MSCA of all 18 years. In the Canadian Arctic Archipelago the MSCA reached from 31.5 % in 2011 to 39.2 % in 2013, which meant a deviation from the average MSCA of 3.4 % and 4.3 %. In comparison to the Canadian part, Greenland had a MSCA of 69 % in 2004 and 72.3 % in 2013 — 2.0 % below and 1.3 % above the average.

Hence, in all three regions 2013 showed the largest extent of the MSCA. In the whole area and the Canadian Arctic Archipelago, the smallest extent occurred in 2011 and in Greenland in 2004. The deviation from the 18-year average was larger for the record high year than for the record low year, except for Greenland, where the record low year was stronger than the record high year.

Table 5.3: The minimum snow/ice-covered area (MSCA) in %, relative to the total land area of the respective region, based on 10d MODIS NDSI calculations. WA = Whole Area, CA = Canadian Arctic Archipelago, GL = Greenland.

	WA	CA	GL
2000	48.5	34.4	72.1
2001	49.1	36.4	71.5
2002	48.9	36.0	71.8
2003	47.9	34.7	71.0
2004	48.5	37.0	**69.0**
2005	48.6	35.5	72.0
2006	49.5	36.8	72.1
2007	48.2	35.0	71.7
2008	46.8	33.3	70.7
2009	47.3	34.0	71.0
2010	47.5	34.1	70.8
2011	**45.4**	**31.5**	70.0
2012	45.8	32.0	70.2
2013	**51.1**	**39.2**	**72.3**
2014	48.3	35.3	71.1
2015	46.7	33.2	70.3
2016	46.4	32.8	70.6
2017	48.9	36.7	70.6
Mean	48.0	34.9	71.0

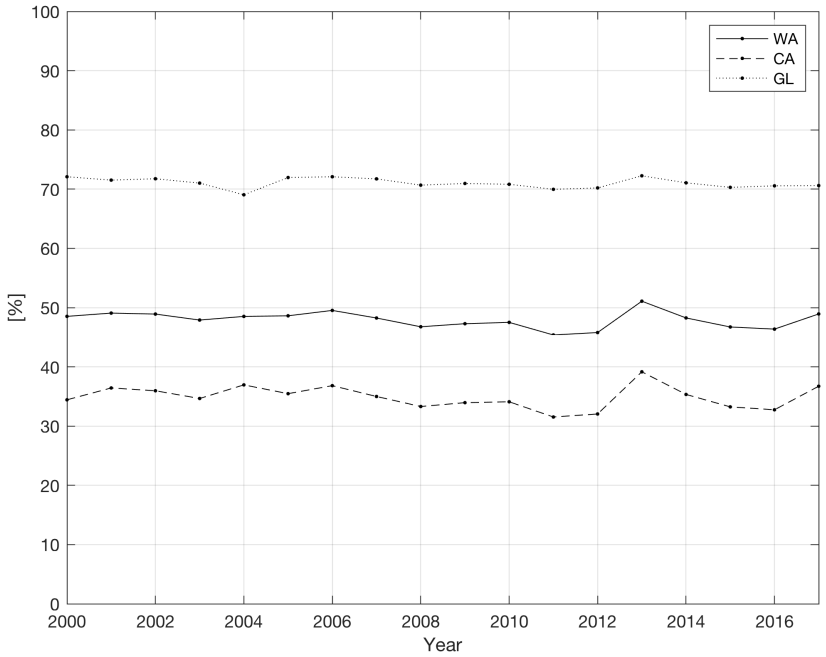

Figure 5.3: The minimum snow/ice-covered area (MSCA) in %, relative to the total land area of the respective region, based on 10d MODIS NDSI calculations. WA = Whole Area, CA = Canadian Arctic Archipelago, GL = Greenland.

The minimum snow/ice-covered area (MSCA) was also analysed in each elevation band. Here, the two highest elevation bands were left out, since they were almost completely snow-covered. The results can be seen in table 5.4 on the following page and in figure 5.4 on page 30.

In elevation bands 0 m to 499 m and 500 m to 999 m, the smallest MSCA was observed in 2011 with 11.6 % and 42.5 % respectively, which was 2.5 % and 4.3 % below the respective 18-year average. The largest MSCA was observed in 2013 with values of 17.4 % and 52.5 %, 3.3 % and 5.7 % above the average. In the highest elevation band (1000 m to 1499 m), the smallest MSCA occurred in 2004 with 93.4 %, while the largest MSCA occurred in 2006 with 97.2 % — a deviation from the 18-year average of 2.4 % and 1.4 %.

Thus, similar to the number of snow/ice-covered days (SCD), the MSCA of the lower to elevation bands behaved similar to the subset regions, except for the highest elevation band. Here again, the deviation from the average MSCA was higher for the record high year than the record low year.

Table 5.4: The minimum snow/ice-covered area (MSCA) in %, relative to the total land area of the respective elevation band, based on 10d MODIS NDSI calculations. E05 = 0 - 499m, E10 = 500 - 999m, E15 = 1000 - 1499m.

	E05	E10	E15
2000	14.4	48.1	95.3
2001	16.0	47.8	96.3
2002	14.6	48.4	96.7
2003	14.1	46.4	96.2
2004	15.2	47.6	**93.4**
2005	14.3	48.6	96.8
2006	15.4	49.9	**97.2**
2007	14.0	47.7	96.5
2008	12.8	45.1	95.5
2009	13.3	45.9	95.9
2010	13.3	45.1	95.3
2011	**11.6**	**42.5**	94.5
2012	12.0	43.3	94.7
2013	**17.4**	**52.5**	97.1
2014	14.7	46.3	95.4
2015	12.4	44.6	95.6
2016	12.4	44.2	95.6
2017	15.4	47.5	95.5
Mean	14.1	46.8	95.8

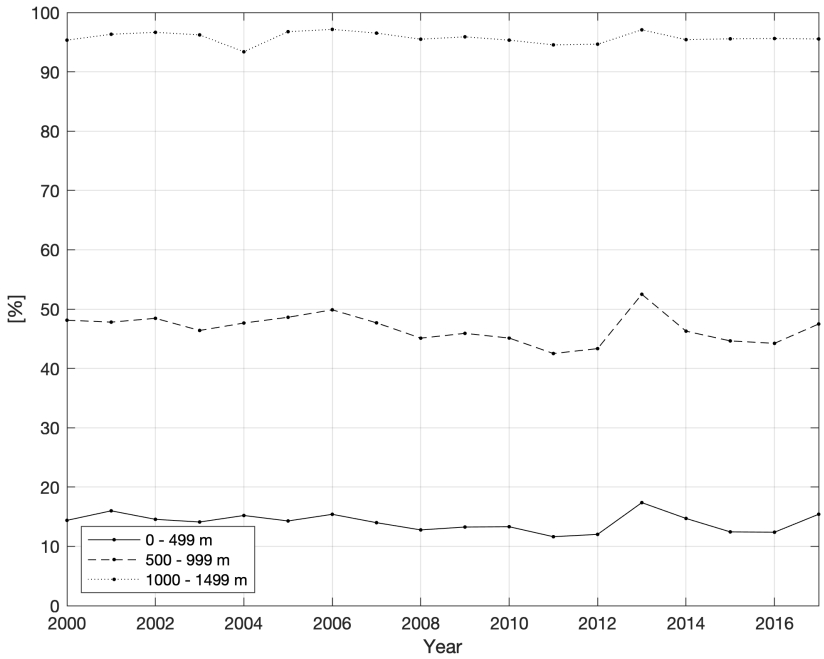

Figure 5.4: The minimum snow/ice-covered area (MSCA) in %, relative to the total land area of the respective elevation band, based on 10d MODIS NDSI calculations. E05 = 0 - 499m, E10 = 500 - 999m, E15 = 1000 - 1499m.

5.1.3 Snow/Ice-Free Season

The calculation of the snow-/ice-free season length, as described in chapter 4.2.3 on page 18, was applied for several years, using different patterns for the detection of the first and the last occurrence of snow-free pixels. The metric was, however, omitted for several reasons:

- Due to the changing nature of the weather, there might be multiple snow/ice-free periods in a year. A first melting might occur in June or July, followed by a new onset of snowfall later in the year, again followed by melting. Using the described algorithm, the occurrence of two seasons would not be detected.
- The fact, that the optical data are only available as composites over 10 days (in order to be cloud-free, see e.g. Trishchenko et al. (2016)), additionally exacerbates the above mentioned problem. If a higher temporal resolution was available, the problem could be tackled.
- No valuable gain in information compared to the number of snow/ice-covered days could be found.
- The algorithm has shown to be very computationally demanding.

Given these considerations, it was decided to leave out the snow/ice-free season as a metric.

5.1.4 Change Analysis

Change detection was applied to the snow/ice-covered days (SCD) and the minimum snow/ice-covered area (MSCA) datasets, according to chapter 4.2.4 on page 19. The results are presented in table 5.5 and figure 5.5 on the following page, and in figure 5.6 on page 32.

Table 5.5: Change analysis statistics for SCD and MSCA for the three regions of interest. SEN = Sen's Slope, τ = Kendall's Tau. WA = Whole Area, CA = Canadian Arctic Archipelago, GL = Greenland.

	SCD [d]		MSCA [%]	
	SEN	τ	SEN	τ
WA	-0.38	-0.11	-0.13	-0.28
CA	-0.20	-0.06	-0.15	-0.23
GL	0.00	-0.01	-0.08	-0.31

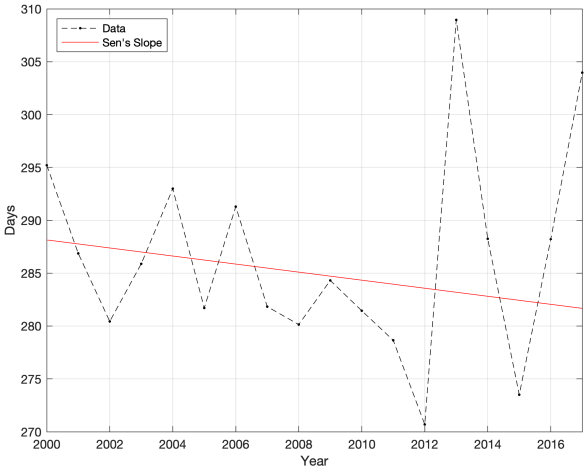

(a) Whole Area

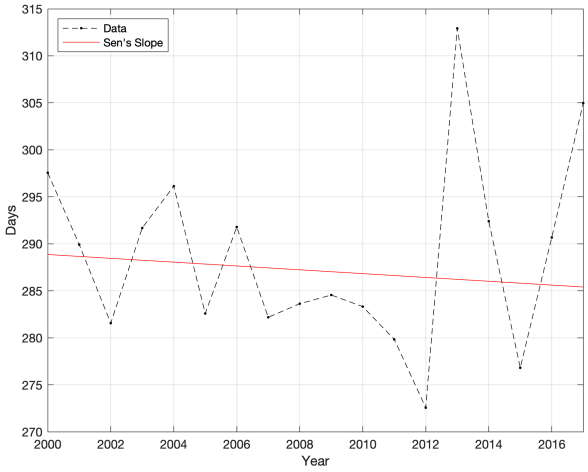

(b) Canadian Arctic Archipelago

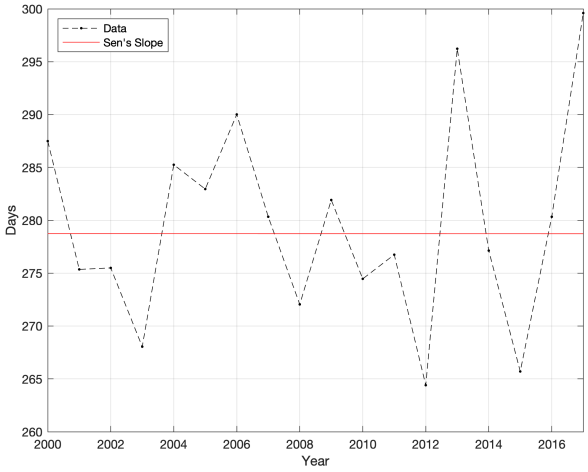

(c) Greenland

Figure 5.5: SCD, based on MODIS NDSI calculations, for different locations: change analysis (Sen's Estimator).

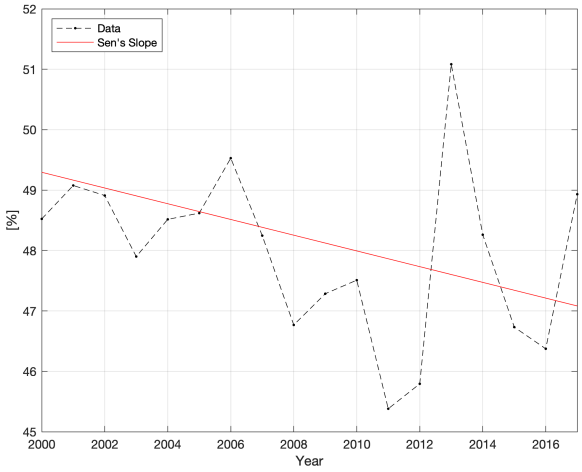

(a) Whole Area

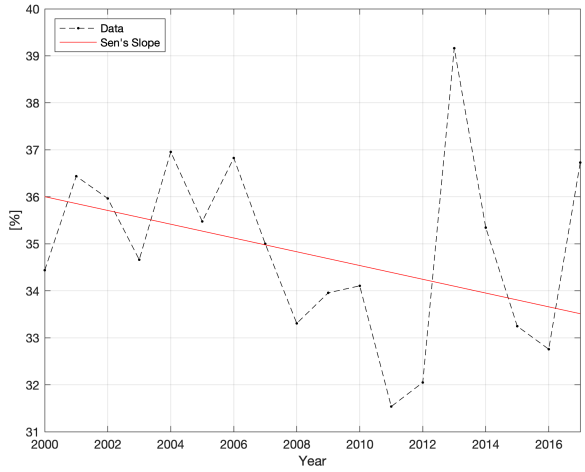

(b) Canadian Arctic Archipelago

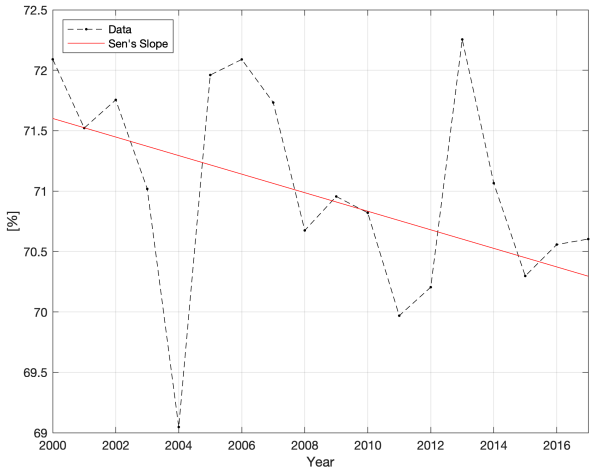

(c) Greenland

Figure 5.6: MSCA, based on MODIS NDSI calculations, for different locations: change analysis (Sen's Estimator).

For the number of SCD, the change had τ values of -0.01 to -0.11, a rather weak negative correlation. The slope of the decrease had values between -0.38 days/year for the whole area and rounded down 0 days/year for Greenland. The MSCA showed a slightly stronger negative correlation, with τ values between -0.23 and -0.31. The slope of the decrease had values between 0.15 %/year for the Canadian Arctic Archipelago and 0.08 %/year for Greenland.

In addition to the three regions of interest, the different elevation bands were analysed. The results can be seen in table 5.6 and figures 5.7 to 5.8 on pages 33–34.

Table 5.6: Change analysis statistics for SCD and MSCA for the three elevation bands. SEN = Sen's Slope, τ = Kendall's Tau. E05 = 0 - 499m, E10 = 500 - 999m, E15 = 1000 - 1499m.

	SCD [d]		MSCA [%]	
	SEN	τ	SEN	τ
E05	-0.40	-0.12	-0.13	-0.25
E10	0.15	0.02	-0.22	-0.35
E15	-0.60	-0.15	-0.05	-0.35

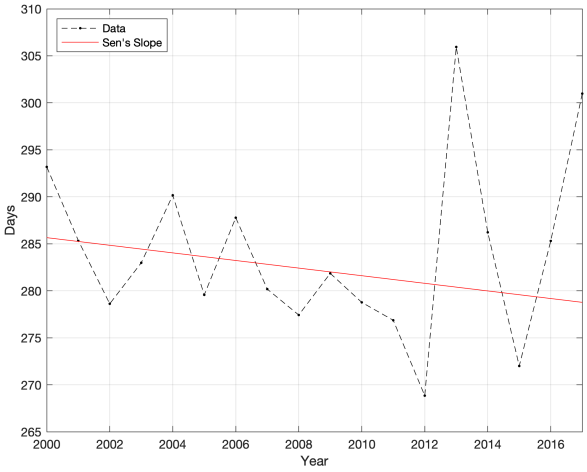

(a) 0 - 499m

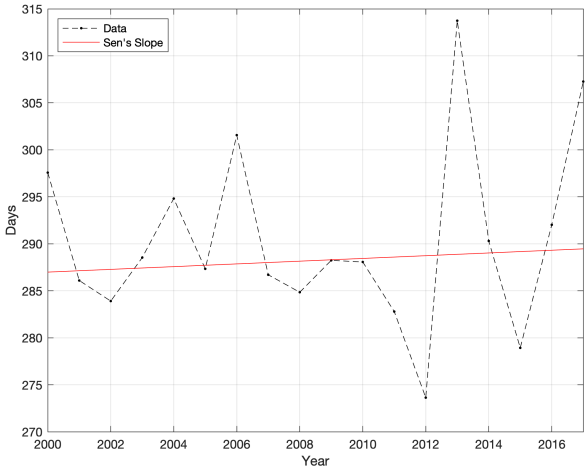

(b) 500 - 999m

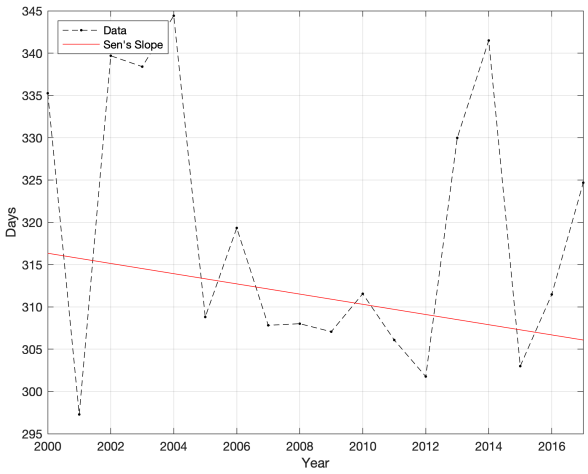

(c) 1000 - 1499m

Figure 5.7: SCD, based on MODIS NDSI calculations, for different elevation bands: change analysis (Sen's Estimator).

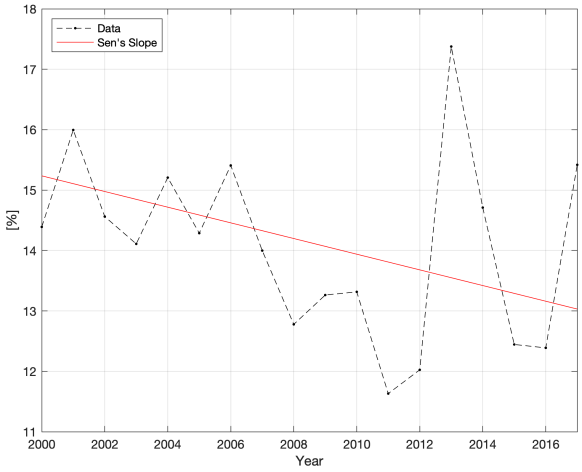

(a) 0 - 499m

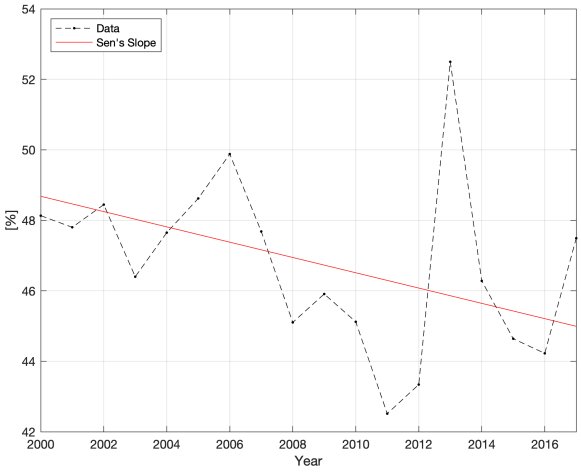

(b) 500 - 999m

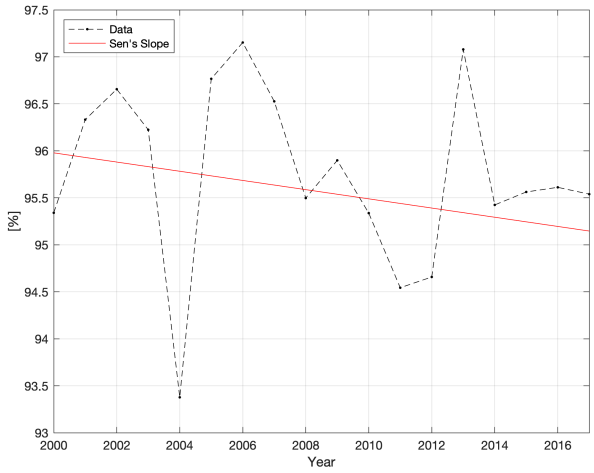

(c) 1000 - 1499m

Figure 5.8: MSCA, based on MODIS NDSI calculations, for different elevation bands: change analysis (Sen's Estimator).

The number of SCD showed a change with τ values of -0.12 in the lowest elevation band and -0.15 in the highest elevation band, implying rather weak negative correlations. They led to an average decrease in SCD of -0.40 days/year in the lowest elevation band and average decrease of -0.60 days/year in the highest elevation band. The middle elevation band had a τ value of 0.02, implying a weak positive correlation with an increase of 0.15 days/year.

The MSCA generally showed larger τ values and thus stronger correlations. In the lowest elevation band, a τ value of -0.25 indicated a decrease in MSCA of -0.13 %/year. The middle elevation band showed a τ value of -0.35 with a decrease in MSCA of -0.22 %/year. And the highest elevation band also showed a τ value of -0.35 and a decrease in MSCA of -0.05 %/year.

5.2 Melting

5.2.1 Melting Days

The number of melting days (MD) per year was calculated according to a modified version of the algorithm of Nagler et al. (2016), see chapter 4.3.2 on page 20. The average number of MD per year for the complete landmass (i.e. permanent + non-permanent snow/ice cover), based on the 10d SAR composites, can be discerned from table 5.7a and figure 5.9a.

In 2010, the region-based average number of MD varied between 24.4 days in the Canadian Arctic Archipelago and 25.3 days in Greenland. In 2015, the span was slightly larger, with 19.2 days in the Canadian Arctic Archipelago as the smallest value and 27.7 days in Greenland as the highest value. In 2016, Greenland showed again the highest number of MD with a value of 28.9, while the Canadian Arctic Archipelago had 18.4 MD. And in 2017, the smallest value of 15.4 days occurred in the Greenland part and the highest value of 18.9 days in the Canadian Arctic Archipelago.

In summary, Greenland showed the highest number of MD in three of four years when the complete landmass was considered, while the Canadian Arctic Archipelago showed the lowest number.

Table 5.7: Average number of melting days (MD) per year and per region, based on 10d SAR composite data (HH), for the complete landmass as well as the area of permanent snow/ice. WA = Whole Area, CA = Canadian Arctic Archipelago, GL = Greenland.

	WA	CA	GL
2010	24.7	24.4	25.3
2015	22.3	19.2	27.7
2016	22.2	18.4	28.9
2017	17.7	18.9	15.4

(a) Complete

	WA	CA	GL
2010	41.4	51.7	32.6
2015	40.0	42.2	38.2
2016	39.5	42.0	37.4
2017	23.9	29.0	19.2

(b) Permanent

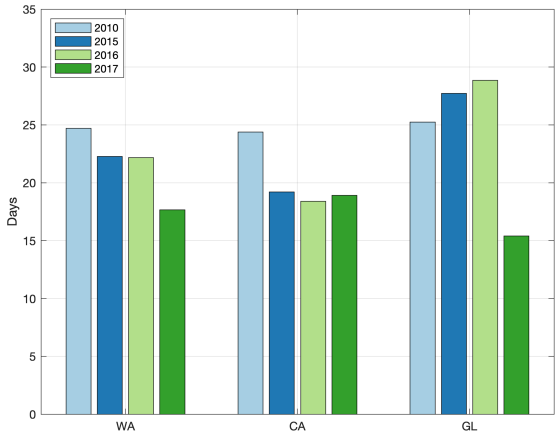

(a) Complete

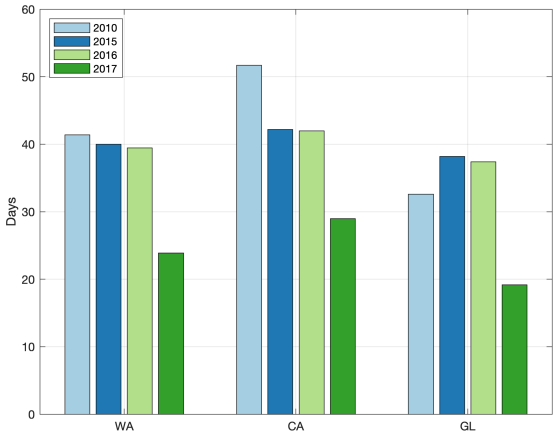

(b) Permanent

Figure 5.9: Average number of melting days (MD) per year and per region, based on 10d SAR composite data (HH), for the complete landmass as well as the area of permanent snow/ice. WA = Whole Area, CA = Canadian Arctic Archipelago, GL = Greenland.

Masked to the area of permanent snow/ice cover (obtained from the minimum snow/ice-covered area (MSCA) calculations), the results appeared slightly different, as can be seen in table 5.7b and figure 5.9b on the preceding page.

In 2010, the region-based average number of MD varied between 32.6 days (+ 7.3 days, compared to the non-masked calculation) in Greenland and 51.7 days (+ 27.3 days) in the Canadian Arctic Archipelago. The variation was smaller in 2015, similar to the results for the whole land mass. The smallest number of MD was observed in Greenland with 38.2 days (+ 10.5 days), while the highest number was observed on the Canadian Arctic Archipelago with 42.2 days (+ 23.0 days). In 2016, Greenland showed the smallest number of MD with a value of 37.4 days (+ 8.5 days) and the Canadian Arctic Archipelago showed the largest number (42.0 days, + 23.6 days). The smallest values were observed in 2017, with a minimum of 19.2 days for Greenland (+ 3.7 days) and a maximum of 29.0 days (+ 10.1 days) for the Canadian Arctic Archipelago.

The masking to the area of permanent snow/ice led to an increase in the number of MD. In 2010 the average increase was 18.7 days, in 2015 it was 17.9 days, in 2016 it was 17.5 days and in 2017 it was 7.9 days. Furthermore, the masking shifted the highest number of melting days from Greenland to the Canadian Arctic Archipelago.

Additionally, the number of MD were analysed within the three different elevation bands (see chapter 2.4 on page 6). The results of the analysis for the complete land mass (i.e. non-permanent + permanent snow/ice) can be seen in table 5.8a and figure 5.10a on the following page.

In 2010, the highest number of MD was observed in the middle elevation band E15 with 44.9 days, while the lowest elevation band E05 showed only 13.1 MD. In 2015 and 2016, the highest number of MD was found in the E15 band again, with a value of 45.8 days and 42.5 respectively. The lowest number of MD was found in the highest elevation band E25, with 2.0 and 0.4 MD. In 2017, the values had the smallest range. The highest number of MD occurred in the elevation band E10 with 23.0 days, while the lowest was found in the highest elevation band E25 with (rounded) 0.0 days.

In summary, the largest number of melting days was observed in the elevation band from 1000 m to 1499 m and the lowest number was observed in the elevation band above 2000 m.

Table 5.8: Average number of melting days (MD) per year and per elevation band, based on 10d SAR composite data (HH), for the complete landmass as well as the area of permanent snow/ice. E05 = 0 - 499m, E10 = 500 - 999m, E15 = 1000 - 1499m, E20 = 1500 - 1999m, E25 = > 2000m.

	E05	E10	E15	E20	E25
2010	**13.1**	29.5	**44.9**	23.1	23.8
2015	11.2	23.3	**42.5**	29.4	**2.0**
2016	11.4	29.2	**44.0**	9.4	**0.4**
2017	17.2	**23.0**	20.4	1.6	**0.0**

(a) Complete

	E05	E10	E15	E20	E25
2010	35.6	**53.5**	46.2	**23.1**	23.8
2015	40.6	**44.3**	44.0	39.4	**2.0**
2016	46.4	**55.0**	45.4	9.4	**0.4**
2017	36.6	**39.7**	20.9	1.6	**0.0**

(b) Permanent

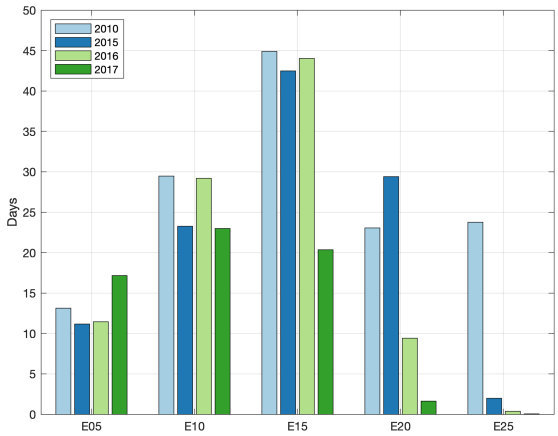

(a) Complete

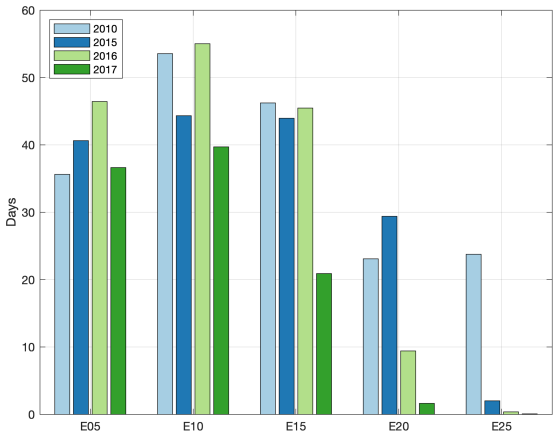

(b) Permanent

Figure 5.10: Average number of melting days (MD) per year and per elevation band, based on 10d SAR composite data (HH), for the complete landmass as well as the area of permanent snow/ice. E05 = 0 - 499m, E10 = 500 - 999m, E15 = 1000 - 1499m, E20 = 1500 - 1999m, E25 = > 2000m.

Here again, the number of MD was calculated masked to the area of permanent snow/ice cover, see table 5.8b and figure 5.10b above.

The results almost only differed in the lower three elevation bands (E05 - E15), the reason being that the upper elevation bands E20 and E25 were nearly completely covered by permanent snow/ice. In all four years, the bands E05 and E10 showed an average increase of 26.6 days and 21.9 days respectively. The biggest increase was observed for band E05 in 2016, with 35.0 more MD compared to the non-masked calculation.

In summary, the masking led to a general increase in MD in the lower three elevation bands and to a change of the elevation band with the highest number of MD from 1000 m to 1499 m to 500 m to 999 m.

5.2.2 Melting Days: Compositing Intervals

Additionally, the different available compositing intervals in 2017 (1d, 2d, 10d), were analysed and compared, see table 5.9 and figure 5.11 below.

For the whole area, the 2d composites showed the highest number of melting days (MD) with a value of 20.2 days, while the 10d composites led to the lowest value of 17.7 days. In the Canadian Arctic Archipelago, the 2d composites led to the highest value of 22.0 days, while the 10d composites led to the lowest value of 18.9 days. In the parts of Greenland covered by the imagery the 2d composites showed the highest number with 17.1 MD, while the 1d and 10d composites both led to a result of 15.4 MD.

Hence, in all three regions (WA, CA, GL) the 2d composites led to the highest number of MD, while the 10d composites led to the lowest number of MD. The range between the highest and the smallest number of MD was roughly 3 days for WA and CA and 2 days for GL.

Table 5.9: Average number of melting days (MD) in 2017 per region, based on 1d, 2d and 10d SAR composite data (HH). WA = Whole Area, CA = Canadian Arctic Archipelago, GL = Greenland.

	WA	CA	GL
10d	17.7	18.9	15.4
2d	20.2	22.0	17.1
1d	18.3	20.0	15.4
Range	2.6	3.0	1.8

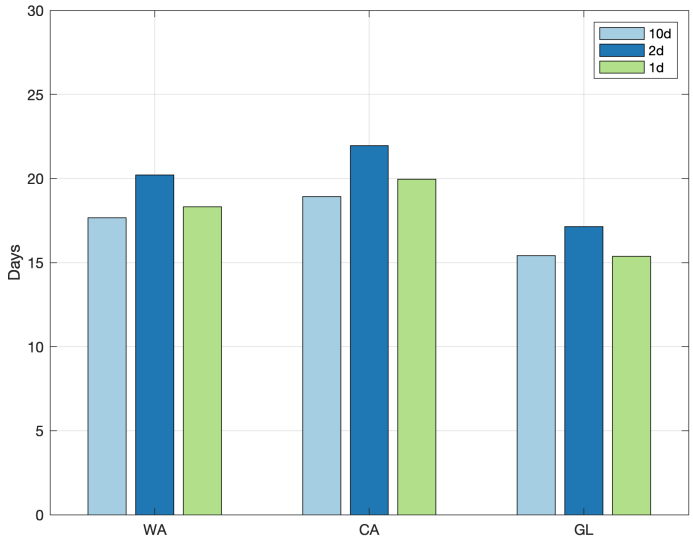

Figure 5.11: Average number of melting days (MD) in 2017 per region, based on 1d, 2d and 10d SAR composite data (HH). WA = Whole Area, CA = Canadian Arctic Archipelago, GL = Greenland.

5.2.3 Average Melting Intensity

The average melting intensity (AMI) was calculated as described in chapter 4.4.2 on page 22. The results can be seen in table 5.10a and figure 5.12a below.

Out of all four years of observation, 2015 showed the strongest AMI. In all four years, Greenland showed the strongest melting, with average values as high as −9 dB in 2015. The lowest values occurred in 2017, where all three regions showed quite similar values between −4 dB and −5 dB.

Table 5.10: The average melting intensity (AMI) in dB, based on 10d SAR composite data (HH), for the different regions and years, masked to the complete landmass and to the area of permanent snow/ice. WA = Whole Area, CA = Canadian Arctic Archipelago, GL = Greenland.

	WA	CA	GL
2010	-4.9	-4.4	-5.6
2015	-7.1	-5.6	-9.0
2016	-5.4	-4.6	-6.4
2017	-4.3	-4.1	-4.9

(a) Complete

	WA	CA	GL
2010	-6.0	-5.7	-6.3
2015	-8.6	-7.5	-9.5
2016	-6.5	-5.9	-7.0
2017	-4.9	-4.6	-5.2

(b) Permanent

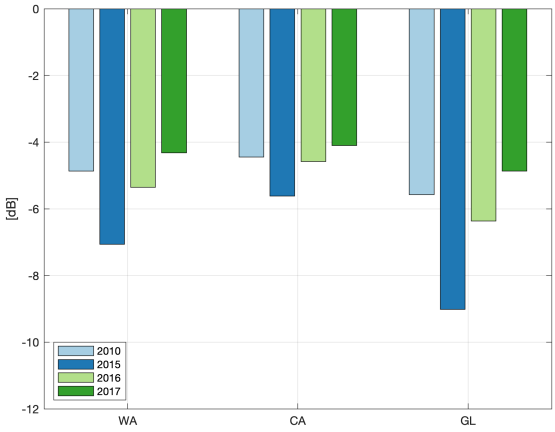

(a) Complete

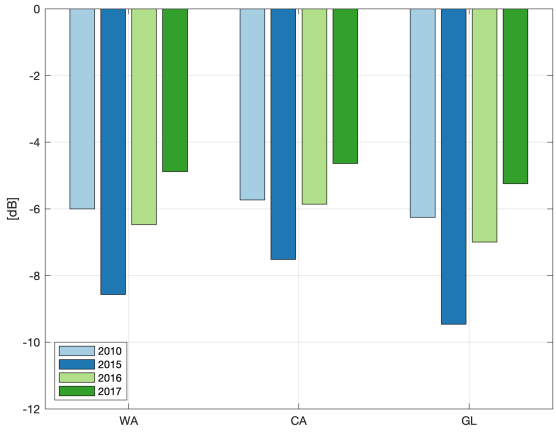

(b) Permanent

Figure 5.12: The average melting intensity (AMI) in dB, based on 10d SAR composite data (HH), for the different regions and years, masked to the complete landmass and to the area of permanent snow/ice. WA = Whole Area, CA = Canadian Arctic Archipelago, GL = Greenland.

Here again, a masking to the area of permanent snow/ice cover led to slightly different results, as can be seen in table 5.10b and figure 5.12b above.

2015 showed the highest AMI and in all four years. Greenland showed the strongest AMI, with the maximum value of −9.5 dB in 2015 (a change of 0.5 dB compared to the whole land mass). The lowest values were observed in 2017, with values roughly between −4.5 dB and −5.5 dB, which meant a strengthening of the melting of about 0.5 dB.

The masking of the AMI to the area of permanent snow/ice cover led to an amplification of

the values of about 1 dB. The distribution of the highest and lowest values remained, however, the same.

Similar to the number of melting days (MD), the AMI was also analysed on different elevation bands. The results for the complete landmass (i.e. non-permanent + permanent snow/ice cover) of the respective elevation bands can be found in table 5.11a and figure 5.13a below.

In 2010, the strongest AMI was found in band E15 with −6.5 dB, while band E25 showed the lowest AMI with −3.1 dB. In 2015, the AMI was distinctly stronger: band E15 again showed the strongest melting with −10.1 dB. The lowest AMI was found in band E05 with −3.4 dB. In 2016 the AMI was lower again. The highest value was found in E15 with −7.4 dB, while the lowest value occurred in band E25 with −2.7 dB. 2017 showed an ever smaller AMI. The highest value was found in band E10 with −4.8 dB, whereas the lowest value was found in band E25 with −2.1 dB.

In summary, band E15 from 1000 m to 1499 m usually showed the strongest AMI and band E25 above 2000 m usually showed the lowest AMI.

Table 5.11: The average melting intensity (AMI) in dB, based on 10d SAR composite data (HH), for the different elevation bands and years, masked to the complete landmass and to the area of permanent snow/ice. E05 = 0 - 499m, E10 = 500 - 999m, E15 = 1000 - 1499m, E20 = 1500 - 1999m, E25 = > 2000m.

	E05	E10	E15	E20	E25
2010	-3.7	-4.6	**-6.5**	-5.7	**-3.1**
2015	**-3.4**	-5.1	**-10.1**	-10.0	-4.9
2016	-3.6	-4.9	**-7.4**	-5.8	**-2.7**
2017	-3.9	**-4.8**	-4.7	-2.9	**-2.1**

(a) Complete

	E05	E10	E15	E20	E25
2010	-4.9	-5.8	**-6.6**	-5.7	**-3.1**
2015	**-4.5**	-6.0	**-10.3**	-10.0	-4.9
2016	-4.8	-6.0	**-7.5**	-5.8	**-2.7**
2017	-4.7	**-5.4**	-4.7	-2.9	**-2.1**

(b) Permanent

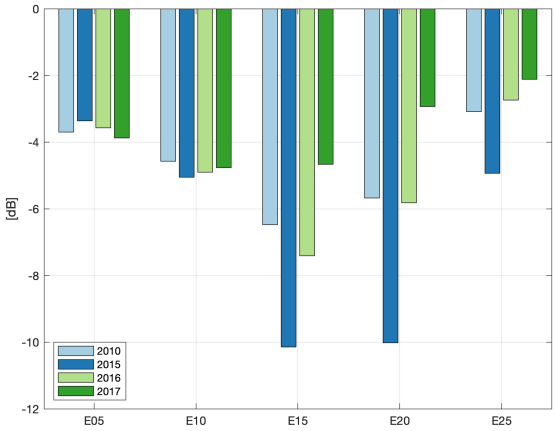

(a) Complete

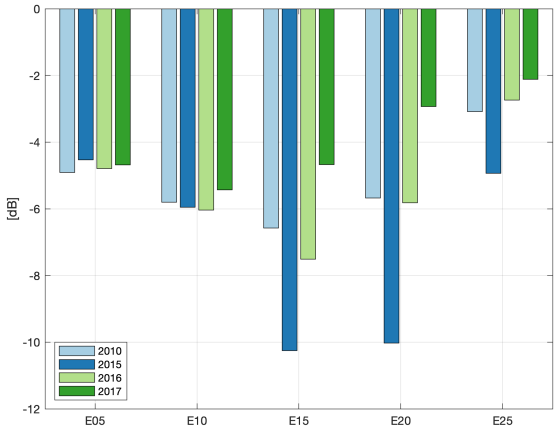

(b) Permanent

Figure 5.13: The average melting intensity (AMI) in dB, based on 10d SAR composite data (HH), for the different elevation bands and years, masked to the complete landmass and to the area of permanent snow/ice. E05 = 0 - 499m, E10 = 500 - 999m, E15 = 1000 - 1499m, E20 = 1500 - 1999m, E25 = > 2000m.

The masking of the AMI to the area of permanent snow/ice cover (see table 5.11b and figure 5.13b on the previous page) revealed stronger values for the lower elevation bands (E05 - E15), while the masking had no impact on the higher elevation bands E20 and E25. The average increase in band E05 and E10 was 1.1 dB and 1.0 dB.

5.2.4 Average Melting Intensity: Compositing Intervals

Similar to the number of melting days, the different available compositing intervals for 2017 were compared, see table 5.12 and figure 5.14 below.

Generally, the results received from the different intervals were quite similar. Looking at the whole area and Greenland, the 2d composites showed the strongest melting. For the Canadian Arctic Archipelago, the strongest melting values came from the 1d and 2d data (equal values).

Thus in all three regions, the 2d composites led to the strongest average melting intensity (AMI), while the 10d composites led to the weakest values. The range for WA and CA was, however, rather small, while the range for GL was slightly larger.

Table 5.12: The average melting intensity (AMI) in dB in 2017 per region, based on 1d, 2d and 10d SAR composite data (HH). WA = Whole Area, CA = Canadian Arctic Archipelago, GL = Greenland.

	WA	CA	GL
10d	-4.3	-4.1	-4.9
2d	-4.8	-4.3	-5.9
1d	-4.7	-4.3	-5.5
Range	0.5	0.2	1.0

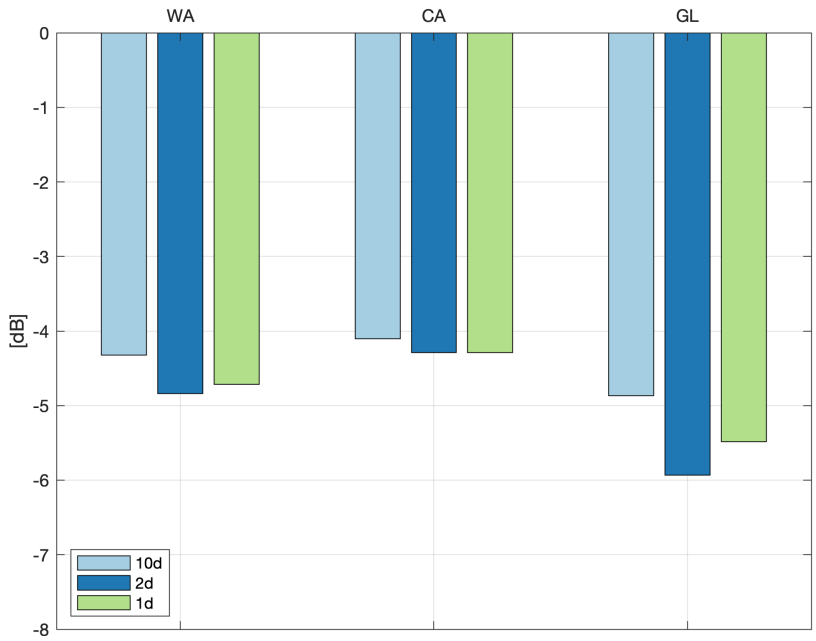

Figure 5.14: The average melting intensity (AMI) in dB in 2017 per region, based on 1d, 2d and 10d SAR composite data (HH). WA = Whole Area, CA = Canadian Arctic Archipelago, GL = Greenland.

5.3 Vegetation

5.3.1 Vegetation Days

The NDVI calculations were performed according to chapter 4.5 on page 23, based on the 10d MODIS data. The average number of vegetation days (defined here as days with an NDVI > 0.2) can be seen in table 5.13 below and in figure 5.15 on the following page.

The highest average number of vegetation days (VD) occurred for all areas in 2007. The whole area showed 10.8 days (2.8 days above average), the Canadian Arctic Archipelago showed 12.5 days (3.4 days above average) and Greenland showed 7.2 days (1.6 days above average). For the whole area and the Canadian Arctic Archipelago, 2013 was the year with the lowest average number of vegetation days with values of 5.0 days (3 days below average) and 5.6 days (3.5 days below average), while for Greenland the year 2017 with 3.5 days (2.1 days below average) showed the lowest average number of VD.

Thus, in all three regions the year 2007 showed the strongest vegetation activity, while 2013 showed the weakest activity (except for Greenland, where 2017 showed an even lower activity). In all three regions the record low year showed a stronger deviation from the 18-year average than the record high year.

Table 5.13: Average number of vegetation days (VD) for the three different regions, based on 10d MODIS NDVI calculations. WA = Whole Area, CA = Canadian Arctic Archipelago, GL = Greenland.

	WA	CA	GL
2000	6.4	7.2	4.6
2001	6.3	7.0	4.9
2002	6.7	7.5	5.0
2003	8.1	9.0	6.6
2004	6.1	7.0	3.6
2005	9.3	10.8	5.5
2006	8.9	10.3	5.9
2007	**10.8**	**12.5**	**7.2**
2008	8.7	9.8	6.6
2009	7.1	8.1	5.5
2010	9.1	10.3	6.6
2011	10.1	11.6	7.2
2012	9.7	11.1	6.8
2013	**5.0**	**5.6**	3.7
2014	7.3	8.3	5.3
2015	10.3	11.8	6.7
2016	8.2	9.2	6.4
2017	5.5	6.4	**3.5**
Mean	8.0	9.1	5.6

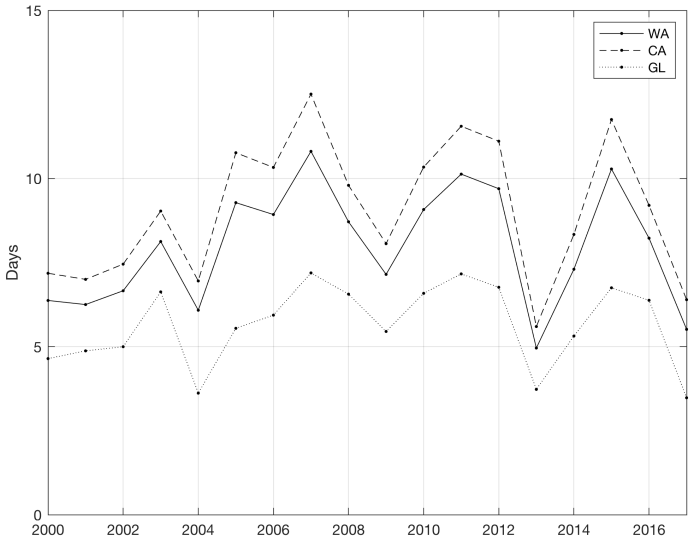

Figure 5.15: Average number of vegetation days (VD) for the three different regions, based on 10d MODIS NDVI calculations. WA = Whole Area, CA = Canadian Arctic Archipelago, GL = Greenland.

The results of the analysis of the vegetation in different elevation bands are shown in table 5.14 and figure 5.16 on the next page. Here again, the two highest elevation bands were excluded, since they were almost completely covered in snow/ice.

In the lowest elevation bands E05 and E10, the highest number of VD was found in 2007 with 13.0 days (3.1 days above average) and 4.6 days (1.4 days above average) respectively, while the lowest number was found in 2013 with 6.1 days (3.8 days below average) and 1.8 days (1.4 days below average) respectively. In the elevation band E15, the highest number was found in 2003 with 0.6 days (0.2 days above average) and the lowest value in 2005, where 0.2 days (0.2 day below average) were measured.

Hence, in the lower two elevation bands the record years occurred in 2007 and 2013 (similar to the subset regions), while the higher elevation band had different record years. Here again, the negative deviation from the 18-year average was stronger than the positive deviation.

Table 5.14: Average number of vegetation days (VD) for three different elevation bands, based on 10d MODIS NDVI calculations. E05 = 0 - 499m, E10 = 500 - 999m, E15 = 1000 - 1499m.

	E05	E10	E15
2000	7.9	2.8	0.4
2001	7.8	2.8	0.5
2002	8.3	2.9	0.4
2003	10.2	3.4	**0.6**
2004	7.6	2.3	0.3
2005	11.3	3.8	**0.2**
2006	10.8	3.3	0.5
2007	**13.0**	**4.6**	0.3
2008	10.9	3.5	0.4
2009	8.9	3.0	0.4
2010	11.3	3.6	0.4
2011	12.5	4.1	0.4
2012	12.1	3.7	0.3
2013	**6.1**	**1.8**	0.2
2014	9.0	3.3	0.5
2015	12.7	3.8	0.4
2016	10.4	3.1	0.2
2017	6.9	2.4	0.2
Mean	9.9	3.2	0.4

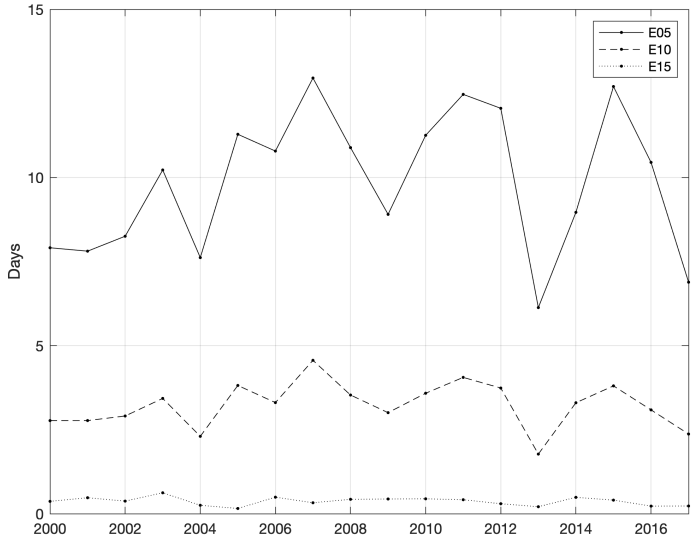

Figure 5.16: Average number of vegetation days (VD) for three different elevation bands, based on 10d MODIS NDVI calculations. E05 = 0 - 499m, E10 = 500 - 999m, E15 = 1000 - 1499m.

5.3.2 Change Analysis

The change in average number of vegetation days (VD) was calculated in the same way as the change in number of snow/ice-covered days (SCD). The results can be seen in table 5.15 and figure 5.17 on the following page.

Table 5.15: Change analysis statistics for vegetation days (VD) in the three different regions. SEN = Sen's Slope, τ = Kendall's Tau. WA = Whole Area, CA = Canadian Arctic Archipelago, GL = Greenland.

	SEN	τ
WA	0.11	0.15
CA	0.12	0.15
GL	0.05	0.14

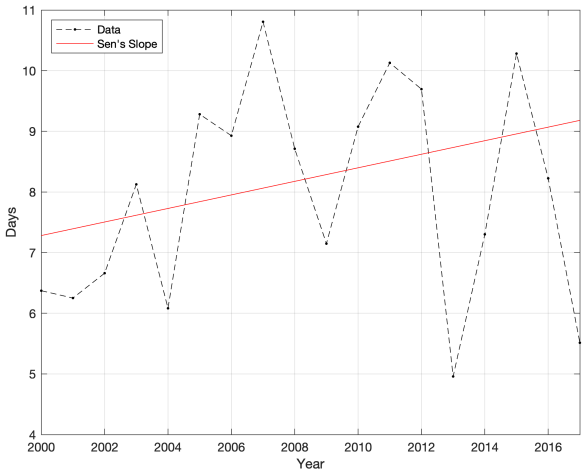

(a) Whole Area

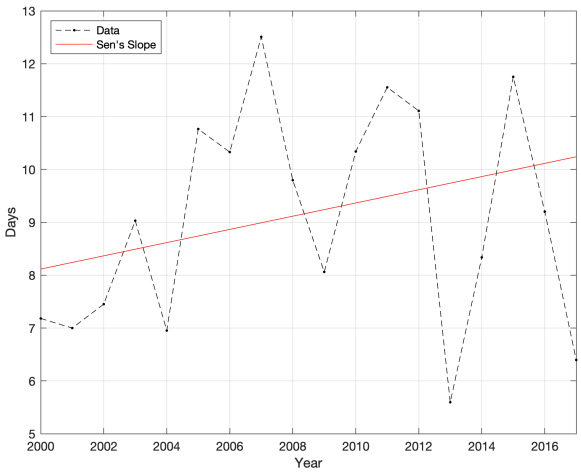

(b) Canadian Arctic Archipelago

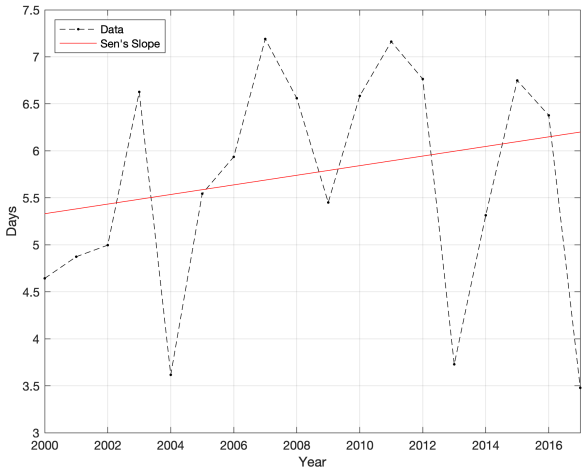

(c) Greenland

Figure 5.17: Average number of vegetation days (VD) in the three different regions: change analysis (Sen's Estimator).

The τ value of all three regions varied between 0.12 and 0.15, implying a small positive temporal correlation of the average number of vegetation days (VD). The strongest change occurred in the Canadian Arctic Archipelago with an increase of 0.12 days per year, while the weakest change occurred in Greenland with 0.05 additional VD per year.

The change in VD for the elevation bands can be found in table 5.16 and figure 5.18 below.

Table 5.16: Change analysis statistics for vegetation days (VD) in three different elevation bands. SEN = Sen's Slope, τ = Kendall's Tau. E05 = 0 - 499m, E10 = 500 - 999m, E15 = 1000 - 1499m.

	SEN	τ
E05	0.13	0.16
E10	0.02	0.11
E15	-0.01	-0.19

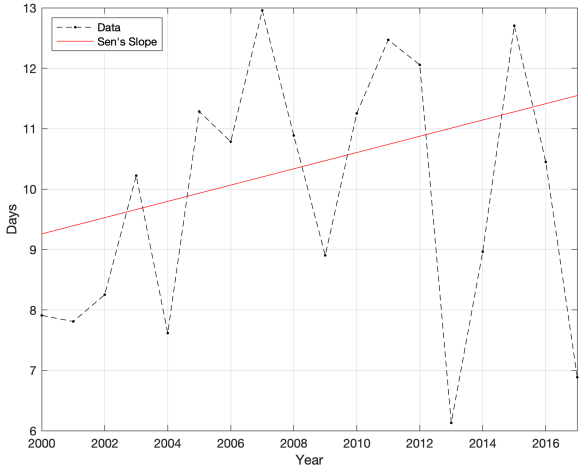

(a) 0 - 499m

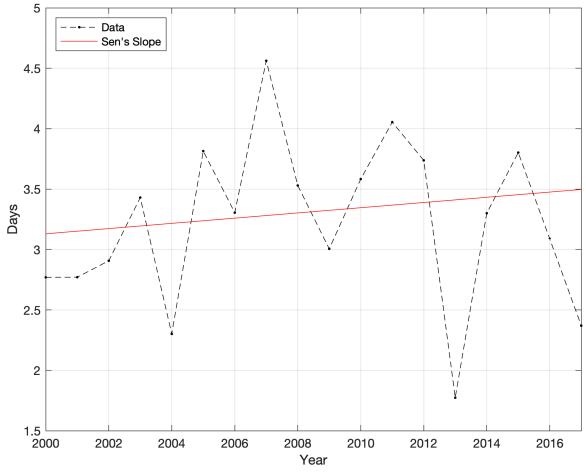

(b) 500 - 999m

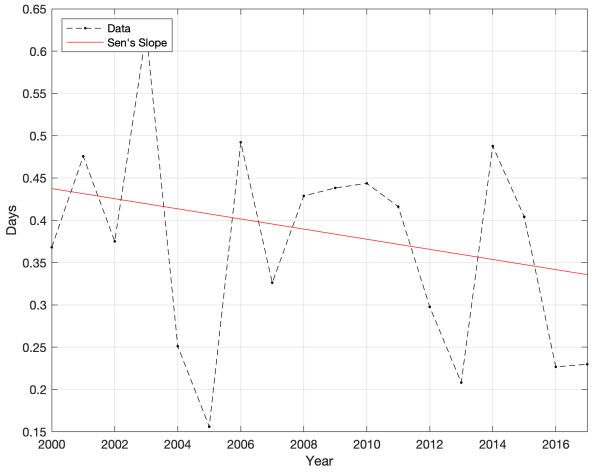

(c) 1000 - 1499m

Figure 5.18: Average number of vegetation days (VD) in three different elevation bands: change analysis (Sen's Estimator).

The τ value varied between -0.19, which means a weak negative correlation, and 0.16, which means a weak positive correlation. The strongest trend occurred in elevation band E05, where a τ value of 0.16 and an increase of 0.13 days per year could be found. In the elevation band E10, both the τ

value and the change were smaller. In elevation band E15, a negative τ value of -0.19 and a weak decrease in VD of -0.01 days per year could be found.

5.4 Snow Cover vs. Melting

The optical data-based measurements and the radar-based measurements can be brought together by comparing time series of NDSI and snow wetness calculations. Figure 5.19 below shows the snow wetness, i.e. the melting activity three weeks before and after the average first snow-free day for the Canadian Arctic Archipelago, based on the 1d Sentinel-1 data.

It can be observed, that roughly one and a half week before the first snow-free day a distinct drop of the radar backscatter difference occurred, after which the value stayed below the threshold of $-2\,\mathrm{dB}$ for a couple of days. After the melting of the snow cover, the backscatter difference generally reached less negative values again, implying no more melting activity.

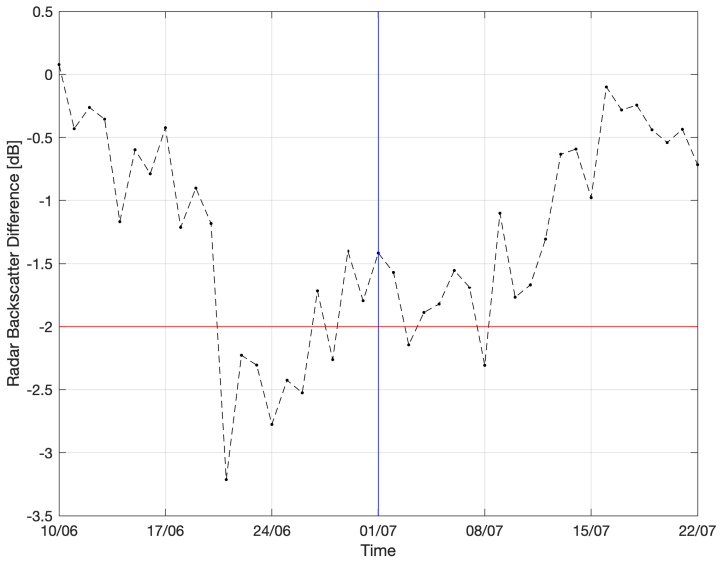

Figure 5.19: Radar backscatter difference [dB], based on 1d Sentinel-1 data, around the average first snow-free day (blue line) for the Canadian Arctic Archipelago. Snow wetness threshold of -2 dB marked with a red line.

5.5 Lake Hazen

5.5.1 Ice Cover

The ice-covered area of Lake Hazen was analysed using the same NDSI algorithm as used for the minimum snow/ice-covered area (MSCA) and the snow/ice-covered days (SCD), slightly altered to count the ice-covered area of the lake in each available image. The average ice-covered area of three different intervals was analysed: the yearly average ice cover, the June, July, August (JJA) ice cover and the May to September snow cover (as analysed in Lehnherr et al. (2018)). The results are presented in table 5.17 and figure 5.20 on the next page.

All three metrics showed the highest ice-covered area in 2004 and the lowest area in 2012, and in all years, the yearly average area was the largest, followed by the May to September area and the JJA area. With 45.2 %, the JJA area showed the largest spread, while the average area and the May to September area had smaller spreads of 30.4 % and 36.2 %.

Table 5.17: Ice cover of Lake Hazen in %, relative to the total lake area, for different time intervals, based on 10d MODIS NDSI calculations. AVG = average, JJA = June to August, MtS = May to September.

	AVG	JJA	MtS
2000	80.0	75.9	76.2
2001	63.4	45.1	54.3
2002	66.8	54.5	61.0
2003	67.6	58.3	63.5
2004	**90.8**	**86.6**	**88.0**
2005	65.5	48.8	57.3
2006	73.5	69.1	71.6
2007	69.0	53.7	61.9
2008	71.1	60.3	65.6
2009	88.5	83.3	84.7
2010	62.2	41.5	52.5
2011	72.1	55.8	64.3
2012	**60.4**	**41.4**	**51.7**
2013	69.3	54.4	61.1
2014	62.6	48.2	55.2
2015	65.7	52.6	59.6
2016	67.2	57.0	62.7
2017	72.0	55.8	63.1
Mean	70.4	57.9	61.1

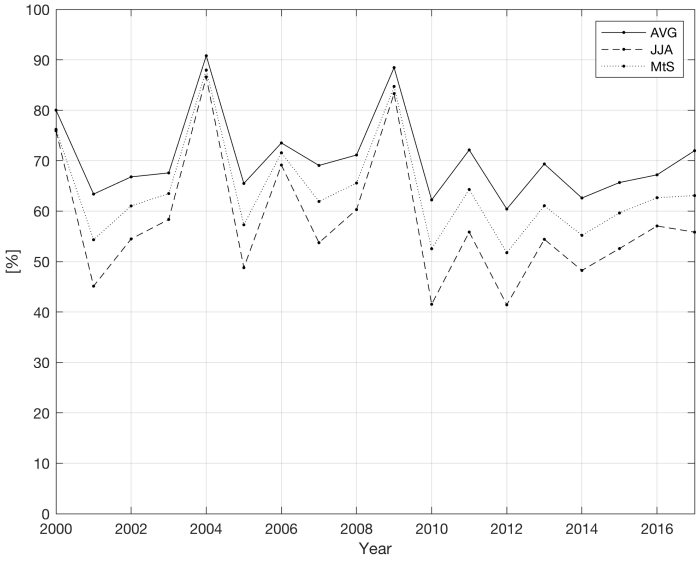

Figure 5.20: Ice cover of Lake Hazen in %, relative to the total lake area, for different time intervals, based on 10d MODIS NDSI calculations. AVG = average, JJA = June to August, MtS = May to September.

5.5.2 Change Analysis

Similar to the other analysed cryosphere metrics in the previous sub-chapters, change analysis methods were applied to the lake ice cover dataset. In addition to the above mentioned metrics, the May to September interval was analysed from 2000 to 2012, to allow comparisons to the findings obtained by Lehnherr et al. (2018). The results are presented in table 5.18 and figure 5.21 below.

Table 5.18: Change analysis of the Lake Hazen ice cover. SEN = Sen's Slope, τ = Kendall's Tau.

	SEN	τ
Yearly average	-0.21	-0.10
June, July, August	-0.40	-0.16
May to September (00-12)	-0.54	-0.13
May to September (00-17)	-0.29	-0.14

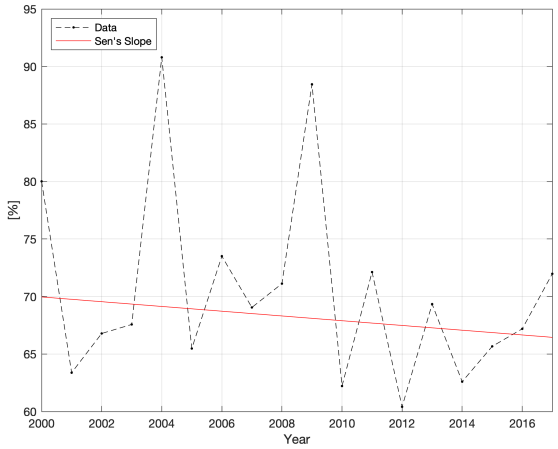

(a) Average

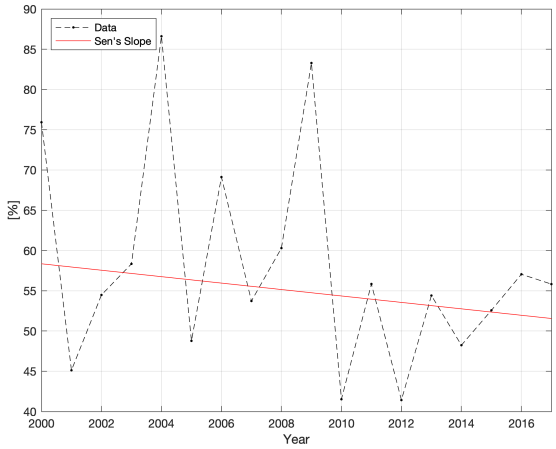

(b) June, July, August

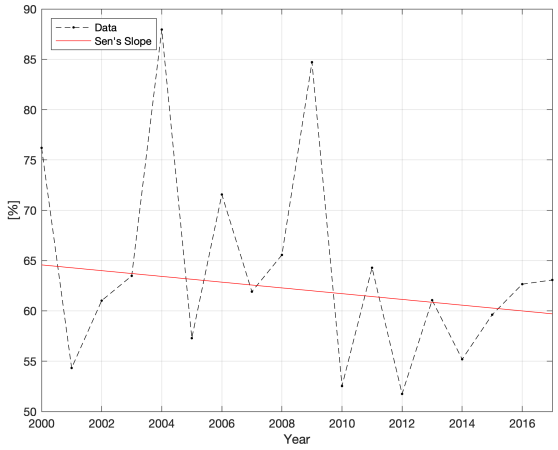

(c) May to September, 2000-2017

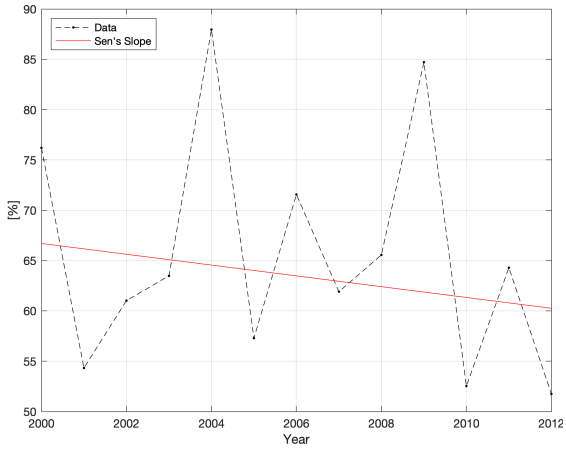

(d) May to September, 2000-2012

Figure 5.21: Change analysis of the Lake Hazen ice cover in %, relative to the total lake area.

All four metrics showed a negative trend, although the τ values did not signify a strong correlation. The strongest decrease of $-0.54\,\%$ per year was observed for the May to September interval between 2000 and 2012. Analysed between 2000 and 2017, the interval showed a smaller decrease with a value of $-0.29\,\%$ per year. While the JJA interval also showed a quite strong decrease of $-0.40\,\%$ per years, the yearly average showed the smallest decrease with a value of $-0.20\,\%$ per year.

6 Discussion

Remotely sensed data have proven to be valuable for monitoring the state of snow and ice over a large spatial and temporal extent. They offer the possibility to get deep insights into the processes and changes on Earth's surface for a fraction of the price and time of field measurements.

Optical data allow statements about the presence or absence of snow and ice cover. Precise assessments of the temporal and spatial extent of the cryosphere are achievable. Using a time series of optical data additionally enables detection of changes over a certain period in time.
SAR data, as used in this thesis, can be used for the identification of wet snow or wet ice, but not for differentiating between snow or ice and other land cover. Wetness detection capabilities are of great value, especially in regions with mostly permanent snow or ice, where the optical data cannot detect any effects of a warming climate, by allowing the detection of melting processes.

The following sub-chapters discuss the results presented in the previous chapters and place them within a broader context. The optical and SAR data are brought together to evaluate their complementarity.

6.1 Snow and Ice Cover

6.1.1 Snow/Ice-Covered Days

For the different regions and elevation bands, the years 2012 and 2013 were striking years. While 2012 showed the lowest number of snow/ice-covered days (SCD) throughout almost all regions and elevations bands, the following year 2013 showed the highest number.

Brown and Mote (2009) noted that the snow cover duration is the most sensitive snow cover variable to climate and that it is strongly negatively correlated with air temperature. The 2012 and 2013 weather data from three weather stations in the Canadian Arctic Archipelago (Alert, Eureka, Grise Fiord, see chapter 3.3.2 on page 14) could thus help to explain these extreme years. Figure 6.1 on the next page shows the weather characteristics, composited in the same 10d intervals as the satellite data, for the years 2010 to 2015, two years before and after the record years 2012 and 2013.

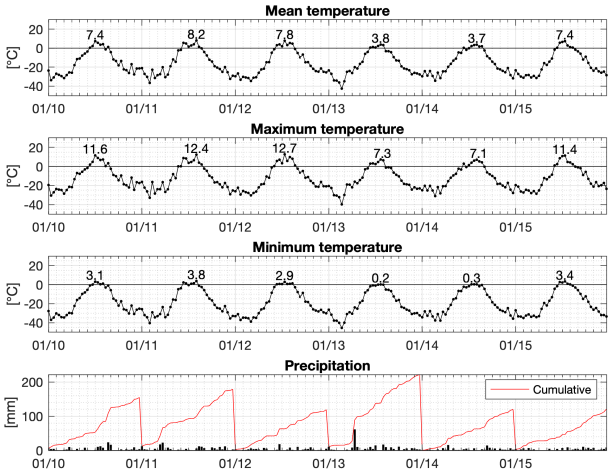

(a) Alert

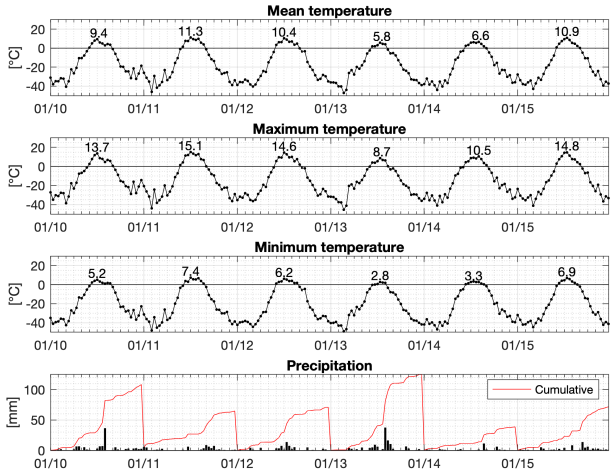

(b) Eureka

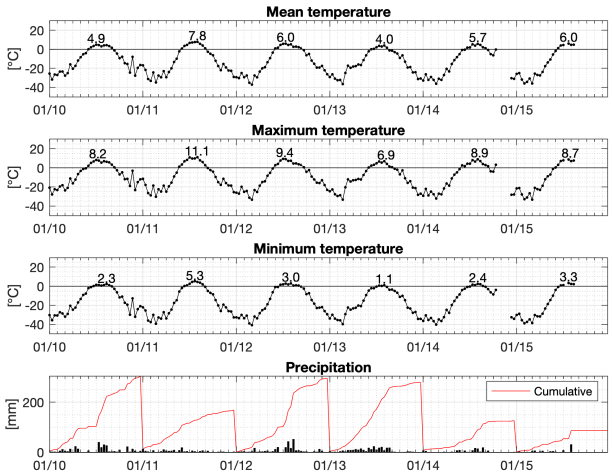

(c) Grise Fiord

Figure 6.1: Weather data at the three weather stations, 2010 to 2015. Highest mean, maximum, and minimum temperature per year in numbers.

In all three locations, the maximum and the minimum temperatures of 2012 were among the highest of the measuring period. Additionally, the cumulative precipitation of Alert and Eureka was lower than in other years. By contrast, the year 2013 showed the lowest mean, maximum and minimum temperatures at all three weather stations, while the cumulative precipitation was distinctly larger compared to other years.

A comparison of the yearly mean temperatures to the average temperature of the 18 years of weather data showed that the temperatures in 2012 were only 2 % to 5 % higher compared to the 18-year average, but the temperatures in JJA were 60 % above the 18-year average in Alert, 36 % in Eureka and 29 % in Grise Fiord. In 2013, the yearly average temperatures were 6 % to 9 % above average, except for the summer months (JJA), which were 70 % below the 18-year average in Alert,

73 % in Eureka and 56 % in Grise Fiord (see figure 6.5a on page 56).

Precipitation is also a key factor for the amount of snow cover. Figure 6.2 below gives an overview of the precipitation in December, January, February (DJF) and March, April, May (MAM), prior to the melting season in summer. For 2012 it could be observed that in Alert, the DJF precipitation rates were 58 % below the average, while the MAM precipitation rates were not prominent. In Eureka both the DJF and MAM precipitation rates were slightly below average, while Grise Fiord had an average DJF precipitation rate and a 50 % above-average MAM precipitation. In 2013, however, the DJF and MAM precipitation rates were almost throughout the data remarkably higher compared to 2012, reaching record high values. In Alert and Grise Fiord the MAM precipitation rates of 2013 were at 270 % and 251 % of the 18-year average — the highest MAM precipitation rates recorded during the 18 years for both stations. In Eureka they reached 227 % of the 18-year average, which was the second highest MAM value for the station.

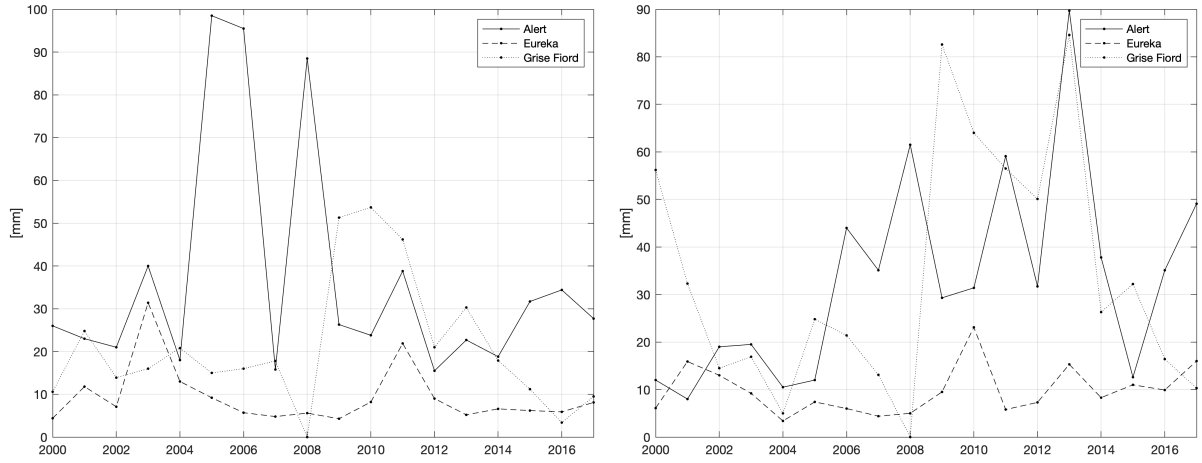

(a) DJF **(b)** MAM

Figure 6.2: Precipitation in the winter months (DJF) and the spring months (MAM) for the three weather stations.

This suggests that the highest number of SCD in 2013 were an effect of the low summer temperatures in combination with high precipitation rates (especially in spring). The lowest number of SCD in 2012 was less clear to explain. Although the precipitation rates in Alert and Eureka, especially in winter and spring, were rather low, there were other years with similarly low numbers. The rather high summer temperature might thus have been the main factor, supported by the rather low precipitation rates. This observation is consistent with the findings by Brown and Mote (2009), who found that the air temperature has the largest impact on snow cover, while precipitation rates only have a small effect.

A widely-used meteorological metric, especially in cold regions, is the number of positive degree days (PDD). Positive degree days are defined as the cumulative temperature higher than the

melting point, i.e. 0 °C, over a certain period (Wake and Marshall, 2015). Ten consecutive days with a temperature of 10 °C would for instance imply 100 PDD. A comparison between the number of SCD and the number of PDD revealed a strong negative correlation ($\tau \approx$ -0.71), as can be seen in figure 6.3.

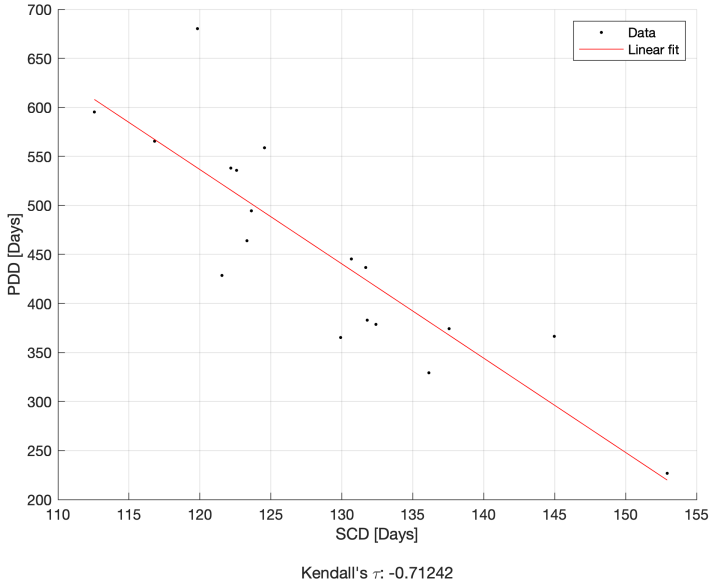

Figure 6.3: Positive degree days (PDD) in Eureka vs. snow/ice-covered days (SCD) in the Canadian Arctic Archipelago.

6.1.2 Change in Snow/Ice-Covered Days

The changes in number of snow/ice-covered days (SCD), masked and averaged to different regions and elevation bands, were presented in chapter 5.1.4 on page 30. The calculations showed a weak negative temporal correlation with the number of SCD. For the whole area, the observed decrease in number of SCD was at a rate of -0.38 days/year and for the Canadian Arctic Archipelago it was at -0.20 days/year. The elevation band from 0 m to 499 m showed a slightly more pronounced decrease at a rate of -0.40 days/year. The obtained values coincide with the 2 to 4 days per decade mentioned in AMAP (2017).

Figure 6.4 on the following page shows the result of a pixel-based calculation of the change in number of SCD. As can be seen in the map, there were both areas of increasing and decreasing SCD. Ellesmere Island in the centre of the study site showed relatively large areas of increasing SCD, which were mostly close to the coastline. The largest areas of decreasing SCD could be found in the south-western part of the study area and at low elevations. The part of Greenland covered by the study area showed both areas of increase and decrease. The areas of decrease were close to the Greenland Ice Cap, while the areas of increase were close to a coast.

The areas of decreasing SCD could be explained by the increasing air temperatures, as men-

tioned in chapter 6.1.1. By contrast, the areas of increasing SCD could not be explained using the available climatological data. Environment and Climate Change Canada (2018a) observed, however, the same areas of increasing SCD in their comparison of the Canadian snow cover relative to the reference period 1998 to 2010, but did not provide an explanation. Potential factors might have been influences of ocean currents or a change in sea ice extent, as for instance observed in northern Alaska by Brock (2016), who found that decreases in sea ice led to an increased water vapour flux, resulting in increased snowfall.

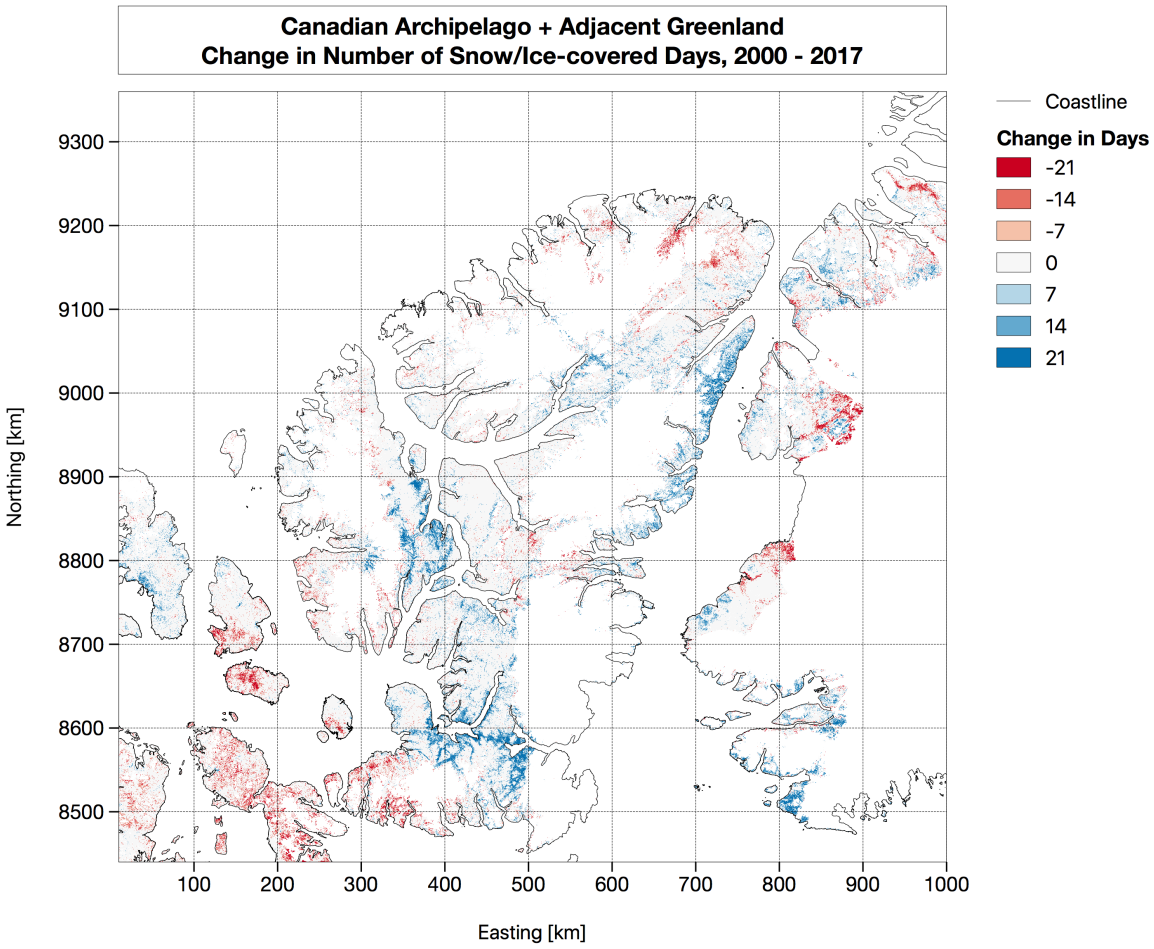

Figure 6.4: Change in snow/ice-covered days (SCD) over the 18 years period. Based on MODIS imagery, calculated with Sen's Slope Estimator, see results in chapter 5.1.4 on page 30.

6.1.3 Minimum Snow/Ice-Covered Area

The minimum snow/ice-covered area (MSCA) showed record low values in the year 2011 and record high values in the year 2013 throughout all regions and elevation bands, except for the highest elevation band (above 2000 m). In other studies, for instance Trishchenko and Wang (2018), the smallest MSCA was found in 2012. In their research, a larger study site was analysed, with a larger share of lower latitude regions. The largest MSCA was, however, found in 2013 as well.

The record high of 2013 can be explained in the same way as the record high number of snow/ice-covered days (SCD) in the previous chapter 6.1.1: high precipitation rates throughout the year in combination with low summer temperatures. The record low year 2011 showed very high December, January, February (DJF) precipitation rates at 234 % of the 18-year average in Eureka and at 207 % in Grise Fiord, while Alert showed regular precipitation rates at 105 % of the average. The high DJF precipitation rates were followed by rather high March, April, May (MAM) precipitation rates (except for Eureka), which do not point towards a low MSCA. Remarkable in 2011 were, however, the summer temperatures (see figure 6.5a below), which were 182 % of the 18-year average in Grise Fiord, 155 % in Eureka and 155 % in Alert, marking the highest June, July, August (JJA) temperatures for Grise Fiord and Eureka and the second highest for Alert. This led to the highest number of PDD in Eureka and Grise Fiord and the third highest number in Alert (figure 6.5b below).

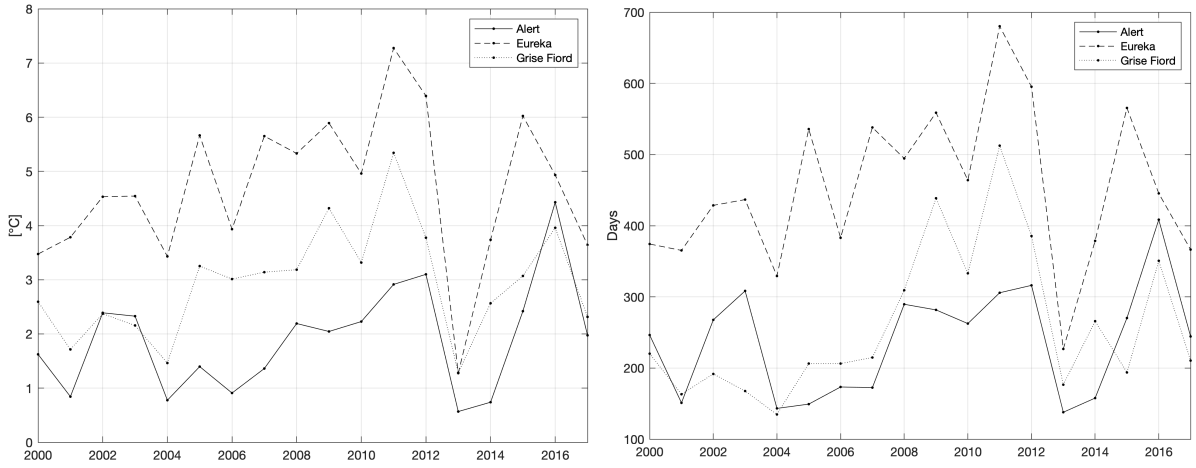

(a) Mean temperatures JJA

(b) Positive degree days (PDD)

Figure 6.5: Yearly mean temperatures in the summer months and number of positive degree days (PDD).

Since the date of the MSCA usually lies in July/August, the high summer temperatures as well as the number of PDD might explain the lowest MSCA in 2011. This theory is also supported by Fontana et al. (2010), which found a strong relationship between the MSCA and the number of PDD.

This relationship indeed appears to be strong. Figure 6.6 on the next page shows a comparison of the number of PDD in Eureka and the MSCA of the Canadian Arctic Archipelago. A Kendall's τ analysis resulted in a τ value of $\approx$ -0.67, implying a considerably strong negative correlation, i.e. a decreasing percentage of MSCA with an increasing number of PDD.

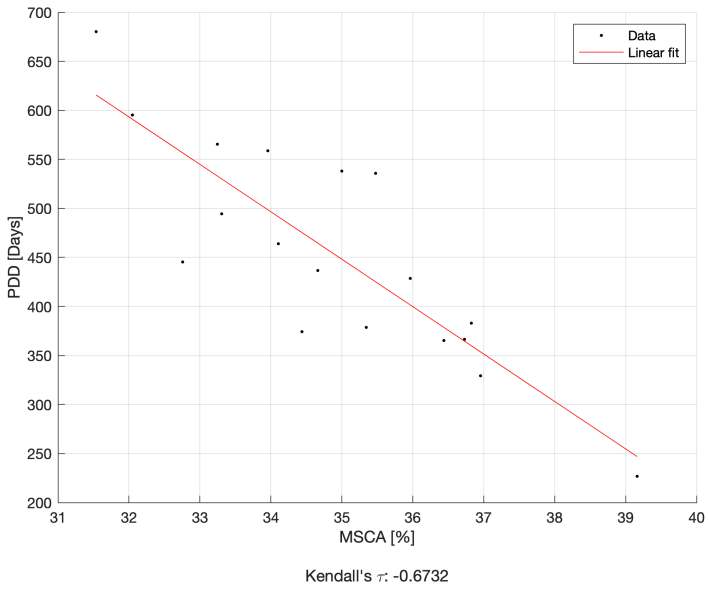

Figure 6.6: Positive degree days (PDD) in Eureka vs. minimum snow/ice-covered area (MSCA) in the Canadian Arctic Archipelago.

6.1.4 Change in Minimum Snow/Ice-Covered Area

As seen in chapter 4.2.4 on page 19, the minimum snow/ice-covered area (MSCA) distinctly decreased in the study area over the course of 18 years. The largest decrease was observed in the Canadian Arctic Archipelago ($-0.15\,\%$ per year or $-1.5\,\%$ per decade) and in the elevation band from 500 m to 999 m ($-0.22\,\%$ per year or $-2.2\,\%$ per decade). This was lower than the values by Environment and Climate Change Canada (2018a) and Vaughan et al. (2013), who observed a decrease of $-4\,\%$ and $-11.7\,\%$. They both, however, calculated the change averaged over a large area (whole Canada and the whole Northern Hemisphere, respectively), potentially influenced by areas at lower latitudes. The discussion in chapter 6.1.3 on page 55 showed that the decrease was strongly related to an increase in positive degree days (PDD). This motivates further analysis of the spatial representation of the decrease.

Figure 6.7 on the following page shows the extent of the smallest and the largest MSCA in 2011 and 2013. It can be observed that almost all the differences were concentrated in the Canadian Arctic Archipelago, whereas Greenland did show big variations in MSCA. The south-western part of the Canadian Arctic Archipelago did not have any perennial snow cover. Woo and Young (2014) found in their research that especially snow banks and snow beds that lay throughout the year had lost their perennial status, and Wang et al. (2018) concluded that perennial snow cover faces a transition to seasonal snow cover. This is consistent with the map: the hot spots of change in the Canadian Arctic Archipelago were around the borders of the ice caps, where a decreasing perennial cover could be expected, as well as close to the coastline. A comparison with the digital elevation model showed that the areas of change were concentrated at low and medium elevations (up to 1000 m), confirming the large observed decrease in the 500 m to 999 m elevation band.

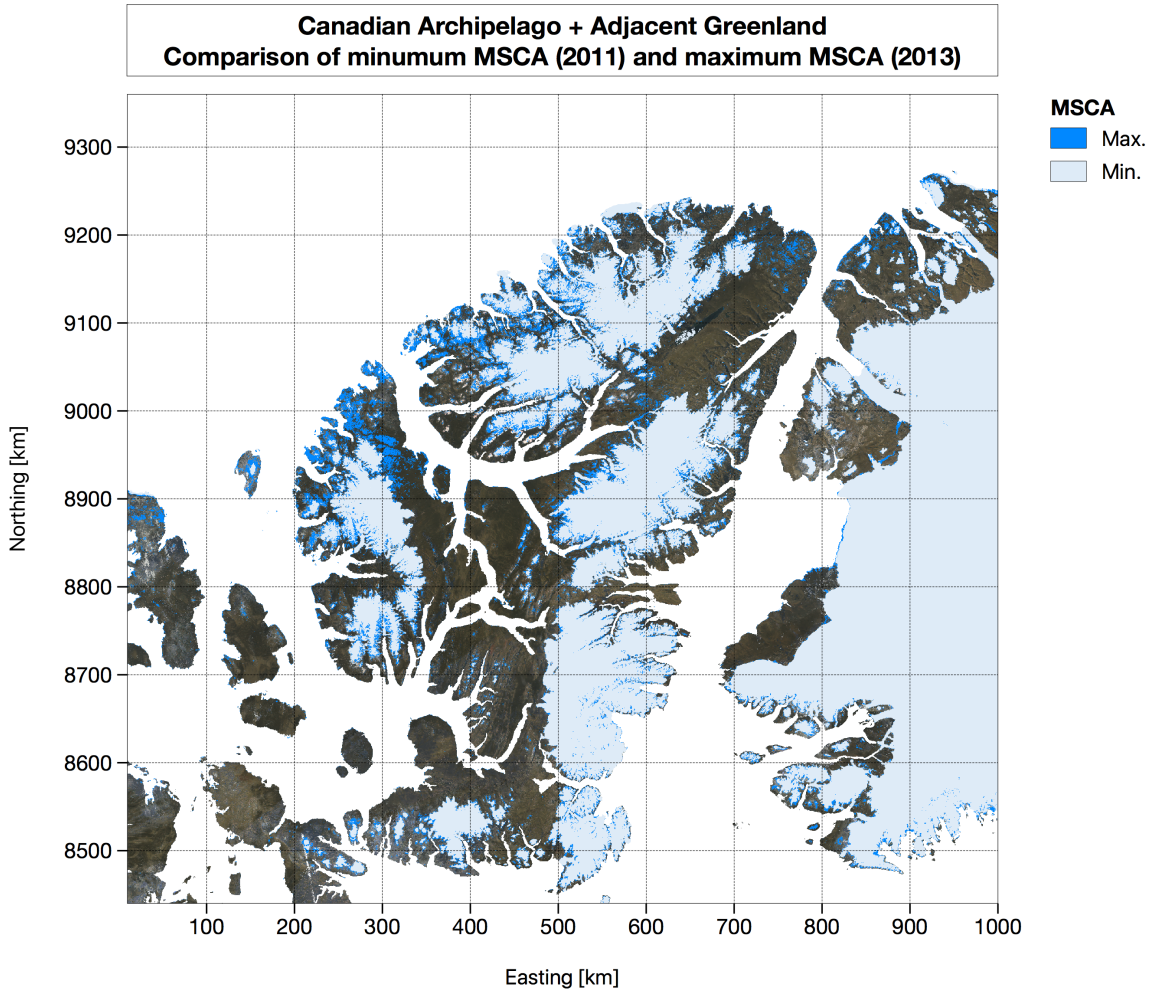

Figure 6.7: Comparison of the smallest and largest minimum snow/ice-covered area (MSCA) in 2011 and 2013 respectively. Background: MODIS RGB.

6.2 Melting

6.2.1 Melting Days

Insights into the melting behaviour in the study area were available for the years 2010 and 2015 to 2017. In all four years, there appeared to be a good agreement between the number of melting days (MD) and the number of positive degree days (PDD). Eureka, which lies in the centre of Ellesmere Island, offers a good opportunity for a comparison.

Table 6.1: A comparison of positive degree days (PDD) in Eureka and melting days (MD) in the Canadian Arctic Archipelago.

	PDD	MD	Ratio
2010	464.0	24.4	19.0
2015	565.5	19.2	29.4
2016	445.4	18.4	24.2
2017	366.5	18.9	19.4

Table 6.1 above shows the relation of the number of PDD and the number of MD. The two values had a similar development in the four years, i.e. an increased number of MD due to an increased number of PDD, with a ratio of roughly 20 to 30 PDD per MD.

A connection between MD and snow/ice-covered days (SCD) or minimum snow/ice-covered area (MSCA) was harder to find. On the one hand, the presence of melting processes does not necessarily imply an areal loss of snow or ice. And on the other hand, a year with a low number of SCD, which are neither related to high temperatures nor to melting, but for example to a lack of precipitation and thus snow, can lead to a lower number of MD.

6.2.2 Average Melting Intensity

Similar to the number of melting days (MD), analyses of the average melting intensity (AMI) were possible for 2010 and 2015 - 2017. The largest AMI in all regions could be observed in 2015. The part of Greenland adjacent to the Canadian Arctic showed an AMI magnitude as high as $-9\,\mathrm{dB}$, linked to an Arctic cut-off high, which led to an all-time melting record for whole Greenland (Tedesco et al., 2016). Here again, the consistency between the AMI and the number of positive degree days (PDD) appeared to be very good — additional years of observations would, however, have helped solidify this correlation. Table 6.2 below compares the two parameters, again for Eureka and the Canadian Arctic Archipelago.

Table 6.2: A comparison of positive degree days (PDD) in Eureka and average melting intensity (AMI) in the Canadian Arctic Archipelago.

	PDD	AMI	Ratio
2010	464.0	-4.4	-104.3
2015	565.5	-5.6	-100.6
2016	445.4	-4.6	-97.2
2017	366.5	-4.1	-89.3

It can be seen that the number of PDD as well as the AMI behaved in a similar manner, i.e. an increased AMI due to an increased number of PDD, and that in the four years of observation roughly 100 PDD equalled $-1\,\mathrm{dB}$ in AMI.

6.2.3 Compositing Intervals

As the SAR imagery for 2017 was available in 1-day, 2-day and 10-day composites, comparisons between the different compositing intervals were possible. The 1-day composites had a pixel coverage of 93.5 %, the 2-day composites 97.8 % and the 10-day composites 99.9 %.

In all three regions, the smallest number of melting days (MD) was obtained from the 10-day composites. The difference to the largest number (mainly the 2-day composites) was roughly 10 % to 15 %. The smallest number, obtained by the 10-day composites, could be explained by the often short-lived nature of melting. By calculating the melting in a 10-day composite and multiplying it by 10 days, not necessarily every melting event could be recorded. The highest number in the 2-day composites could be explained by the same process — the calculation of the melting in a 2-day composite (with overlap) and by dividing it by 2 days.
When the pixel coverage (see figure 3.3e and 3.3f on page 12) and the number of MD in the 1-day and 2-day composites are evaluated, it can be observed that the difference in MD is smaller for Greenland (1d: 15.4 days, 2d: 17.1 days) with a larger pixel coverage, compared to the whole Canadian Arctic Archipelago (1d: 20.0 days, 2d: 22.0 days) with a smaller pixel coverage (especially in the western part of the area). This suggests that the results of the 1-day and 2-day composites would be closer if both had a 100% pixel coverage.

In summary, there appears to be a trade-off between a good temporal versus a good spatial coverage. The 10-day composites provided the best spatial coverage, while the 1-day composites provided the best temporal coverage. When a large number of image acquisitions is available, the 1-day composites should be preferred. When the image availability is smaller, the 10-day composites provide a quite solid approximation. The observations made for the number of MD also hold for the average melting intensity (AMI).

6.3 Vegetation

6.3.1 Vegetation Days

In chapter 5.3.1 on page 42, the years 2007 and 2013 showed as record years: 2007 had the highest number of days with vegetation in all three regions, and 2013 showed the lowest number of VD, aside from Greenland, where 2017 was the year with the weakest vegetation signal.

The record low in 2013 can be explained in the same manner as the record high values for the number of snow/ice-covered days (SCD) and the minimum snow/ice-covered area (MSCA). The record low year 2007, however, did not show any strong meteorological anomalies. The yearly average precipitation was 45 % below the 18-year average in Eureka and 67 % below the average in Grise Fiord — only in Alert it was with 117 % of the 18-year average slightly surpassing, which can be explained by a high autumn precipitation rate. The annual mean temperatures in all three stations were 0 % to 11 % above the 18-year average, which resulted in positive degree days (PDD)

below the average in Alert and Grise Fiord, whereas Eureka showed a slight excess of PDD at 19 % above the 18-year average.

However, a quite strong relationship between the number of VD and the number of PDD was found. Figure 6.8 below shows the number of PDD in Eureka plotted against the number of VD. The τ value of ≈ 0.73 implies a strong positive correlation, i.e. an increase of VD with an increase of PDD.

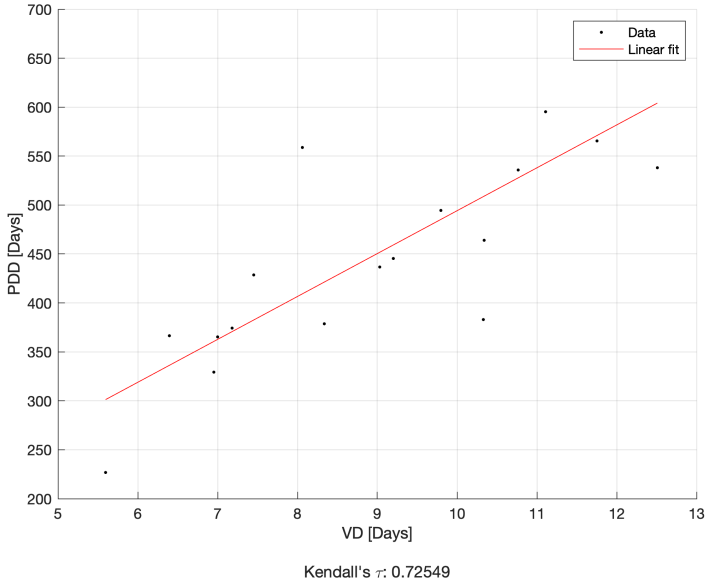

Figure 6.8: Positive degree days (PDD) in Eureka vs. vegetation days (VD) of the Canadian Arctic Archipelago.

Yet it remains unclear, why the year 2007 with just average PDD presented such a high number of VD. The year 2011, by comparison, which showed by far the highest number of PDD of the 18-year period only scored the third highest number of VD. A comparison of the areas of vegetation activity between 2007 and 2013 revealed no large differences, implying a stronger, but not more spatially extensive activity in 2007.

6.3.2 Change in Vegetation Days

The observed changes in the occurrence of vegetation days were discussed in chapter 5.3.2 on page 44. The most pronounced changes occurred in the Canadian Arctic Archipelago, where the number of vegetation days (VD) – on average – increased by 0.12 days/year.

The map in figure 6.9 on the next page shows the changes in more detail. There were relatively large areas of increasing VD in the south-western and centre part of the Canadian Arctic Archipelago, close to Lake Hazen as well as in the lower third of the west coast of Greenland. The areas of increasing vegetation overlapped to a certain degree with the areas of decreasing snow from figure 6.4 on page 55.

A comparison between the obtained increases in vegetation in figure 6.9 on the next page and the circumpolar Arctic vegetation map from 2003 showed the largest increases in regions of tundra

and dwarf-shrub. This was supported by Henry and Elmendorf (2010), who found that the largest increases in vegetation signal (i.e. biomass) could be observed in wet sedge tundra regions and dwarf-shrub regions and by Edwards and Treitz (2017), who found a significantly increased greening, concentrated in areas of dry to mesic (i.e. moderately moist) vegetation. They observed, however, that the change in vegetation was spatially heterogeneous. This was also observed by Jia et al. (2009), who realised, that the magnitudes of change in vegetation activity showed a non-linear response to climate change.

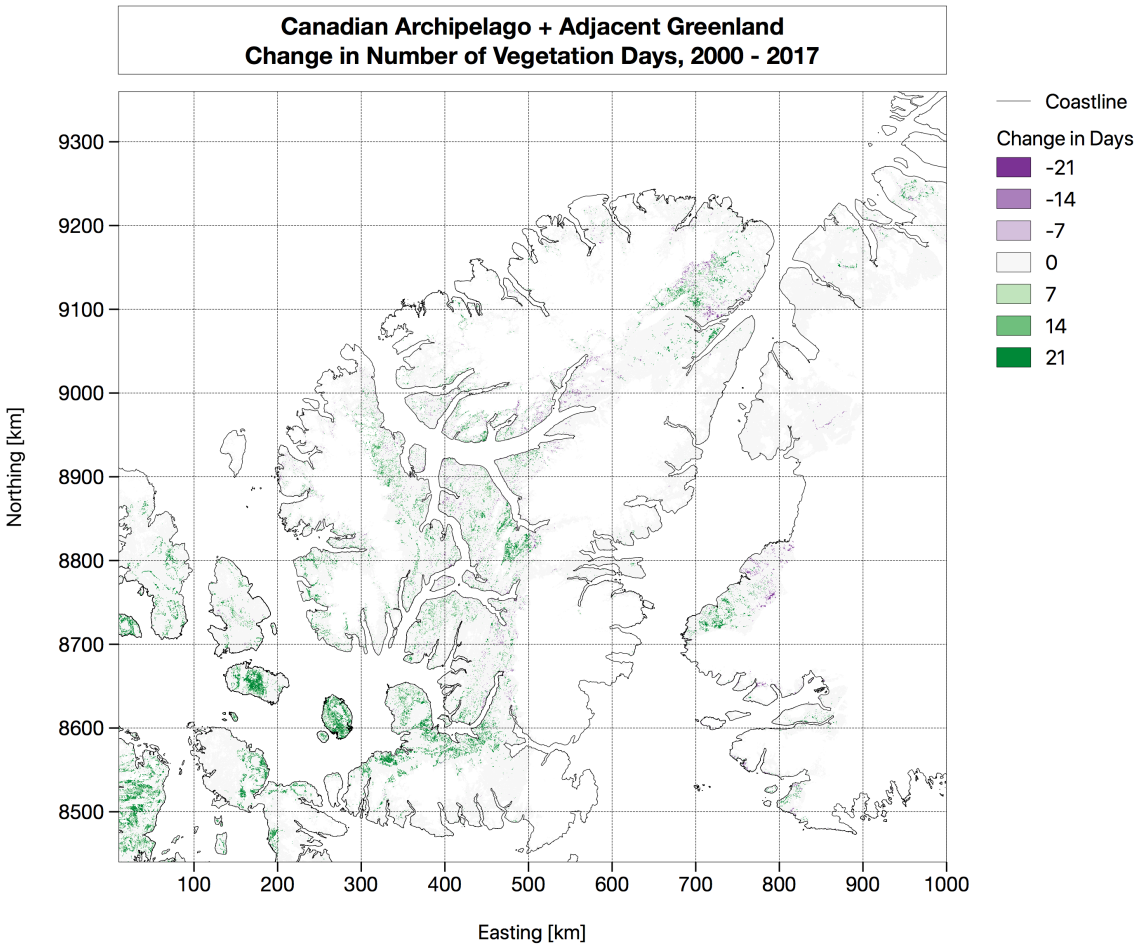

Figure 6.9: Change in vegetation days (VD) over the 18 years period. Based on MODIS imagery, calculated with Sen's Slope Estimator.

6.4 Lake Hazen

6.4.1 Ice Cover

The ice cover of Lake Hazen showed strong variations during the 18 years of observation. The lowest ice cover for all analysed intervals (i.e. yearly average, June, July, August (JJA) average and May to September average) occurred in 2012, although 2010 showed almost similarly low values.

This is consistent with the record low values of the snow/ice-covered days (SCD) and the minimum snow/ice-covered area (MSCA) in 2012 and can be explained by the high summer temperatures. The highest ice cover for all intervals occurred in 2004. Although 2004 was the second coldest year in the closest weather station (Alert) in terms of positive degree days (PDD), no strong connection between the temperatures in Alert and the ice cover was found: 2013 showed the lowest number of PDD and did not have an accordingly high lake ice cover.

The correlation between the ice cover and meteorological variables, such as the PDD, indeed appears to be rather weak (see table 6.3 below). Kendall's τ analyses showed almost no correlation between the PDD in Alert and the ice cover in the analysed intervals. The correlations with other temperature parameters (such as the mean, maximum or minimum temperature) were slightly stronger. The strongest correlations were, however, found with the precipitation: a higher precipitation appears to lead to a larger ice cover. A reason for the weak connection to the regional weather measurements might be the topography of Lake Hazen, described by Surdu et al. (2016) as sheltered from cold Arctic Ocean air.

Table 6.3: The correlation of the Lake Hazen ice cover (based on MODIS NDSI calculations) to different meteorological parameters of the nearest weather station, Alert.

	AVG		JJA		MtS	
	SEN	τ	SEN	τ	SEN	τ
Poistive degree days	-0.01	-0.07	0.01	0.07	0.01	0.02
Mean temperature	-1.97	-0.19	-1.90	-0.15	-1.97	-0.15
Maximum temperature	-2.27	-0.19	-2.37	-0.15	-1.65	-0.15
Minimum temperature	-0.77	-0.11	-1.48	-0.12	-1.06	-0.10
Precipitation	0.05	**0.31**	0.06	**0.22**	0.06	**0.27**

The map in figure 6.10 on the next page shows the average ice cover of Lake Hazen between 2000 and 2017. It can be seen that the centre of the lake showed a larger average ice cover throughout the 18 years of observations, than the areas close to the coast. An interesting feature could be observed in the square from 660 km to 670 km easting and 9090 km to 9100 km northing. This area covers the only outflow of Lake Hazen (Ruggles River). In the outflow area, a smaller ice cover could be observed than in the surroundings. Another area of low ice cover could be found at the south-western end of the lake, in an isolated, shallow part (cf. figure 2.2 on page 5).

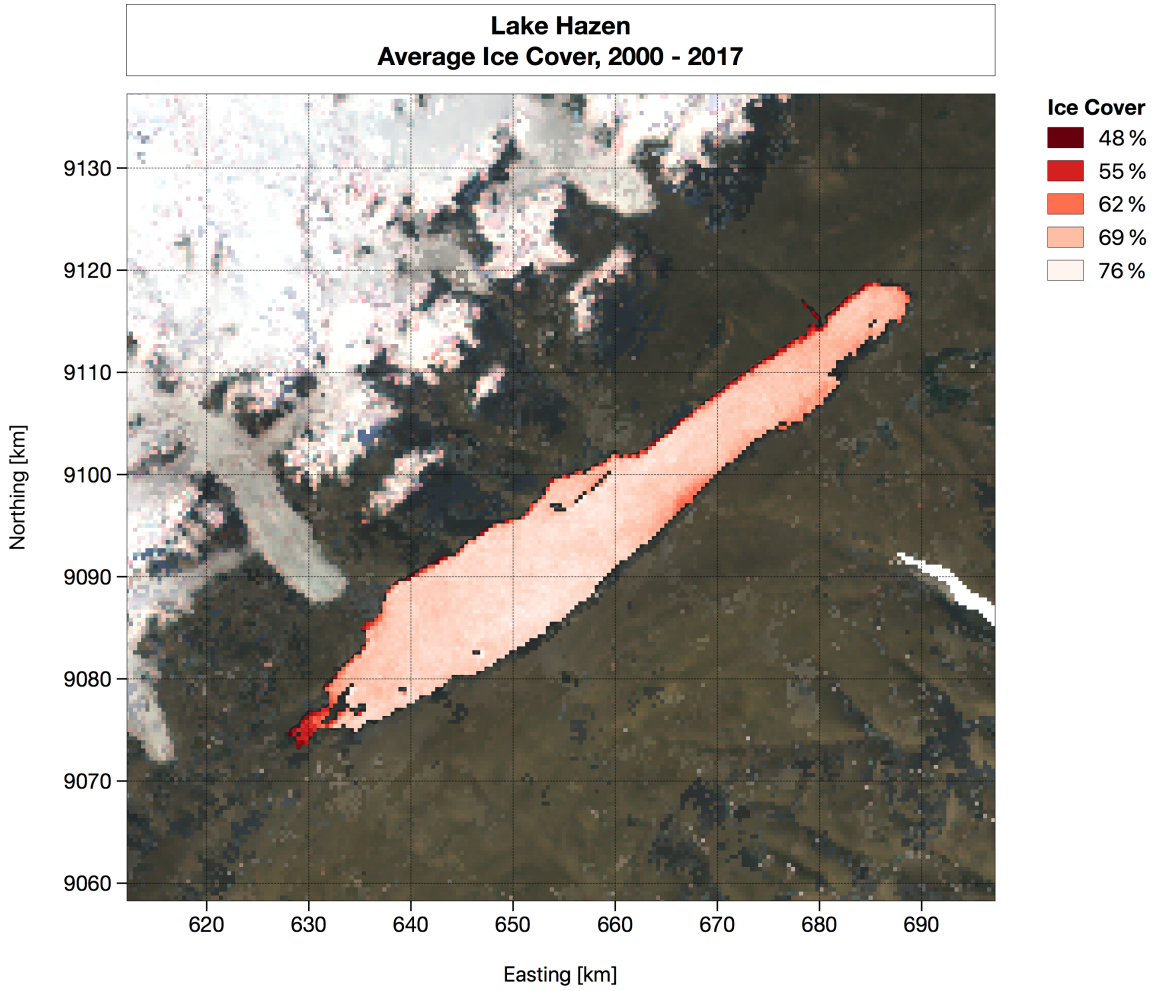

Figure 6.10: Average ice cover of Lake Hazen for the period 2000 - 2017 in %, based on MODIS NDSI calculations. Background: MODIS RGB.

6.4.2 Change Analysis

The observed changes in ice cover depend on the analysed temporal interval. The strongest decrease in ice cover was observed between 2000 and 2012 for the interval May to September with a value of $-0.54\,\%$ per year. This is consistent with the $-0.5\,\%$ observed by Lehnherr et al. (2018), also using MODIS data, validating the applied methods and data of this thesis. Another strong decrease could be observed in the interval June, July, August (JJA), with a magnitude of $-0.40\,\%$ per year.

The map in figure 6.11 on the next page shows the trend in number of ice-covered days of the Lake Hazen area. It can be observed that the north-eastern part was more resilient to changes, and that most of the changes occurred in the south-western part of the lake. A visual analysis of MODIS time series has shown that the south-western part usually thaws a couple of weeks before the north-eastern part. A potential factor might have been the input of glacial meltwater from the

nearby glacier. Lehnherr et al. (2018) found, however, that the number of ice-covered days was not related to the run-off of glaciers in Lake Hazen's watershed. They mention an advanced onset of the ice break-up due to more rapid warming in spring and a delayed freeze-up due to less intense warming in August as contributing factors.

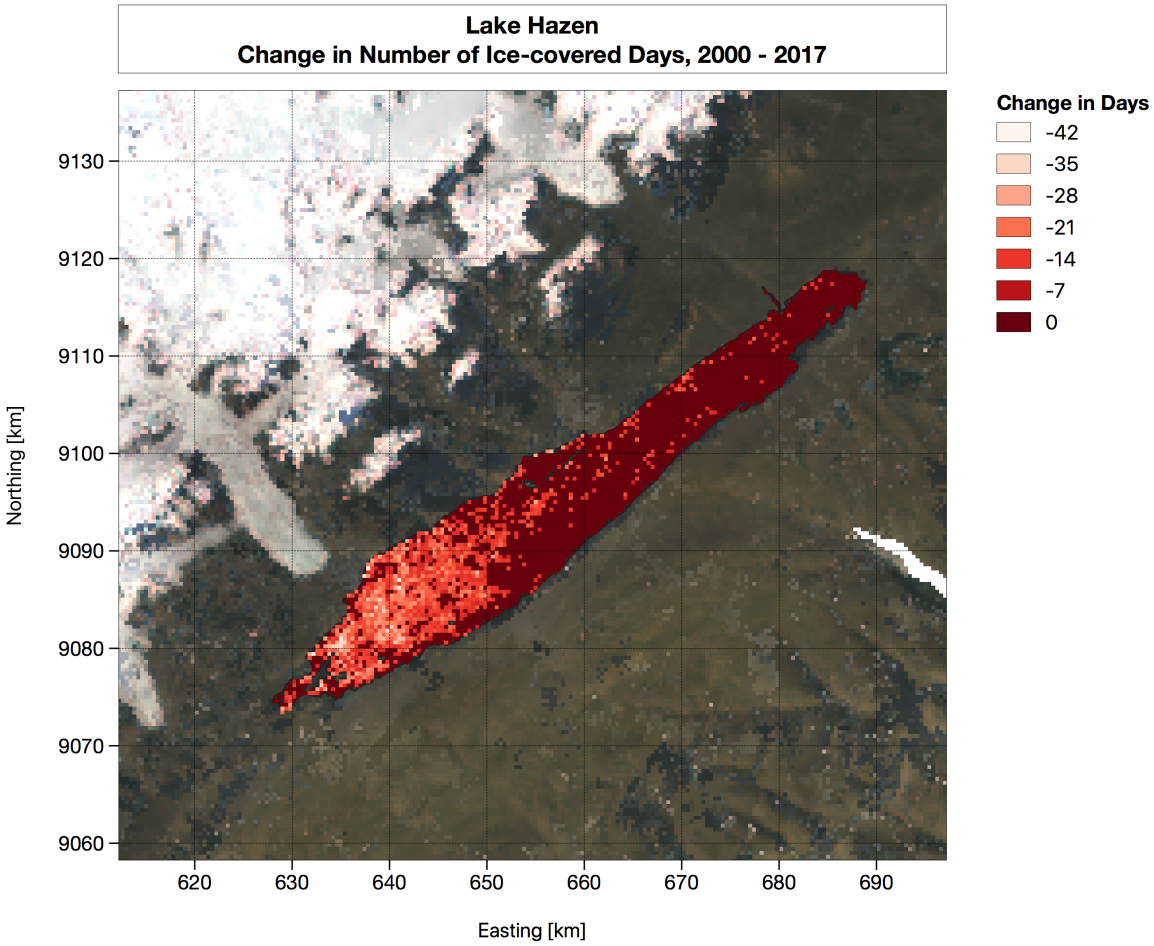

Figure 6.11: Trend in number of ice-covered days of Lake Hazen between 2000 and 2017, based on MODIS NDSI calculations and Sen's Slope Estimator. Background: MODIS RGB.

The observed change in lake ice cover, besides other substantial changes (such as large mass losses of the surrounding glaciers and a decreased lake water residence time) have large impacts on the local ecosystem. Lehnherr et al. (2018) mention a jeopardized security of freshwater foods for the indigenous peoples as a decisive issue. And moreover, the fact that the largest High Arctic lake, previously thought to be resilient to changes, showed such a critical response, raises an uncertain future for the rest of the High Arctic environment.

6.5 Changes in Land Cover

Chapters 6.1 to 6.4 highlighted some of the changes the Canadian Arctic has faced in the last 18 years in terms of land and cryosphere cover. Although some areas of increasing snow/ice-covered days (SCD) were revealed, a general decrease was seen in the share of the cryosphere, especially in the south-western part of the Canadian Arctic Archipelago. At the same time, a clear increase in vegetation was observed — mostly concentrated in the areas of decreasing cryosphere.

The changes in land cover could not directly be linked to the melting intensity — as discussed in chapter 6.2 on page 58, no clear connection between changes in melting and changes in snow cover was found. Both parameters were, however, linked to temperature.

A comparison between the Canadian Arctic Archipelago and Greenland revealed, that the Canadian Arctic Archipelago showed a much stronger response to increasing air temperatures. Most snow cover-related parameters, i.e. snow/ice-covered days (SCD) and minimum snow/ice-covered area (MSCA) showed stronger changes in the Canadian Arctic Archipelago. With a focus on the area of permanent snow/ice, the Canadian Arctic Archipelago showed a higher number of MD. In contrast to the number of MD, the average melting intensity (AMI) was larger in Greenland. As can be expected from the previously mentioned changes, the Canadian Arctic Archipelago also showed a larger increase in vegetation.

The different elevation bands responded heterogeneously to a changing climate with a concentration to the elevation from 1000 m to 1499 m. While the largest changes in SCD could be observed in the elevation bands from 1000 m to 1499 m, the elevation band from 500 m to 999 m showed the largest changes in MSCA. The elevation band from 1000 m to 1499 m showed the largest number of MD without masking to the area of permanent snow/ice. Masked to this area, the highest number of MD could be observed in the band from 500 m to 999 m. The strongest AMI occurred from 1000 m to 1499 m. The largest increase in vegetation could be observed in the band between 0 m to 499 m. This implies that, depending on the elevation, different processes played the major role. In the lowest elevation band, low snow cover coincided with low melting and a high vegetation. In the higher elevation bands with more snow, and especially perennial snow, more melting and a lower vegetation share were observed.

6.6 Combination of Optical Data and SAR Data

The previous chapters have shown that it is vital to use both optical and SAR data for a comprehensive analysis of the state of the snow and ice in an Arctic to High Arctic environment. Thanks to their different physical principles, the optical data can detect processes that cannot be detected by the SAR data and vice versa. Chapter 5.4 on page 47 showed that the SAR data can be used to further investigate events detected using the optical data, such as the first snow-free day, preceded by a series of days with enhanced melting activity.

Optical data allow a precise monitoring of the Earth's surface, as it could be observed with the naked eye. The availability of observations beyond the visible spectrum of the electromagnetic radiation enhances the level of information, enabling for example a differentiation between snow or ice and clouds. Using optical data, an accurate and extensive quantification of different metrics, such as the snow cover duration, the snow/ice-covered area as well as their changes in time are achievable. A clear drawback of optical data is, however, their dependence on daylight and cloud-free conditions. In high latitudes like the Canadian Arctic Archipelago, the optical observation of the land surface is distinctly hampered by the lack of daylight between October and March.

SAR data, on the other hand, provide two-dimensional measurements of the Earth's surface, less intuitively readable by the human eye. As discussed in chapter 4.3 on page 20, dry snow and ice are invisible at some frequencies. In a wet state (i.e. melting snow/ice), however, they are easily detected due to their increased absorption of microwaves, leading to a distinctly decreased backscattering. This allows the detection of a process invisible to the human eye, again at an accurate and extensive level. Thanks to the independence of SAR from weather and light, observations are available around the clock.

The complementarity of optical data and SAR data, however, is ambivalent. At first sight, optical data seem to provide a larger variety of information, when it comes to monitoring the cryosphere. While with optical data accurate spatial and temporal measurements of the cryosphere are achievable, SAR data only provides information about the wetness of the cryosphere. Both measurements can, however, be used for statements about the change of the cryosphere in the context of climate change over a longer period in time. Optical data can for example detect a decrease in snow/ice cover, while SAR data can detect an increase in melting. Put in this way, they can be used for similar applications, and certainly do complement each other.

Especially in high latitude environments, like the Canadian Arctic Archipelago, the SAR data can clearly complement the optical data. With the lack of daylight between October and March, no optical observations of the Earth's surface are available. If the last image in autumn and the first image in spring acquired by the optical sensor show a completely snow-covered land surface, and the SAR sensor does not record any melting activities between autumn and spring, it could be assumed, that the snow cover did not change. Optical data can only detect extreme changes in areas of permanent snow/ice (i.e. a complete loss), while the SAR data can monitor an increased melting activity with unvarying cryosphere extent. This is particularly useful in the High Arctic, where ice caps or glaciers might show an increased melting activity in a warm year, without a visible change in area.

6.7 Outlook

This research could be extended mainly in two ways. On the one hand, longer and additional time series could be used to analyse changes in land surface over a long period of time, making

even climatological statements possible. Especially additional years of SAR data could help to further investigate the relation between melting activity and snow/ice cover. On the other hand, the analysis could be extended to other areas in the Arctic, such as northern Scandinavia or Iceland or high-altitude environments in lower-latitude areas (e.g. the Central European Alps) in order to detect similarities or differences between the regions. Another conceivable widening of the research is the integration of data from multiple sources. As discussed in chapters 6.1 on page 51 and 6.3 on page 60, there are some trends, which could not yet be explained by the combination of remotely sensed data and meteorological records. Additional data, such as information about the sea ice extent and its change as well as information about ocean currents might help to find explanations.

In a broader context, there are many extensions to cryosphere research using remote sensing. Given that remote sensing has proven in being able to monitor the state of the cryosphere, there is plenty of potential for future missions and new approaches. Dietz et al. (2012) and Nolin (2010) mention methods that combine data from the optical and the active microwave domain as encouraging new methods, with need for further research. An example is the approach of Foster et al. (2011), who combined Moderate Resolution Imaging Spectro-Radiometer (MODIS), Advanced Microwave Scanning Radiometer for the Earth Observing System (AMSR-E) and Quick Scatterometer (QuikSCAT) data to produce a daily global snow cover product, combining information about the snow cover extent, the snow water equivalent, the onset of melt and melting snow. In this product, however, the great temporal coverage is counterbalanced by a rather low spatial resolution of 25 km, although the authors mention potentials for an improvement to 5 km.

A promising addition to the existing SAR sensors is the RADARSAT Constellation Mission (RCM), a continuation of the existing RADARSAT satellites, planned by the Canadian Space Agency (CSA). The RCM consists of three C-band SAR sensors with the main applications of maritime surveillance, disaster management and ecosystem monitoring (Thompson, 2015). The planned ecosystem and sea ice monitoring capabilities are of big interest for cryosphere remote sensing. RCM is planned for launch in late 2018 and will provide daily SAR images of Canada (Dabboor et al., 2018).

In the reflective domain, Visible Infrared Imager Radiometer Suite (VIIRS) and the Sentinel family are interesting additions to already established platforms (such as the Landsat family and MODIS) for future cryosphere monitoring. VIIRS is a sensor launched in 2011 onboard the Suomi National Polar-orbiting Partnership (Suomi NPP) satellite. It was designed to improve the capabilities of Advanced Very High Resolution Radiometer (AVHRR) and to continue the MODIS observation history. Key et al. (2013) analysed the capabilities of the ice and snow monitoring products of VIIRS (such as ice surface temperature, snow cover, sea ice concentration) and obtained positive validation results. They rated the products as useful for research and operational applications. From the Sentinel family, the optical satellites Sentinel-2A/B (2015/2017) and Sentinel-3A/B (2016/2018) are interesting candidates for cryosphere monitoring. Sentinel-2 (see e.g. Drusch et al. (2012)) provides high-resolution multi-spectral images. Although it was not primarily designed for snow or ice monitoring, it has successfully been applied for various cryosphere applications, such as

glacier extent mapping (see Kääb et al. (2016) and Paul et al. (2016)). Sentinel-3 (see e.g. Donlon et al. (2012)) measures sea surface topography, sea surface temperature and different visible and infrared radiances, enabling global monitoring of ice/snow, sea ice, ice surface topography every 0.5 to 1 days. As of autumn 2018, only a few studies using Sentinel-3 data could be found. In their pre-launch assessment of the satellite, Solberg et al. (2015) rated Sentinel-3 with its great spatio-temporal coverage as a valuable addition to already operational satellites.

Moreover, there are completely new missions, such as the Cold Regions Hydrology High-Resolution Observatory (CoReH2O), suggested by Rott et al. (2008). CoReH2O was designed to also monitor dry snow (in contrast to previous active microwave missions monitoring wet snow) by using co-polarised and cross-polarised Ku-band and X-band SAR. The mission was, however, not selected for further development by the European Space Agency (ESA) (Lemmetyinen et al., 2017). Another new mission is Ice, Cloud and land Elevation Satellite-2 (ICESat-2), launched during the last weeks of this thesis — the successor of the ICESat mission from 2003. ICESat-2 is a spaceborne laser altimeter with the purpose of measuring elevation changes of sea ice or ice sheets (Markus et al., 2017).

7 Conclusions

7.1 Summary

Using an 18 years long time series of optical data and an additional four years of SAR data, the land cover of the north-eastern most part of Canada was analysed. Different methods, for instance the NDSI and the NDVI for the optical data and a snow wetness algorithm for the SAR data were used to calculate various metrics, such as the number of snow/ice-covered days, the minimum snow/ice-covered area, the number of melting days or the number of vegetation days. Using these, a general characterisation of the land surface was obtained and changes that occurred during 18 years were analysed. Using the gained insights, the research questions proposed at the beginning of the thesis can be answered.

7.2 Findings

Which aspects of snow dynamics can be derived from SAR data, from optical data, and from both?

Both optical and SAR data offer great opportunities to receive timely information about the state of the cryosphere at reasonable spatial and temporal resolutions. In addition to near real-time monitoring, vast archives of satellite imagery can provide a foundation for an investigation of the development of certain phenomena over a longer period in time.

Optical sensors mostly operate in the visible and infrared spectrum of the electromagnetic radiation. They have the capabilities to monitor snow, be it dry snow or wet snow, and ice, while at the same time excluding clouds. Parameters that can be gathered by optical sensors are the extent of the snow/ice cover in terms of temporal extent (number of snow/ice-covered days) and spatial extent (minimum snow/ice-covered area). Using a time series of optical data, the change of these parameters can be analysed. Optical data can further be used to detect the greening of the vegetation, allowing descriptions of the land surface after the disappearance of the snow.

The strongest potential of SAR sensors is the detection of wet snow, that is, melting processes. This is of special interest in areas with permanent snow/ice. In these areas, elevated air temperatures do not necessarily lead to a decrease in the area of snow/ice cover. In this case, SAR sensors can still detect melting processes, and thus confirm the impact of climate change. Another strong asset of SAR sensors is their independence from good weather and daylight, providing reliable data.

This independence of SAR sensors is a point of intersection with optical data for their complementarity. While both systems can individually detect changes of the land surface related to climate change, the largest potential of a dual-use of optical and SAR data is in high-latitude regions between autumn and spring. In this period, there is no sunlight available, making the application of optical sensors impossible. The SAR sensors can, however, step in and help detect whether any

changes (e.g. melting events) occurred on the land surface between the last and the first available optical image acquisition.

Using these, what changes in land cover and snow/ice cover can be observed between 2000 and 2017?

Although 18 years do not allow significant climatological statements, fairly clear observations could be made. The number of snow/ice-covered days decreased over the course of the 18 years. The strongest decrease was observed in the Canadian Arctic Archipelago, where the number of snow/ice-covered days decreased at an average rate of 2.0 days per decade. The spatial representation of the change was heterogeneous. Clear areas of decreasing snow cover could be found in the south-western part of the study area, while there were also areas of increasing snow cover, concentrated to the centre of the Canadian Arctic Archipelago.

An even more pronounced change could be observed for the minimum snow/ice-covered area. Here, the strongest decrease was observed for the whole Canadian Arctic Archipelago, with an average decrease of 1.5% per decade, relative to the complete landmass. Spatially, the largest changes could be observed in the north-western part of the study area, on the west coast of Ellesmere Island and Axel Heiberg Island, and close to the ice caps.

Given that only four years of SAR data were available, no profound inter-annual comparisons could be made. The number of melting days and the melting intensity correlated well with meteorological variables, such as the number of positive degree days. Additionally, well-described events, such as the extreme melt in Greenland in 2015, were observed in the data.

In contrast to the decrease of the cryosphere, the vegetation showed an increase. The number of vegetation days distinctly increased, especially in the south-western part of the study site. The locations of increasing vegetation clearly correlated with areas of decreasing snow cover.

Lake Hazen, the largest High Arctic lake showed a distinct decrease in lake ice during the observation period. The findings by Lehnherr et al. (2018) could be confirmed and extended by five more years. Although the obtained decrease in lake ice of $-0.29\,\%$ per year (2000 - 2017, measured between May and September) was slightly lower than the decrease of $-0.5\,\%$ per year (2000 - 2012, same period), as obtained by the authors, the decrease in lake ice is clear and the impacts on the local environment are alarming.

(How) can the observed changes in land cover and snow/ice cover be explained?

The observed changes could nearly universally be explained by an increase in air temperature. The number of snow/ice-covered days, the minimum snow/ice-covered area and the number of vegetation days showed a clear correlation with the number of positive degree days. The number of melting

days was also correlated with temperature, but as only four years of measurements were available, no trend analysis was performed.

There were, however, some phenomena, that could not be explained with the available data. One example was the record high vegetation signal in 2007. Although the year 2007 did not show any meteorological anomalies, the year showed a distinctly larger number of days with vegetation. Another example was the increase in snow/ice-covered days in certain parts of Ellesmere Island over the 18 years of observations. The increase was confirmed by other sources (e.g. Environment and Climate Change Canada (2018a)), but no explanation could be found in literature. However, an impact of a change in sea ice leading to increased water vapour flux and increased snowfall was assumed, as suggested by (Brock, 2016). Other data, such as ocean temperatures or changes in sea ice cover, might thus help to reveal the reasons.

7.3 Closing Remarks

With the available data and methods, a characterisation of the changes in land cover in the north-eastern most part of Canada and adjacent Greenland was achieved. Comparisons between optical remote sensing and SAR remote sensing and an assessment of their complementarity were possible. This yielded answers to the research questions posed at the beginning of the thesis. The potential of remote sensing for cryosphere research was demonstrated. Many new technologies, methods, and research directions further fortify this potential, creating a promising future for the remote sensing of the cryosphere.

Danksagung

Im Rahmen meiner Masterarbeit durfte ich auf die Unterstützung zahlreicher Personen zählen. Als erstes möchte ich mich für die tolle Betreuung durch **Dr. David Small** und **Dr. Rogier de Jong** und ihre Expertise im Bereich SAR und optischer Fernerkundung bedanken. Die zahlreichen Treffen während der rund acht Monaten fruchteten stets in wertvollen Beiträgen für meine Arbeit.

Weiterer Dank geht an **Christoph Rohner** für seine tollen Inputs im Bereich Schnee-/Eisschmelze, an **Elias Mendez** für einige gute Hinweise zum MATLAB-Code und an **Dr. Hendrik Wulf** für konstruktive Gespräche über die Analyse von klimatischen Veränderungen.

Nicht zuletzt möchte ich mich auch bei meinen Büronachbarn **Manuel Luck**, **Joan Sturm**, **Isabelle Helfenstein**, **Sonja Bertschi** und **Sebastian Röthlin** für die gute Gemeinschaft und bei vielen Mitarbeitenden der **RSL-Abteilung** für spannende Diskussionen beim Mittagessen bedanken.

8 References

Adams, P. and Dunbar, M. J. (2016). Arctic Archipelago. In *The Canadian Encylopedia*. Consulted on July 11, 2018. Retrieved from https://www.thecanadianencyclopedia.ca/en/article/arctic-archipelago/.

AMAP (2017). Snow, Water, Ice and Permafrost. Summary for Policy-makers. Arctic Monitoring and Assessment Programme (AMAP), Oslo, Norway. 20 pp.

Brock, B. W. (2016). Shrinking sea ice, increasing snowfall and thinning lake ice: a complex Arctic linkage explained. *Environmental Research Letters*, 11(9):2 pp.

Brown, R. D. and Mote, P. W. (2009). The Response of Northern Hemisphere Snow Cover to a Changing Climate. *Journal of Climate*, 22(8):2124–2145.

Callaghan, T. V., Johansson, M., Brown, R. D., Groisman, P. Y., Labba, N., Radionov, V., Bradley, R. S., Blangy, S., Bulygina, O. N., Christensen, T. R., Colman, J. E., Essery, R. L. H., Forbes, B. C., Forchhammer, M. C., Golubev, V. N., Honrath, R. E., Juday, G. P., Meshcherskaya, A. V., Phoenix, G. K., Pomeroy, J., Rautio, A., Robinson, D. A., Schmidt, N. M., Serreze, M. C., Shevchenko, V. P., Shiklomanov, A. I., Shmakin, A. B., Sköld, P., Sturm, M., Woo, M.-k., and Wood, E. F. (2011). Multiple Effects of Changes in Arctic Snow Cover. *AMBIO*, 40(S1):32–45.

Crane, R. G. and Anderson, M. R. (1984). Satellite discrimination of snow/cloud surfaces. *International Journal of Remote Sensing*, 5(1):213–223.

Crichton, N. (2001). Information Point: Kendall's Tau. *Journal of Clinical Nursing*, 10(5):707–715.

Dabboor, M., Iris, S., and Singhroy, V. (2018). The RADARSAT Constellation Mission in Support of Environmental Applications. *Proceedings*, 2(7):323.

Dietz, A. J., Kuenzer, C., Gessner, U., and Dech, S. (2012). Remote sensing of snow - a review of available methods. *International Journal of Remote Sensing*, 33(13):4094–4134.

Donlon, C., Berruti, B., Buongiorno, A., Ferreira, M.-H., Féménias, P., Frerick, J., Goryl, P., Klein, U., Laur, H., Mavrocordatos, C., Nieke, J., Rebhan, H., Seitz, B., Stroede, J., and Sciarra, R. (2012). The Global Monitoring for Environment and Security (GMES) Sentinel-3 mission. *Remote Sensing of Environment*, 120:37–57.

Drusch, M., Del Bello, U., Carlier, S., Colin, O., Fernandez, V., Gascon, F., Hoersch, B., Isola, C., Laberinti, P., Martimort, P., Meygret, A., Spoto, F., Sy, O., Marchese, F., and Bargellini, P. (2012). Sentinel-2: ESA's Optical High-Resolution Mission for GMES Operational Services. *Remote Sensing of Environment*, 120:25–36.

Edwards, R. and Treitz, P. (2017). Vegetation Greening Trends at Two Sites in the Canadian Arctic: 1984–2015. *Arctic, Antarctic, and Alpine Research*, 49(4):601–619.

Environment and Climate Change Canada (2018a). Canadian Environmental Sustainability Indicators: Snow cover. Consulted on August 24, 2018. Retrieved from: https://www.canada.ca/en/environment-climate-change/services/environmental-indicators/snow-cover.html.

Environment and Climate Change Canada (2018b). Technical Documentation. Digital Archive of Canadian Climatological Data. Consulted on June 28, 2018. Retrieved from: ftp://ftp.tor.ec.gc.ca/Pub/Documentation_Technical/Technical_Documentation.pdf.

Esau, I., Miles, V. V., Davy, R., Miles, M. W., and Kurchatova, A. (2016). Trends in normalized difference vegetation index (NDVI) associated with urban development in northern West Siberia. *Atmospheric Chemistry and Physics*, 16(15):9563–9577.

European Space Agency (2012). Sentinel-1: ESA's Radar Observatory Mission for GMES Operational Services (ESA SP-1322/1). Consulted on June 05, 2018. Retrieved from http://esamultimedia.esa.int/multimedia/publications/SP-1322_1/.

Fisher, D., Zheng, J., Burgess, D., Zdanowicz, C., Kinnard, C., Sharp, M., and Bourgeois, J. (2012). Recent melt rates of Canadian arctic ice caps are the highest in four millennia. *Global and Planetary Change*, 84:3–7.

Fontana, F. M. A., Trishchenko, A. P., Luo, Y., Khlopenkov, K. V., Nussbaumer, S. U., and Wunderle, S. (2010). Perennial snow and ice variations (2000–2008) in the Arctic circumpolar land area from satellite observations. *Journal of Geophysical Research*, 115(F4):1–11.

Foster, J. L., Hall, D. K., Eylander, J. B., Riggs, G. A., Nghiem, S. V., Tedesco, M., Kim, E., Montesano, P. M., Kelly, R. E. J., Casey, K. A., and Choudhury, B. (2011). A blended global snow product using visible, passive microwave and scatterometer satellite data. *International Journal of Remote Sensing*, 32(5):1371–1395.

Gregory, J. M., White, N. J., Church, J. A., Bierkens, M. F. P., Box, J. E., van den Broeke, M. R., Cogley, J. G., Fettweis, X., Hanna, E., Huybrechts, P., Konikow, L. F., Leclercq, P. W., Marzeion, B., Oerlemans, J., Tamisiea, M. E., Wada, Y., Wake, L. M., and van de Wal, R. S. W. (2013). Twentieth-Century Global-Mean Sea Level Rise: Is the Whole Greater than the Sum of the Parts? *Journal of Climate*, 26(13):4476–4499.

Hall, D. K., Foster, J. L., Verbyla, D. L., Klein, A. G., and Benson, C. S. (1998). Assessment of Snow Cover Mapping Accuracy in a Variety of Vegetation Cover Densities in Central Alaska. *Remote Sensing of the Environment*, 66(2):129–137.

Hall, D. K. and Riggs, G. A. (2011). Normalized-Difference Snow Index (NDSI). In Singh, V. P., Singh, P., and Haritashya, U. K., editors, *Encyclopedia of Snow, Ice and Glaciers*, pages 779–780. Springer Netherlands, Dordrecht.

Hall, D. K., Riggs, G. A., and Salomonson, V. V. (1995). Development of methods for mapping global snow cover using moderate resolution imaging spectroradiometer data. *Remote Sensing of Environment*, 54(2):127–140.

Hall, D. K., Riggs, G. A., Salomonson, V. V., Digirolamo, N. E., and Bayr, K. J. (2002). MODIS snow-cover products. *Remote Sensing of Environment*, 83(1-2):181–194.

Heisel, D. and Hirsch, R. (2002). *Statistical Methods in Water Resources*. U.S. Geological Survey.

Henry, G. and Elmendorf, S. (2010). Greening of the Arctic. In CAFF International Secretariat, editor, *Arctic Biodiversity Trends 2010*, chapter 11, pages 62–64. CAFF International Secretariat, Akureyri.

Howat, I. M., Negrete, A., and Smith, B. E. (2014). The Greenland Ice Mapping Project (GIMP) land classification and surface elevation data sets. *Cryosphere*, 8(4):1509–1518.

Jia, G. J., Epstein, H. E., and Walker, D. A. (2009). Vegetation greening in the canadian arctic related to decadal warming. *Journal of Environmental Monitoring*, 11(12):2231–2238.

Kääb, A., Winsvold, S., Altena, B., Nuth, C., Nagler, T., and Wuite, J. (2016). Glacier Remote Sensing Using Sentinel-2. Part I: Radiometric and Geometric Performance, and Application to Ice Velocity. *Remote Sensing*, 8(7):1–22.

Key, J. R., Mahoney, R., Liu, Y., Romanov, P., Tschudi, M., Appel, I., Maslanik, J., Baldwin, D., Wang, X., and Meade, P. (2013). Snow and ice products from Suomi NPP VIIRS. *Journal of Geophysical Research: Atmospheres*, 118(23):12,816–12,830.

Köck, G., Muir, D., Yang, F., Wang, X., Talbot, C., Gantner, N., and Moser, D. (2012). Bathymetry and sediment geochemistry of Lake Hazen (Quttinirpaaq National Park, Ellesmere Island, Nunavut). *Arctic*, 65(1):56–66.

Lehnherr, I., St Louis, V. L., Sharp, M., Gardner, A. S., Smol, J. P., Schiff, S. L., Muir, D. C. G., Mortimer, C. A., Michelutti, N., Tarnocai, C., St Pierre, K. A., Emmerton, C. A., Wiklund, J. A., Köck, G., Lamoureux, S. F., and Talbot, C. H. (2018). The world's largest High Arctic lake responds rapidly to climate warming. *Nature Communications*, 9(1):1–9.

Lemmetyinen, J., Rautiainen, K., Luojus, K., Rott, H., Nagler, T., Parrella, G., Hajnsek, I., Derksen, C., Macelloni, G., Brogioni, M., Wiesmann, A., Matzler, C., and Kern, M. (2017). Future mission concepts for measuring snow mass. In *2017 IEEE International Geoscience and Remote Sensing Symposium (IGARSS)*, number 1, pages 1370–1371. IEEE.

Livingstone, C. E., Sikaneta, I., Gierull, C., Chiu, S., and Beaulne, P. (2005). RADARSAT-2 System and Mode Description. In *Integration of Space-Based Assets within Full Spectrum Operations*, number 15, pages 1–22, Neuilly-sur-Seine.

Luojus, K. P., Pulliainen, J. T., Blasco Cutrona, A., Metsamaki, S. J., and Hallikainen, M. T. (2009). Comparison of SAR-Based Snow-Covered Area Estimation Methods for the Boreal Forest Zone. *IEEE Geoscience and Remote Sensing Letters*, 6(3):403–407.

Luojus, K. P., Pulliainen, J. T., Metsämäki, S. J., and Hallikainen, M. T. (2006). Accuracy assessment of SAR data-based snow-covered area estimation method. *IEEE Transactions on Geoscience and Remote Sensing*, 44(2):277–287.

Markus, T., Neumann, T., Martino, A., Abdalati, W., Brunt, K., Csatho, B., Farrell, S., Fricker, H., Gardner, A., Harding, D., Jasinski, M., Kwok, R., Magruder, L., Lubin, D., Luthcke, S., Morison, J., Nelson, R., Neuenschwander, A., Palm, S., Popescu, S., Shum, C., Schutz, B. E., Smith, B., Yang, Y., and Zwally, J. (2017). The Ice, Cloud, and land Elevation Satellite-2 (ICESat-2): Science requirements, concept, and implementation. *Remote Sensing of Environment*, 190:260–273.

Marsh, J. H. (2018a). Baffin Island. In *The Canadian Encylopedia*. Consulted on July 04, 2018. Retrieved from https://www.thecanadianencyclopedia.ca/en/article/baffin-island.

Marsh, J. H. (2018b). Ellesmere Island. In *The Canadian Encylopedia*. Consulted on July 04, 2018. Retrieved from https://www.thecanadianencyclopedia.ca/en/article/ellesmere-island.

Nagler, T. and Rott, H. (2000). Retrieval of Wet Snow by Mean of Multitemporal SAR Data. *IEEE Trans. Geosci. Remote Sens.*, 38(2):754–765.

Nagler, T., Rott, H., Ripper, E., Bippus, G., and Hetzenecker, M. (2016). Advancements for snowmelt monitoring by means of Sentinel-1 SAR. *Remote Sensing*, 8(4):1–17.

Natural Resources Canada (2016). Canadian Digital Elevation Model Product Specifications. Edition 1.1. Consulted on March 06, 2018. Retrieved from ftp://ftp.geogratis.gc.ca/pub/nrcan_rncan/elevation/cdem_mnec/doc/CDEM_product_specs.pdf.

Nolin, A. W. (2010). Recent advances in remote sensing of seasonal snow. *Journal of Glaciology*, 56(200):1141–1150.

Ohlson, J. A. and Kim, S. (2015). Linear valuation without OLS: the Theil-Sen estimation approach. *Review of Accounting Studies*, 20(1):395–435.

Park, J.-W., Korosov, A. A., Babiker, M., Sandven, S., and Won, J.-S. (2018). Efficient Thermal Noise Removal for Sentinel-1 TOPSAR Cross-Polarization Channel. *IEEE Transactions on Geoscience and Remote Sensing*, 56(3):1555–1565.

Paul, F., Winsvold, S. H., Kääb, A., Nagler, T., and Schwaizer, G. (2016). Glacier remote sensing using Sentinel-2. part II: Mapping glacier extents and surface facies, and comparison to Landsat 8. *Remote Sensing*, 8(7):1–15.

Rott, H., Cline, D., Nagler, T., Pulliainen, J., Rebhan, H., Yueh, S., Duguay, C., Essery, R., Haas C.an Macelloni, G., Malnes, E., Pulliainen, J., Rebhan, H., and Yueh, S. (2008). CoReH2O - A Ku- and X-Band SAR Mission for Detailed Studies of Snow and Ice Processes. In *EUSAR 2008. 7th European Conference on Synthetic Aperture Radar*, pages 111–114.

Rouse, J. W., Hass, R. H., Schell, J., and Deering, D. (1973). Monitoring vegetation systems in the great plains with ERTS. *Third Earth Resources Technology Satellite (ERTS) symposium*, 1:309–317.

Salomonson, V. V., Barnes, W. L., Maymon, P. W., Montgomery, H. E., and Ostrow, H. (1989). MODIS: Advanced Facility Instrument for Studies of the Earth as a System. *IEEE Transactions on Geoscience and Remote Sensing*, 27(2):145–153.

Small, D. (2011). Flattening Gamma: Radiometric Terrain Correction for SAR Imagery. *IEEE Transactions on Geoscience and Remote Sensing*, 49(8):3081–3093.

Small, D. (2012). SAR backscatter multitemporal compositing via local resolution weighting. *International Geoscience and Remote Sensing Symposium (IGARSS)*, pages 4521–4524.

Snehmani, Singh, M. K., Gupta, R. D., Bhardwaj, A., and Joshi, P. K. (2015). Remote sensing of mountain snow using active microwave sensors: a review. *Geocarto International*, 30(1):1–27.

Solberg, R., Amlien, J., Koren, H., Eikvil, L., Malnes, E., and Storvold, R. (2004). Multi-sensor and time-series approaches for monitoring of snow parameters. In *IGARSS 2004. 2004 IEEE International Geoscience and Remote Sensing Symposium*, volume 3, pages 1661–1666. IEEE.

Solberg, R., Trier, O. D., and Rudjord, O. (2015). Monitoring of Snow Properties with Sentinel-3. In *Sentinel-3 for Science Workshop*, volume 734 of *ESA Special Publication*.

Surdu, C. M., Duguay, C. R., and Fernández Prieto, D. (2016). Evidence of recent changes in the ice regime of lakes in the Canadian High Arctic from spaceborne satellite observations. *The Cryosphere*, 10(3):941–960.

Tedesco, M., Mote, T., Fettweis, X., Hanna, E., Jeyaratnam, J., Booth, J. F., Datta, R., and Briggs, K. (2016). Arctic cut-off high drives the poleward shift of a new Greenland melting record. *Nature Communications*, 7:1–6.

The Editors of Encyclopaedia Britannica (2017). Ellesmere Island. In *Encyclopædia Britannica*. Consulted on July 04, 2018. Retrieved from https://www.britannica.com/place/Ellesmere-Island.

Thompson, A. A. (2015). Overview of the RADARSAT Constellation Mission. *Canadian Journal of Remote Sensing*, 41(5):401–407.

Tiuri, M., Sihvola, A., Nyfors, E., and Hallikaiken, M. (1984). The complex dielectric constant of snow at microwave frequencies. *IEEE Journal of Oceanic Engineering*, 9(5):377–382.

Torres, R., Navas-Traver, I., Bibby, D., Lokas, S., Snoeij, P., Rommen, B., Osborne, S., Ceba-Vega, F., Potin, P., and Geudtner, D. (2017). Sentinel-1 SAR system and mission. In *2017 IEEE Radar Conference (RadarConf)*, pages 1582–1585. IEEE.

Trishchenko, A. P. (2017). MODIS Time Series for Ellesmere Island Derived From Canada 10-Day Composites Over 2000-2017 Period. Product Details. Natural Resources Canada/Earth Sciences Sector/Long Term Satellite Data Record.

Trishchenko, A. P., Leblanc, S. G., Wang, S., Li, J., Ungureanu, C., Luo, Y., Khlopenkov, K. V., and Fontana, F. (2016). Variations of Annual Minimum Snow and Ice Extent over Canada and Neighboring Landmass Derived from MODIS 250-m Imagery for 2000–2014. *Canadian Journal of Remote Sensing*, 42(3):214–242.

Trishchenko, A. P. and Wang, S. (2018). Variations of climate, surface energy budget, and minimum snow/ice extent over Canadian Arctic landmass for 2000-16. *Journal of Climate*, 31(3):1155–1172.

University of Ottawa (2018). Milne Ice Shelf Weather Station. Consulted on June 25, 2018. Retrieved from https://datagarrison.com/users/300034012631040/300034012631040/index.php.

Vaughan, D., Comiso, J., Allison, I., Carrasco, J., Kaser, G., Kwok, R., Mote, P., Murray, T., Paul, F., Ren, J., Rignot, E., Solomina, O., Steffen, K., and Thang, T. (2013). Observations: Cryosphere. *Climate Change 2013 the Physical Science Basis: Working Group I Contribution to the Fifth Assessment Report of the Intergovernmental Panel on Climate Change*, pages 317–382.

Wake, L. and Marshall, S. (2015). Assessment of current methods of positive degree-day calculation using in situ observations from glaciated regions. *Journal of Glaciology*, 61(226):329–344.

Wang, Y., Huang, X., Liang, H., Sun, Y., Feng, Q., and Liang, T. (2018). Tracking snow variations in the Northern Hemisphere using multi-source remote sensing data (2000-2015). *Remote Sensing*, 10(1):1–22.

Woo, M.-k. and Young, K. L. (2014). Disappearing semi-permanent snow in the High Arctic and its consequences. *Journal of Glaciology*, 60(219):192–200.

Personal Declaration

I hereby declare that the submitted thesis is the result of my own, independent work. All external sources are explicitly acknowledged in the thesis.

Hendschiken, 27.09.2018

Marius Vögtli

Place, Date

Signature